Table 7.7 Summary of imperfections considered from the target to the end of the positron linac, with RMS error values reported for each parameter

Imperfection	Unit	Value
Transverse position error	µm	100
Transverse angular error (solenoids and dipoles)	µrad	200
Transverse angular error (other elements)	µrad	100
Magnetic strength error	%	0.1
RF gradient error	%	1
RF phase error	°	0.1
Beam position error	µm	100
Beam divergence error	µrad	100

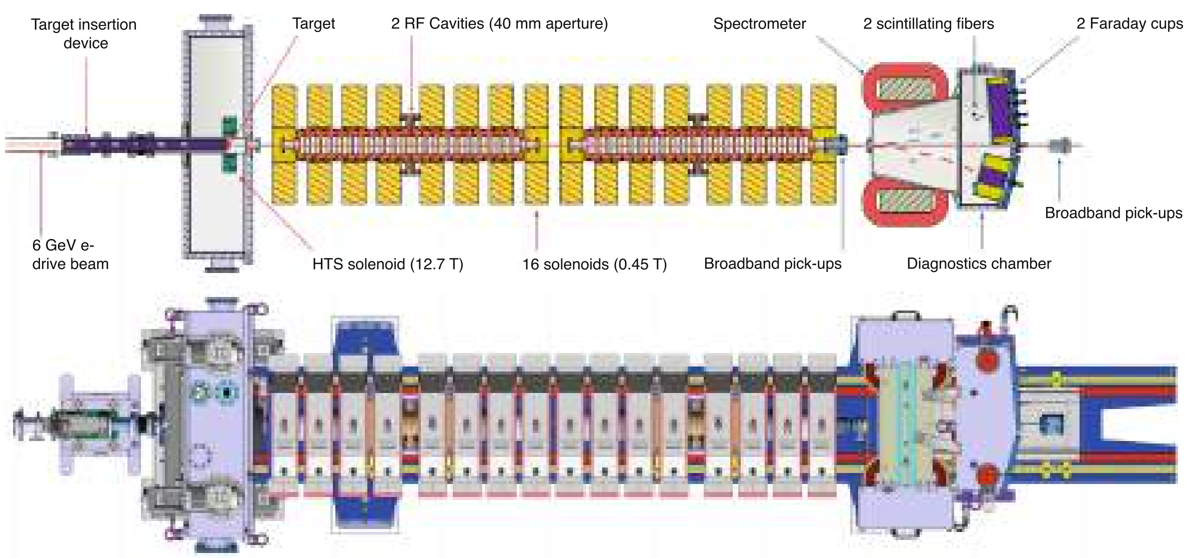

Fig. 7.16 Overview of the technology for the P^3 experiment

superconducting (HTS) solenoid around the target region, as well as a novel standing-wave solution for the RF cavities that provides a large iris aperture.

Figure 7.16 presents a technical drawing of the experiment, illustrating all the technologies developed or under development at PSI and CERN. These technologies have been carefully designed and optimised based on an in-depth study involving advanced beam dynamics simulations. This detailed simulation work made it possible to model and predict the behaviour of particle beams under various conditions, thereby refining the experimental setup and ensuring the optimal performance of each component. The figure also illustrates the integration of these technologies, highlighting key aspects such as the integration of the target in the cryostat that houses the HTS coils, the RF structures surrounded by normal conducting solenoids, and the diagnostics chamber that will allow measurement of the charge and energy spectrum of the positrons generated.

The procurement and assembly of most accelerator and diagnostic components are progressing on schedule, ensuring the timely completion of the project milestones. A key achievement has been the successful demonstration of the HTS solenoid at PSI, which achieved magnetic fields up to 18 T, a significant step forward for this advanced component.

Figure 7.17 shows photos of the P^3 component production process, including the HTS coils and their cryostat, the broadband pickups, and the first accelerating RF structure. Overall, the P^3 experiment is making steady progress, with installation work at SwissFEL proceeding smoothly during scheduled shutdown periods, which take place three times a year. Essential infrastructure components, such as segments of the extraction line and the high-voltage klystron-modulator system, are being installed in the tunnel according to plan. The primary installation phase is expected to conclude by the end of 2025, paving the way for the experiment to begin positron operations in 2026. It is worth noting that the SwissFEL facility is an ideal location for hosting the P^3 experiment, as it can deliver an electron beam energy of up to 6 GeV, matching the maximum drive beam energy required for the FCC-ee positron source. Currently, two beamlines (Aramis and Athos) are operational at SwissFEL, and the

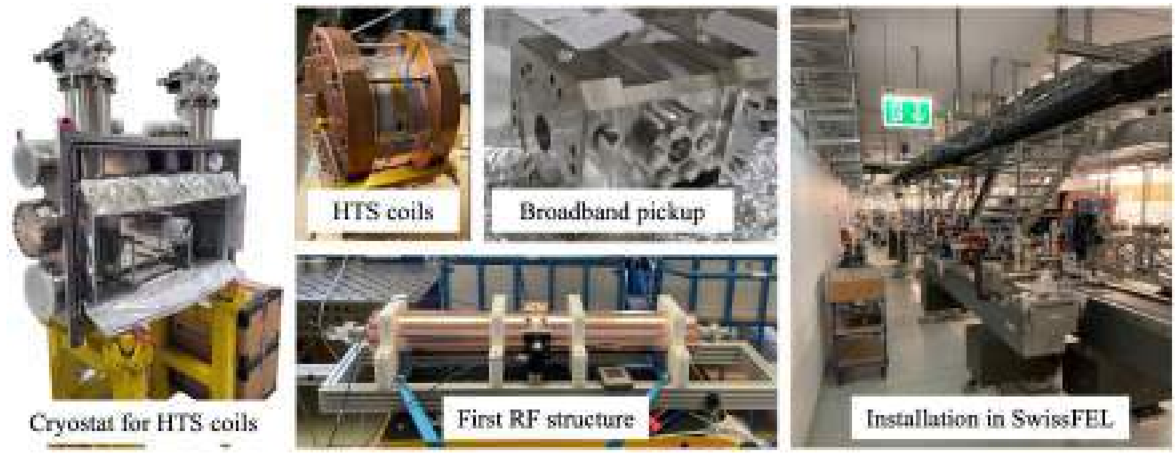

Fig. 7.17 P^3 components production and installation in SwissFEL

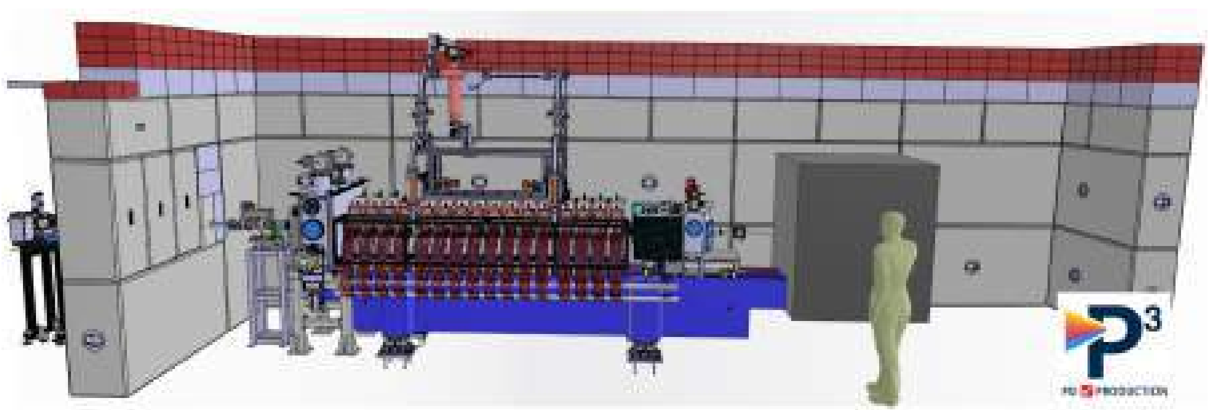

Fig. 7.18 The PSI Positron Production (P^3) Experiment

accelerator tunnel has reserved space for a future third beamline (Porthos). This layout provides sufficient room for the temporary installation of the P^3 experiment and switchyard. Figure 7.18 illustrates the current design of the P^3 experiment in its planned final configuration within the SwissFEL tunnel.

7.5 Damping ring and bunch compressor

The new optimised FCC-ee injector layout imposed a review of the intrinsic structure of damping ring (DR) Transfer Lines (TLs). The presence of two independent linacs for electron and positron beams, and the elimination of the common linac, naturally led to increased DR energy which, to avoid spin resonances, was set at the value of 2.86 GeV.

The main concept driving the DR and TLs design consists of achieving an overall efficiency of the order of 80% in transporting electron and positron beams from the respective linacs, through the DR for emittance cooling, to the end of the TLs conveying extracted beams toward the collider booster. Electron and positron linacs produce beam pulses at 100 Hz, each pulse consists of 4 bunches spaced by 25 nsec, each bunch stores a variable charge intensity up to 5 nC. The DR is mainly needed to reduce the emittance of the incoming positron beam by more than three orders of magnitude, from 2.36×10^{-6} m·rad to about 1.8×10^{-9} m·rad.

However, in the latest injector layout, the DR will also be used for electron beam cooling to cure possible emittance dilution induced by misalignments and space-charge effects. Several options have been studied and evaluated for the DR arcs, such as using multi-bend cells, and FODO cells. One of the options studied is based on a 6-fold symmetry ring, and has multi-bend arc cells. This design is presented as the main option in the following section. An alternative design of the DR has also been studied. A FODO cell is chosen and this alternative DR design, consists of three arcs and three straight sections that locate damping wiggler magnets, the RF cavity and injection/extraction equipment. The ring is about 384 m long, and its energy is 2.86 GeV. The injected beam emittance could be reduced to the required emittance value of 1.76 nm·rad, horizontal damping time is 6.4 ms

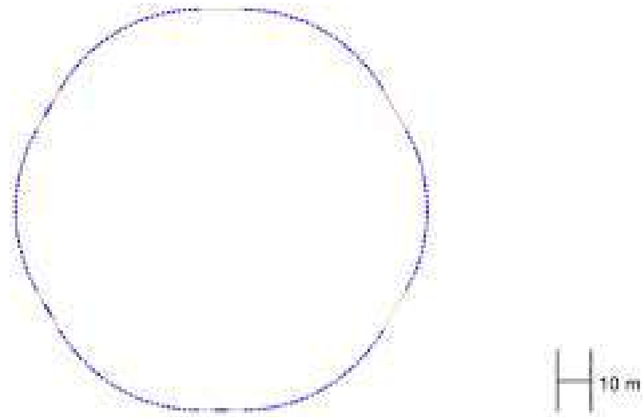

Fig. 7.19 Damping Ring layout. The six-fold symmetry allows having straight sections dedicated for different equipment: RF cavity, injection/extraction septa and kickers and wigglers (to reduce damping time and equilibrium emittance)

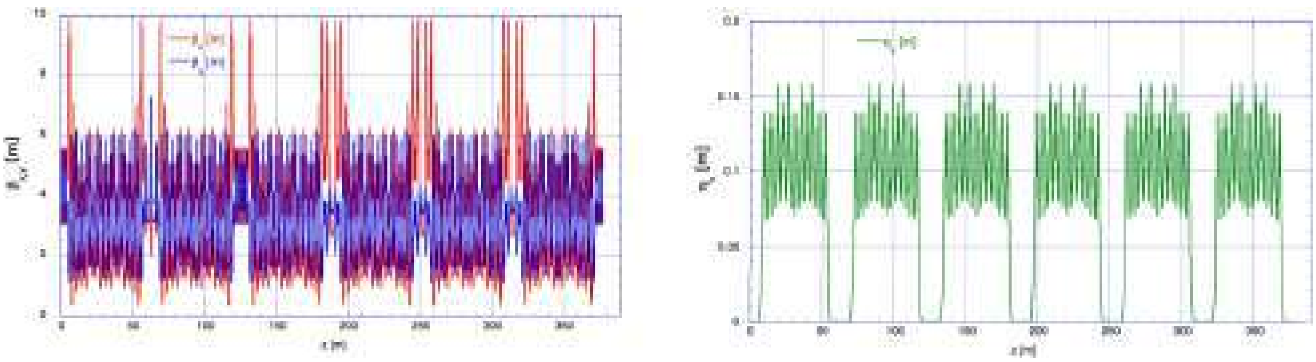

Fig. 7.20 Damping Ring optics: betatron amplitude (left) and dispersion (right)

and the energy loss per turn is 1.13 MeV. The total length of the damping wiggler magnets is about 36.45 m. They have a 2 T magnetic field and are distributed in the three straight sections. It could be possible to lower the magnetic field of the damping wiggler to 1.5 T for optimising the phase advance for minimum emittance (around 135°). However, this may cause even more challenging dynamic aperture optimisation.

7.5.1 New damping ring design

The new DR lattice features a six-fold symmetry, as shown in Fig. 7.19. It consists of six arc cells connected by six straight sessions. Each straight session is used to host three wiggler magnet insertions, one RF cavity module, and two independent injection/extraction sections. Injection and extraction will be implemented in the same branch for the two-particle species in order to avoid changing the polarities of the DR magnets, thus ensuring fast and reliable operation modes for both electron and positron. The injection will be performed using an on-axis scheme.

Arc cells are based on an achromatic multi-bend optics, symmetric with respect to the cell centre. Each half cell provides 30° deflection angle, using 15 bends of five different types. This approach allows keeping the maximum excursion of the horizontal dispersion, optimising damping time, and shaping the H_5 function along the cell to achieve low emittance. A further reduction of the damping time is obtained using three 3.5 m long wiggler magnets, each with a moderate magnetic field intensity of 1.8 T. Straight sections are based on the FODO structure and modified according to their function.

The DR optics is presented in Fig. 7.20, it features moderate betatron oscillation amplitudes achieved with a relatively weak focusing lattice producing low chromaticity per cell and, consequently, wide on- and off-momentum dynamic aperture. Limiting betatron oscillation amplitudes in the transverse planes below a maximum value of the order of 10 m is also beneficial in keeping the ring requirement in terms of stay-clear aperture under control, which is crucial especially for DR operation with positron beam. A complete list of the DR parameters is presented in Table 7.8.

Table 7.8 Damping ring parameters

Parameters	Value
Energy [GeV]	2.86
Circumference [m]	373.46
Arc Cell	multi-bend
Lattice shape	six-fold symmetry
Nat. emittance [nm rad] (WGL on/off)	1.3 / 2.3
Bunch Length [mm]	5.1
Damping time $\tau_{x,y}$ (WGL on/off) [ms]	16.9 / 29.4
Nat. Chromaticity (x/y)	−38.2/-28.3
Nat. energy spread (WGL on/off) [10^{-4}]	7.1 / 5.2
Betatron amplitude max (x/y) [m]	9.66 / 6.49
Betatron amplitude min (x/y) [m]	0.5 / 1.1
Tune (Q_x,Q_y)	27.8707 / 22.3728
Momentum compaction (WGL on/off) [10^{-3}]	1.55 / 1.57
Revolution period [µs]	1.2457
Dipole #, length [m], field [T]	180 , 0.7 1.13, 0.34 0.39
Wiggler #, length [m], field [T]	3, 3.5 , 1.8
Cavity #, length, voltage [MV]	1.5, 4
Max. # Bunch stored, Bunch Curr. [mA]	40 / 4
Store time	5 τ_y
Energy loss per turn (WGL on/off) [keV]	422.2 / 246.7
SR power loss wiggler [kW]	27.83
Kicker rise time [ns]	50

7.5.2 Timing

The maximum number of trains that could be simultaneously stored in the damping ring depends on the revolution period (T_{per}), the train length (Δt) and the kicker pulse rise time (t_K)

$$n_{train} = \frac{T_{per}}{\Delta t + t_K}$$

The storing time (T_{store}) for each train of bunches it is fixed by the requirements imposed from the next steps of the injector chain: the positron vertical emittance must be damped from 2.34 mm·mrad (ϵ^y_{inj}) to 0.18 nm·rad (ϵ^y_{ext});

$$\epsilon_y(t) \sim \epsilon^y_{inj} \mathrm{e}^{-\frac{2t}{\tau_y}}$$

The damping required implies:

$$T_{store} = -\frac{\tau_y}{2} \ln \frac{\epsilon^y_{ext}}{\epsilon^y_{inj}} \simeq 5\tau_y$$

Using the values in Table 7.8 for the revolution period and the linac repetition rate of 100 Hz ($T_{RepRate} = 10$ ms) gives:

$$\tau_y \leq \frac{n_{train} T_{RepRate}}{5} \simeq 20 \text{ ms}$$

with $n_{train} \simeq 10$ that corresponds to $T_{per} \geq$1.25 µs.

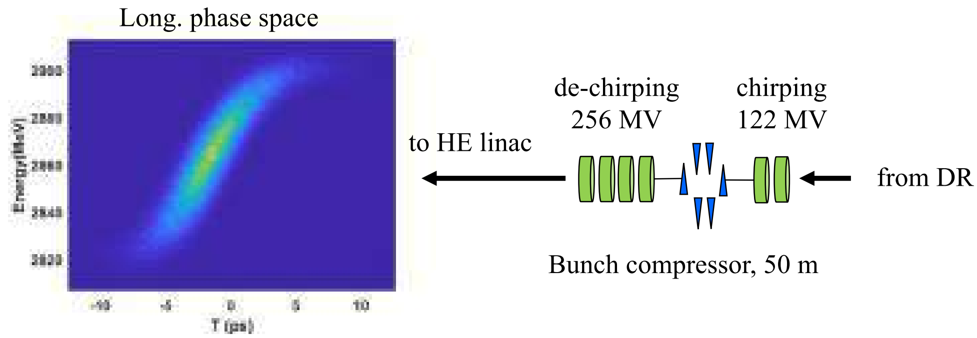

Fig. 7.21 Bunch compressor at 2.86 GeV placed between the DR and the HE-linac. Left: longitudinal phase space after the compression and de-chirping. Right: schematic layout and overall length

7.5.3 Bunch compressor

The bunch compressor is designed to reduce the bunch length of the beam originating from the damping ring, from an initial range of 4–5 mm to a final length of ∼1 mm. Figure 7.21 (right) illustrates the schematic layout of the bunch compressor, which consists of a magnetic chicane formed by four C-shaped bending magnets. Each magnet has a magnetic length of 1.9 m and a maximum magnetic field strength of 1 T. The momentum compaction factor R_{56} is −0.336 m, and the bending angle of each magnet is 11 degrees, resulting in a maximum dispersion of 0.98 m. The distance between dipoles 1 (3) and 2 (4) is 2.9 m, while the separation between dipoles 2 and 3 is 2 m. To induce the necessary energy chirp for compression, two RF structures, providing a maximum accelerating voltage of 122 MV, are employed. Additionally, four RF structures are utilised to partially remove the residual chirp in order to meet the specifications of the high-energy linac (HE-linac). These structures operate with a maximum accelerating voltage of 256 MV. Beam dynamics simulations were performed using the ELEGANT code for a bunch with a maximum charge of 5 nC. Figure 7.21 (left) shows the longitudinal phase space after the compression and de-chirping. The results indicate a residual energy spread of 0.7% after de-chirping, a compression factor of 5.75, and a reduction in the bunch length from 4.6 mm to 0.8 mm. The horizontal emittance growth is approximately 20%, while the vertical emittance growth remains below 1%.

7.6 High energy linac and energy compressor

7.6.1 High energy linac

The high-energy (HE) linac accelerates electron and positron beams from the exit of the chicane downstream of the DR at 2.86 GeV energy up to the transfer line towards the booster ring injection at 20 GeV energy.

Analogous to the e-linac, beam dynamics simulations have been done to study both longitudinal and transverse beam dynamics in the HE-linac. The following beam parameters were used in the simulations: bunch length 1 mm, emittance 1 mm·mrad and 10 mm·mrad in the vertical and horizontal plane, respectively at the start of the HE-linac for a 5 nC electron bunch. The lattice is the same as the electron linac: a FODO lattice with 90° phase advance per cell, one quadrupole, and one BPM per RF structure. The RF structures operate at the peak of the RF electric field (on-crest) to maximise accelerating efficiency and minimise beam quality degradation. The beam tracking simulations described in this document were performed using RF-Track [354].

To evaluate the robustness of the linac design against static misalignments in terms of emittance growth, the same Gaussian-distributed misalignments assumed for the electron linac and reported in Table 7.4 and the BPM resolution of 10 µm were considered.

To mitigate the effects of misalignments, a combination of one-to-one correction and dispersion-free steering (DFS) was applied sequentially, incorporating the randomly distributed errors. In this case, the focus is on the vertical plane, which is much more critical due to the smaller margin between the starting value and the value accepted by the booster. Finally, a maximum emittance growth of 0.6 mm·mrad in the vertical plane was obtained at the end of the linac for 98% or more of the simulation seeds, giving a final emittance of 1.6 mm·mrad below the maximum 2 mm·mrad required at the booster injection. A similar emittance increase is expected in the horizontal plane, which would give a final emittance smaller than 15 mm·mrad, still satisfying the booster requirement (maximum emittance smaller than 20 mm·mrad) in the horizontal plane. These results were achieved by varying the RF structure aperture and optimising the minimum number of sections (resulting in 8 for the HE-linac) in which the linac must be divided to avoid propagating an error in the correction over a long distance. These simulations determined a minimum aperture of the RF structure corresponding to $a/\lambda = 0.12$.

The dynamic effects were investigated using the same approach as the electron linac. The JA was determined by tracking simulations varying the length of the RF structure, impacting the distance among the quadrupoles, the

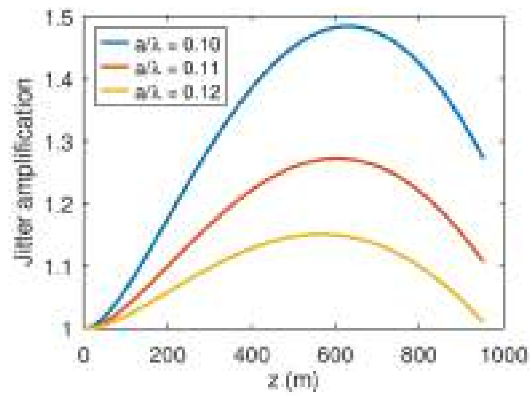

Fig. 7.22 Jitter amplification along the HE-linac for several RF structure apertures. The RF structures are operated on-crest, with a quadrupole spacing of 3.75 m (corresponding to the RF structure length of 3 m)

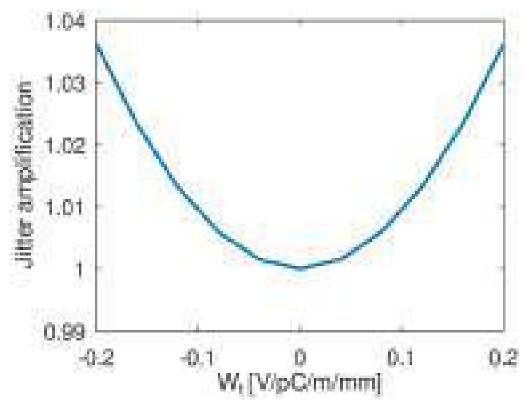

Fig. 7.23 Multi-bunch jitter amplification at the end of the HE-linac

Table 7.9 Summary of the optimised RF and lattice parameters based on the beam dynamics studies

Parameter	Value
Mean RF structure aperture (mm)	13.9 ($a/\lambda = 0.12$)
RF structure length (m)	3
RF structure operating phase	on-crest
Phase advance/cell (degrees)	90
Number of BPM/RF structure	1
Number of quadrupoles/RF structure	1
Distance between the quadrupoles (m)	3.75

phase advance per cell, and the RF structure aperture. Figure 7.22 shows, for example, the JA along the HE-linac assuming a constant RF structure length of 3 m (corresponding to a distance among the quadrupoles of 3.75 m) for several RF structure apertures. In particular, for an RF aperture corresponding to $a/\lambda = 0.12$, a final JA of 1.01 was obtained for 3 m RF structure length. The multi-bunch effects were investigated by imposing a kick from the first to the following bunch, analogous to what was done for the e-linac. The results are shown in Fig. 7.23. The RF structure has been designed to provide a long-range wakefield corresponding to a maximum kick equal to 0.11 V/pC/m/mm for the 5 nC bunch charge. This corresponds to a multi-bunch JA of 1.02.

Single- and multi-bunch JAs give a total JA of 1.03. This allows a very large transverse jitter coming from the upstream sections to be tolerated. The latter is expected to be much smaller than the one at the exit of the gun section, due to the damping in the DR (which is expected to reduce the incoming jitter) and the kickers currently in use (which introduce angle jitter). Table 7.9 summarises the most important lattice and RF structure parameters determined by the beam dynamics simulations. In summary, the RF structure aperture, length, and lattice of the HE-linac fulfil the specifications determined by the transfer line and booster in terms of static and dynamic effects.

Table 7.10 Parameters of the high energy EC assuming the same machine settings for the maximum 5 nC and a minimum 5 pC single-bunch charge. 'Initial' indicates that the parameter is computed at the entrance of the EC chicane and 'final' at the exit of the downstream RF modules. The voltage is 410 MV

Parameter	Q = 5 nC	Q = 5 pC
Initial rms bunch length (mm)	1.00	1.00
Initial single bunch ΔE/E (%)	0.56	0.20
Final rms bunch length (mm)	4.00	1.43
Final single bunch ΔE/E (%)	0.10	0.12

7.6.2 Energy compressor

The Energy Compressor (EC) [363] at the end of the HE-linac is essential to achieve optimal performance along the HE-linac and, at the same time, the beam parameters required by the transfer line and the booster ring. This kind of system, previously utilised in accelerators such as SuperKEK-B to enhance positron capture efficiency in the damping ring (DR), consists of a magnetic chicane followed by RF structures operated at zero-crossing phase. Using the EC presents several advantages:

- Possibility to operate the RF structures of the HE-linac on-crest. This is advantageous for the mitigation of emittance growth and accelerating efficiency.
- It minimises the single-bunch energy spread due to the RF curvature and the longitudinal short-range wakefields.
- It reduces the bunch-to-bunch energy variation due to a very large variation from several nC down to nearly 0 nC bunch charge and associated beam loading effects when using a 'golden' RF pulse during top-up mode operation.
- It reduces the overall bunch-to-bunch energy jitter.
- It manipulates the beam longitudinal phase space to match the booster requirements.

The EC also has some drawbacks:

- It requires more hardware and more space.
- It converts energy jitter and offset to arrival time jitter and offset, which must be within the tolerance of the downstream sections.

While the transfer line and booster requirements can be met without this system, its absence would lead to reduced performance along the HE-linac.

The EC may be utilised exclusively for single-bunch effects, as well as for both single- and multi-bunch effects. In the first case, the R_{56} of the chicane and the integrated voltage of the RF structures are determined by the target bunch length and energy spread, given the incoming chirp. The simulations also incorporate a residual chirp resulting from compression downstream of the DR, estimated at 0.7% for the 5 nC bunch charge. Table 7.10 summarises the results obtained for a maximum and minimum charge of 5 nC and 5 pC, respectively. In this configuration, increasing the integrated voltage can reduce the single-bunch energy spread by a factor of 3 to 4 while maintaining the bunch length. The booster injection does not currently require this, but it is stressed that the system can, in principle, provide it.

Although bunch-to-bunch beam loading compensation can be managed through a low-level RF (LLRF) system, this system must have the capability to modify the RF phase and/or amplitude for each of the infinite combinations of bunch charges in the timescale of the bunch separation (presently 25 ns) for four bunches accelerated during the same RF pulse. Ongoing studies are therefore investigating whether the EC fulfils this task by leveraging a single constant golden pulse optimised by the LLRF, which remains the same for all the possible charge combinations. In this context, the bunch length was identified as a third degree of freedom to fine-tune the single-bunch properties. The bunch length selected is 0.8 mm rms instead of the 1 mm assumed so far. This modification is not detrimental to the other aspects of the design, since a shorter bunch would even be advantageous for static and dynamic effects at the price of a slightly increased single-bunch energy spread of 0.05% at the EC entrance.

Like the previous case, the simulations incorporate the residual chirp resulting from compression downstream of the DR, estimated to be 0.7% for all bunches, and the beam loading effect as a function of the bunch charge calculated assuming the golden pulse discussed in this document, see Fig. 7.30. The optimal R_{56} of the chicane is about 0.55 m and the voltage of the downstream RF structures is equal to 620 MV. This corresponds to a total EC length of less than 90 m including matching sections upstream and downstream of the chicane, the chicane itself, made of normal conducting dipoles, and three RF modules. Table 7.11 summarises the results for the maximum single-bunch charge of 5 nC. The results of the low-charge scenario simulations without modifying

Table 7.11 Parameters of the EC for the maximum 5 nC bunch charge, assuming a target single-bunch energy spread of approximately 0.1%. B_j corresponds to j^{th} bunch along the train. The extra time delay is computed by subtracting an increasing integer number of RF structures periods. The voltage is 620 MV

	B_1	B_2	B_3	B_4
Initial rms bunch length (ps)	0.80	0.80	0.80	0.80
Initial single bunch ΔE/E (%)	0.61	0.61	0.61	0.61
Initial offset centroid ΔE/E from B_1 (%)	0	−0.31	−0.59	−0.93
Final rms bunch length (mm)	4.06	4.07	4.09	4.10
Final single bunch ΔE/E (%)	0.11	0.11	0.10	0.09
Final offset centroid ΔE/E from B_1 (%)	0	−0.01	−0.03	−0.05
Final centroid Δt from B_1 (ps)	0	5.7	11.0	17.3

Table 7.12 Parameters of the EC for a 5 pC bunch charge, assuming the machine parameters optimised for the 5 nC bunch charge (RF structures phasing and strength of the dipoles set using the 5 nC bunch as a reference). The relative energy spread, energy offset, and extra time delay are computed with respect to the B_1 of the 5 nC bunch charge

	B_1	B_2	B_3	B_4
Initial rms bunch length (ps)	0.80	0.80	0.80	0.80
Initial single bunch ΔE/E (%)	0.14	0.14	0.14	0.14
Initial offset centroid ΔE/E from B_1 at 5 nC (%)	1.62	1.97	2.30	2.54
Final rms bunch length (mm)	1.04	1.04	1.03	1.03
Final single bunch ΔE/E (%)	0.13	0.13	0.12	0.12
Final offset centroid ΔE/E reference B_1 at 5 nC (%)	0.14	0.21	0.29	0.36
Final centroid Δt from B_1 at 5 nC (ps)	−29.0	−35.2	−41.0	−44.9

Table 7.13 Spread of the beam parameters at the EC exit for the different charges (assuming the same bunch charge along the four bunches), and considering the maximum single-bunch variation from 5 nC down to 5 pC. The peak-to-peak values are taken for the B_4, which are the maxima

	Initial	Final
Single-bunch rms energy spread @ 5 nC (%)	0.61	0.103±0.009
Single-bunch rms bunch length @ 5 nC (ps)	0.80	4.08±0.02
Single-bunch rms energy spread @ 5 pC (%)	0.14	0.125±0.006
Single-bunch rms bunch length @ 5 pC (ps)	0.80	1.035±0.006
Peak-to-peak centroid energy offset variation from 0-5 nC (%)	±1.74	±0.21
Peak-to-peak centroid Δt variation from 0-5 nC Δt (ps)	0	±31

any machine parameters optimised for the high-charge case are shown in Table 7.12. The shorter single-bunch length compared to the higher charge mode appears to be acceptable for the booster, as lower charges are less susceptible to instabilities.

In conclusion, the EC enables the operation of the HE-linac at settings optimised for beam dynamics and RF structures while ensuring that the target parameters for the downstream lines are matched at its output. The energy jitter and offset caused by substantial bunch charge variations ranging from a few nC to nearly zero are converted into time delays and jitter, which are better tolerated by the transfer line and the booster ring compared to energy variations. Table 7.13 summarises the expected range of parameter variation for the final bunch. Some minor effects, like the variation of the bunch length and the residual chirp from the bunch compressor before HE-linac for the 5 pC charge, are presently neglected. Others are overestimated, such as the single-bunch beam loading, which is included in both the golden pulse calculation (solely the fundamental mode) and the tracking code. Even with these assumptions, the HE-linac and EC design fulfil the requirements of the downstream sections. Further studies are underway to fine-tune the results.

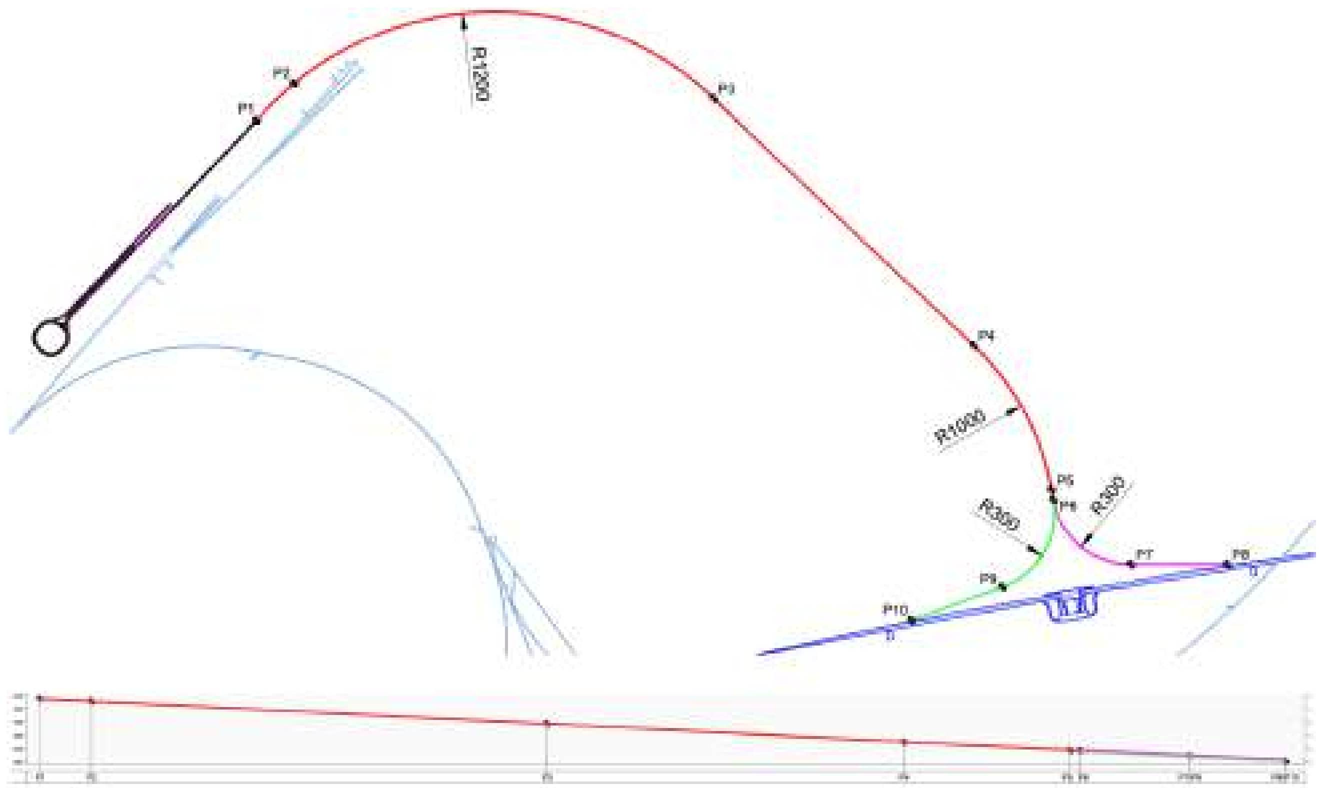

Fig. 7.24 Lepton transfer lines from the injector complex on the surface to the collider tunnel

7.7 Transfer lines from HE-linac to booster

7.7.1 Transfer line geometry

The transfer line geometry has undergone significant changes between MTR and this report. The transfer lines at the MTR stage passed close to the SPS to allow synergy with hadron transfer lines for FCC-hh and for the physics programme in the SPS. The design suggested here provides a direct connection from the output of the HE-linac on the surface at the CERN Prévessin site, see P1 in Fig. 7.24 to the two extremities of the collider tunnel straight section of PA, see P8 and P10, respectively. This design is driven mainly by civil engineering constraints related to scheduling and shaft availability. It also features a symmetric line design for electrons and positrons, ensuring that the beam dynamics impact of synchrotron radiation in the final bending sections is equal for both species. The location of the injector complex allows a very efficient connection between HE-linac and the CERN North Area (NA); see beamlines close to P2 in Fig. 7.24. It remains to be discussed if a beam transfer in the reverse direction from the booster back to, e.g., the NA or a direct line from the HE-linac to the SPS is required and to design the transfer lines accordingly.

7.7.2 Cell design and beam dynamics

As shown in Fig. 7.24, the high-energy linac to booster transport has been designed with a constant negative vertical slope of $-3°$ in the CERN Coordinate System (CSS), combined with horizontal bending in sectors P2-P3, P4-P5, P7-P8 and P9-P10. The slope will be applied and removed at the first and last cells of the line, respectively. To maintain it along the line, the local bending plane must be progressively tilted following the expressions described in Ref. [364]. Figure 7.25 confirms that such a procedure yields the correct beam trajectory. This *twisting reference frame* will introduce a coupling between horizontal and vertical motion. Skew quadrupoles may be needed to control such a coupling, although they have not been included in this initial iteration.

Additionally, the beam transport from the high-energy linac to the booster must be designed to stay within the 'beam quality' budget specified in Table 7.14, which will drive the lattice design choices.

FODO cells have been chosen to design the transfer line due to their simplicity. Later iterations may explore other types of cells, which explicitly aim to minimise the impact of synchrotron radiation (such as theoretical-minimum-emittance cells). The chosen phase advance is 135° as it is close to the optimum for minimising emittance

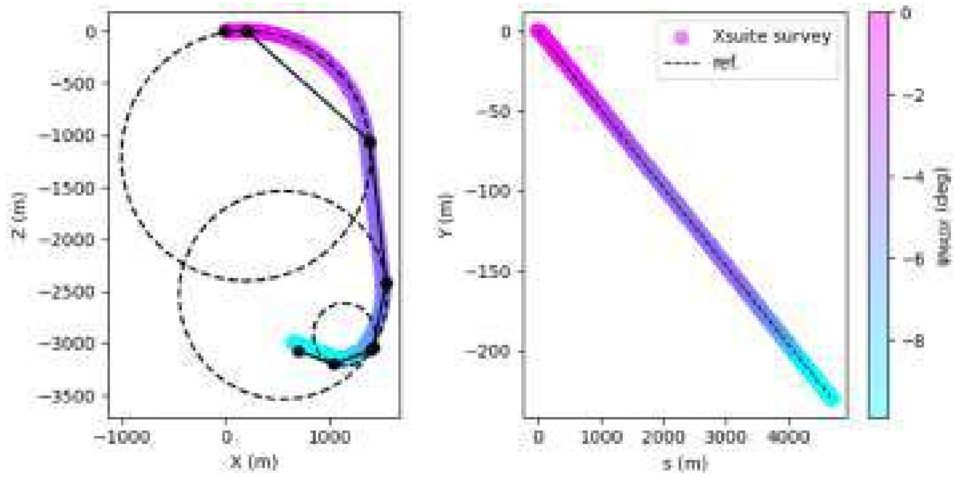

Fig. 7.25 XSUITE survey output and reference trajectory provided by Civil Engineering. The colour bar shows the local roll angle ψ_{MADX}, which is necessary to maintain a constant vertical slope in the global frame

Table 7.14 Summary of Sector Parameters

Sector	Bunch len. (mm)	RMS dp/p (10^{-3})	$\epsilon_{x,N}$ (µm)	$\epsilon_{y,N}$ (µm)
(...)				
HE Linac	1	7.5	16	1.6
E. Compressor	4	1.0	16	1.6
Transfer	TBD	TBD	TBD	TBD
Booster Inj.	4	1	20	2
(...)				

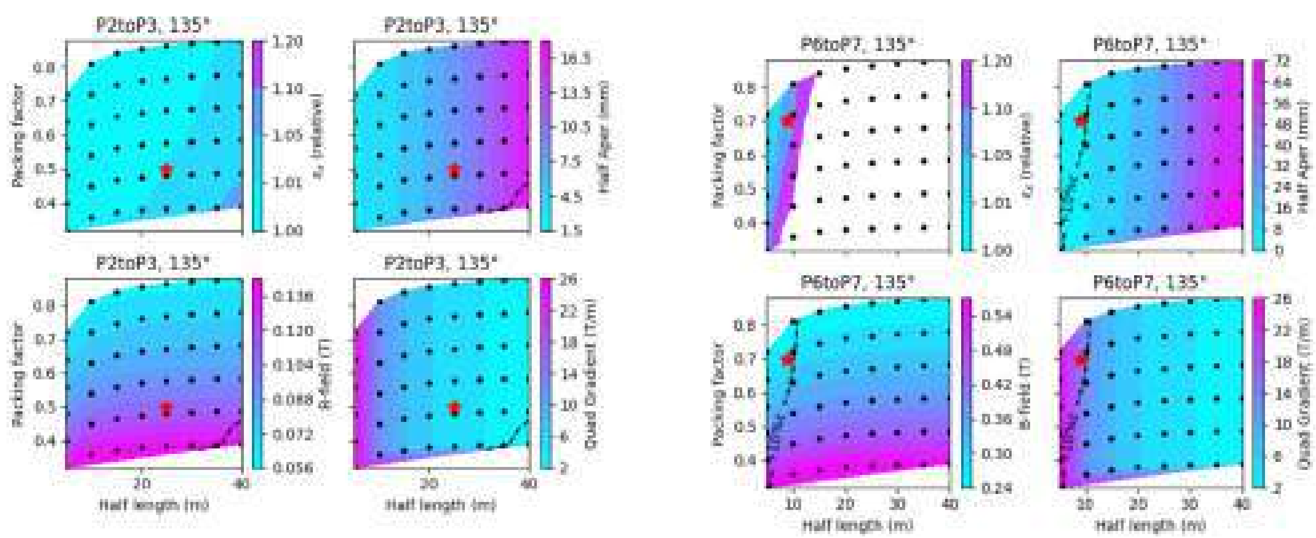

Fig. 7.26 Horizontal emittance blow-up, bending field, quadrupole gradient and aperture as a function of cell half length and dipole fill factor

blow-up [365], while remaining an easy number to work with when designing orthogonal correction schemes. Figure 7.26 shows the horizontal emittance blow-up as a function of the cell length and the dipole fill factor for the sectors P2-to-P3[9] and P6-to-P7 (or equivalently P9-to-P10). The required quadrupole gradients, bending fields

[9]P4-to-P5 has very similar behaviour to P2-to-P3.

Table 7.15 FODO cell parameters

Attribute	Long FODO (P1-to-P6)	Short FODO (P6-to-P8/P10)
Cell length (m)	50	18
Dipole fill factor	0.5	0.67
Dipole field (mT)	130	330
Dipole length (m)	6	6
Dipoles per half cell	2	1
Quadrupole length (m)	1	1
Quadrupole gradient (T/m)	5	14
Cell phase advance (deg)	135	135

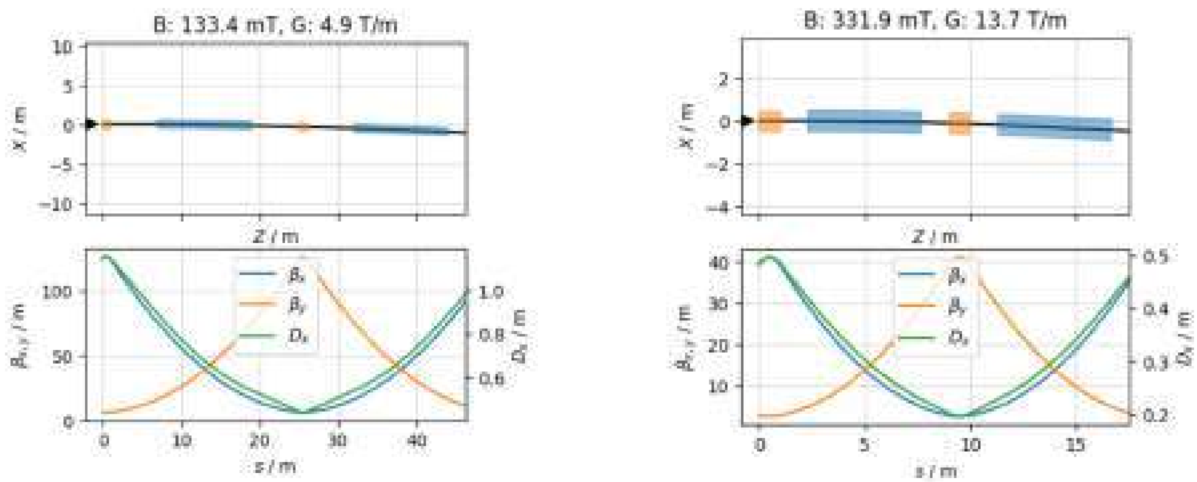

Fig. 7.27 Magnet layout and optics for long and short FODOs (quads in orange and dipoles in blue). Only horizontal dispersion is shown, but a similar vertical dispersion is expected for the cells where the −3 deg, the vertical slope is applied

and apertures are also shown. The aperture required has been calculated with the formula:

$$A_{x,y} = n_\sigma * \sqrt{\beta_{x,y} * \frac{\epsilon_{norm,x,y}}{\gamma}} + D_{x,y} * (2 * \frac{\delta_p}{p} + \delta_{jitter}) + traj * \sqrt{\frac{\beta_{x,y}}{\beta_{max}}} + align \tag{7.1}$$

where $n_\sigma = 6$, $\epsilon_{norm,x/y} = 20/2$ µm, the 1σ momentum spread $\frac{\delta_p}{p}$ is 0.1% ($\pm 2\sigma$ taken into account and dispersion contribution conservatively added linearly). The trajectory variation is assumed to be ±2 mm at the locations of maximum betatron functions, the momentum jitter δ_{jitter} is assumed to be a maximum of ±0.3%, and there are ±2 mm taken into account for alignment errors.

Based on the parametric scans above, two cells have been chosen to build the line: a long FODO for the shared part of the transport (P1-to-P6) and a short FODO for the separate parts of the transport (P6-to-P8, P6-to-P10). The latter is required due to the tight bending radius of $R = 300$ m, which leads to significant synchrotron radiation. Table 7.15 lists the parameters for each FODO cell. The 135° phase advance is close to the optimum for minimising emittance blow-up [365], while remaining an easy number to work with when designing orthogonal correction schemes.

The schematics and optics functions for both cell configurations are shown in Fig. 7.27. The number of magnets required has been documented in Ref. [366]. For the beginning and end of the line, the bending magnets will bend vertically to introduce (and then remove) the −3° slope present along the entire line descending from the HE-linac to the collider tunnel. In those cells, the dispersion will be vertical but similar in amplitude and shape to the one shown in Fig. 7.27. Under such a configuration, tracking simulations show that both the dp/p blow-up and the bunch length increase remain under 5%. However, further investigations might be needed when including matching sections and errors, which have not been considered in this report.

Table 7.16 Summary of magnet specifications, assuming polarity switching and the FODO parameters from Table 7.15. For ease of manufacturing and costing, the 6 m dipoles have been split into 1 m segments. The number of dipoles quoted refers to the number of 1 m segments

	Unit	Quadrupoles	Dipoles	Correctors
Total number		338	286x6 = 1716	224
# magnets in common line		162	192x6 = 1152	108
Length	m	1	1	tbd
Aperture (diameter)	mm	30	30	30
Gradient	T/m	5-15	-	-
Field	mT	-	150-400	tbd
Deflection	µrad			O(10)
Field homogeneity		$O(10^{-3})$	$O(10^{-3})$	tbd
Polarity switching time	s	O(1)	O(1)	

7.7.3 Magnet technology and technical infrastructure needs

The magnet system of the transfer lines is specified in Table 7.16. The constant transfer energy of 20 GeV opens the door to permanent magnet technology, thus both technologies, electro- and permanent magnets were studied and documented in Ref. [367]. It can be concluded that both magnet technologies are technically feasible. The installation and running cost for the permanent magnet option is well below the electromagnet option. The technical infrastructure needs are also much reduced, however the transfer lines as a whole, contribute less than 10% of the injector complex power requirements. The total power requirements of the transfer lines amount to about 2 MW, compared to about 25 MW for the full injector complex. The permanent magnet option would require about a factor 10 less power for e.g., corrector magnets and ventilation. Operational flexibility is the main aspect to consider when choosing between magnet technologies. If the are beam stability issues in the booster, a transfer energy increase can be beneficial. On the other hand, if the booster could accept a lower energy beam at injection, reducing the transfer energy reduces the power consumption of the whole injector complex which is driven by the HE-linac. The main field of permanent magnets can be tuned by about ±20% by increasing or decreasing a leakage field via mechanical shunts. The shunt modification and subsequent magnetic field measurement require several weeks. Another argument for operational flexibility is the duty cycle of the injector complex, which varies between 5 and 75% depending on the operation mode. In particular, in the low-duty modes, the injector beam can be used for experiments beyond FCC physics and shot-to-shot variability of beam parameters, including the transfer energy, open the door to a very diverse physics programme as discussed in Ref. [368]. At this stage, electromagnets have been chosen as the baseline technology due to the higher operational flexibility for the FCC and any science programme beyond the FCC.

7.8 RF system for linacs

7.8.1 RF accelerating structure

The RF design of the accelerating structures FCC injector complex is optimised to deliver efficient beam acceleration in all 3 linacs: the electron (e-)linac, the positron (p-)linac and the high-energy (HE)-linac. While each linac has some unique operational parameters, they share several common design features: all have a RF structure of total length of 3 m, are configured to accelerate 4 bunches with a separation of 25 ns, and operate with a repetition rate of 100 Hz. The HE- and e-linacs are designed to operate at a frequency of 2.8 GHz, with a bunch charge of 5 nC, while the p-linac operates at a lower frequency of 2 GHz to accommodate its higher bunch charge of 15 nC. This difference reflects the tailored optimisation of each linac to the specific beam dynamics requirements described above. The RF structures have tapered geometries, which effectively balance beam transport with short- and long-range wakefield suppression requirements, $W_t < 0.1$ V/pC/mm/m and a value specific to each linac of $< a > /\lambda$. The detailed parameters and design specifications for all three linacs are summarised in Table 7.17. Similar design principles are applied to all 3 linacs, providing a uniform and scalable approach across all structures. The RF design of the HE-linac, is described as an example, in detail below.

The parametric sweep of iris aperture and thickness was utilised to identify structures that satisfy the long-range transverse wakefield constraint $W_t < 0.1$ V/pC/mm/m for a given $< a > /\lambda = 0.12$ related to the short-range wakefields, ensuring stable beam propagation. The long-range transverse wakefields were calculated using a lookup table, which employs frequency-domain parameters of the 20 lowest higher-order modes (HOMs).

Table 7.17 Accelerating structure parameters for e-, p- and HE-linacs

	e-linac	p-linac	HE-linac	Unit
Frequency	2.8	2	2.8	GHz
Length	3	3	3	m
Average aperture	0.15λ	0.2λ	0.12λ	
Cell aperture: first/last	17.13/14.99	30/30	14.85/10.85	mm
Iris thickness: first/last	10.4/13.7	14.3/20.0	2.84/4.04	mm
V_g/c: first/last	3.14/1.38	2.58/1.92	3.92/1.25	%
r/Q: first/last	3.28/3.67	1.49/1.52	3.63/4.38	kΩ/m
Q: first/last	14,599/13,668	20,977/19,102	16,571/16,039	
Filling time	486	447	460	ns
SLED coupling	15	17	15	
$R_{\text{sh, eff}}$ (4 bunches)	81.69	36	95.65	MΩ/m
Repetition rate	100	100	100	Hz
Klystron power per structure	14.2	14.2	14.2	MW
Average power per structure	3.76	3.68	3.72	kW
Bunch charge	5	15	5	nC
Average loaded gradient (4 bunches)	19.50	13.31	21.06	MV/m
$E_{s,\max}$ (instant.)	77	55	73	MV/m
$S_{c,\max}$ (instant.)	453	298	501	mW/mm^2

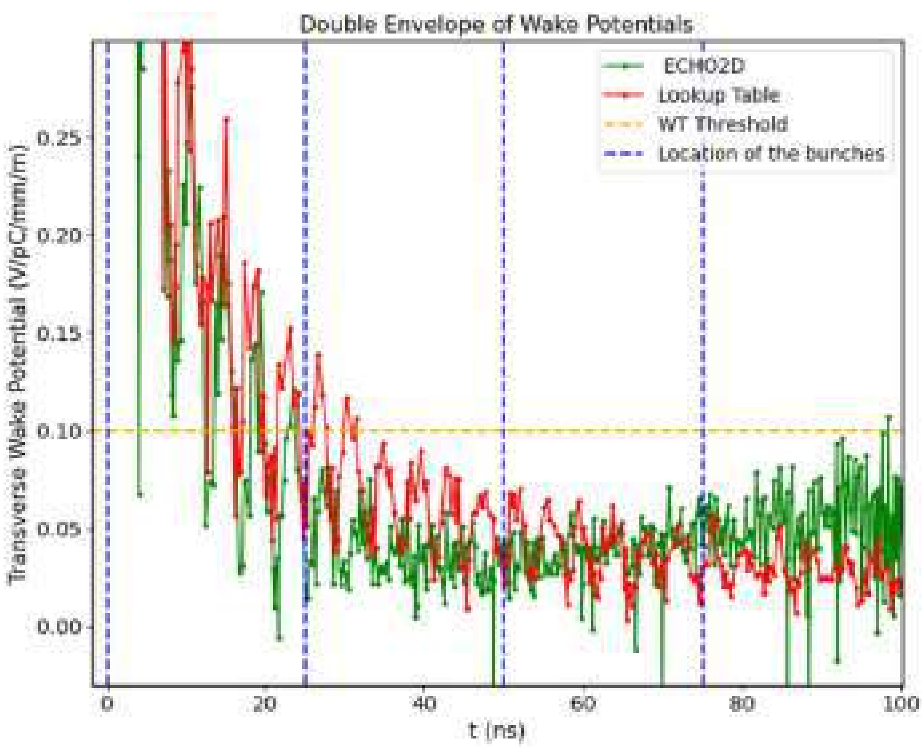

Fig. 7.28 Envelope-of-the-envelope of transverse wakefield potentials for the HE-linac structure, calculated over time using both the lookup table and ECHO2D methods

To achieve more realistic and accurate wakefield predictions and to benchmark the lookup table calculations, the ECHO2D time-domain solver was used for the structure of the final choice. This approach is more accurate, accounting for an infinite number of HOMs and the coupling between cells. The envelope-of-the-envelope approach was applied to the wakefield data from both ECHO2D and the lookup table to rigorously assess worst-case scenarios and long-range wakefield effects. The results are shown in Fig. 7.28.

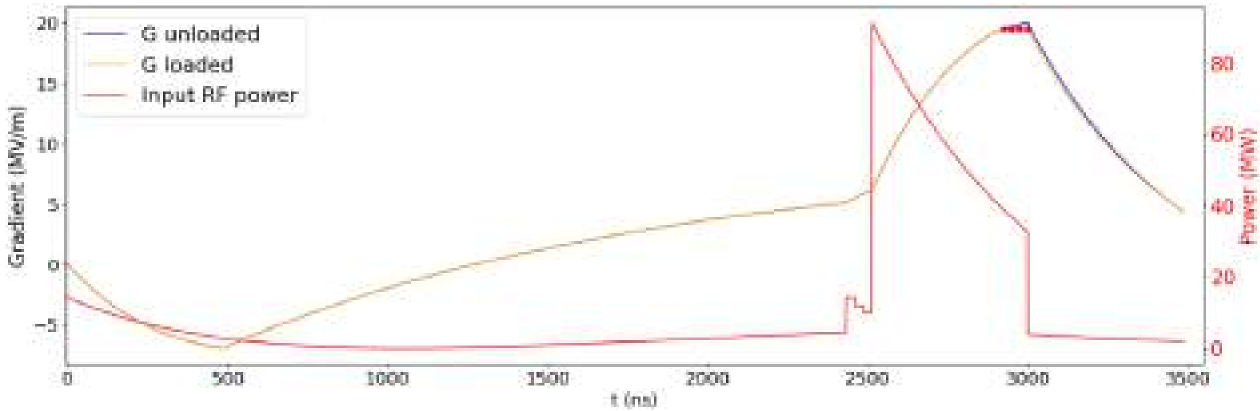

Fig. 7.29 Input RF power and average gradients versus time

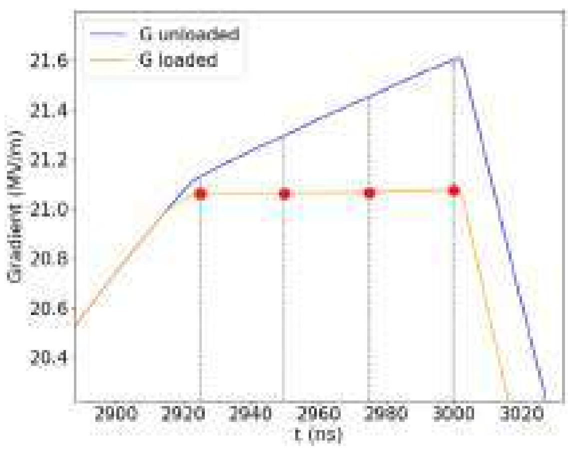

(a) Nominal charge condition.

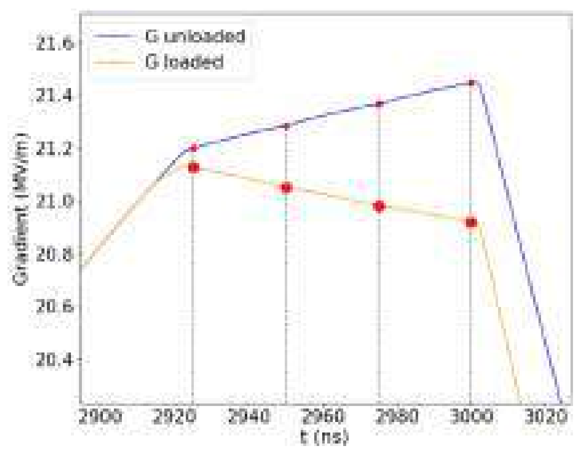

(b) Top-up operation.

Fig. 7.30 Bunch-to-bunch energy minimisation for the nominal bunch charge (a) and top-up operation (b)

In the design of travelling wave accelerating structures, minimising bunch-to-bunch energy spread is a critical objective for ensuring high beam quality and stable accelerator performance. During collider filling with nominal bunch charge, the input RF power pulse shape is optimised to minimise bunch-to-bunch energy spread, taking into account the beam loading effect. As shown in the red trace in Fig. 7.29, the input RF power is modulated using a step-like amplitude modulation. This approach ensures a constant average loaded gradient for all four bunches. The gradients for unloaded and loaded conditions are represented by the blue and orange traces, respectively. The four red dots indicate the temporal positions of the bunches. In Fig. 7.30(a), the unloaded and loaded gradients are shown in more detail for comparison near the position of the 4 bunches, showing a maximum energy difference of 2.4% between unloaded and loaded gradients on the fourth bunch, highlighting the beam loading effect in HE-linac. However, in top-up operation, where bunch charges vary from 0 to 100% among the four bunches, a single optimal input RF pulse must accommodate both extremes. The 'golden pulse' is introduced to address this by averaging the optimised RF pulses for unloaded and loaded voltages. While it does not individually minimise energy variation to ∼0-level, it provides a balanced compromise, reducing energy spread across all possible charge variations. Figure 7.30(b) demonstrates the golden pulse in top-up operation, reducing energy spread to +1.1% and −1.1% for unloaded (4 bunches at 0 bunch charge, small red dots) and loaded cases (4 bunches at nominal intensity of 5 nC, large red dots), respectively. This result underscores the golden pulse's ability to balance energy spread across bunches, ensuring stable performance even under varying charge conditions in top-up mode.

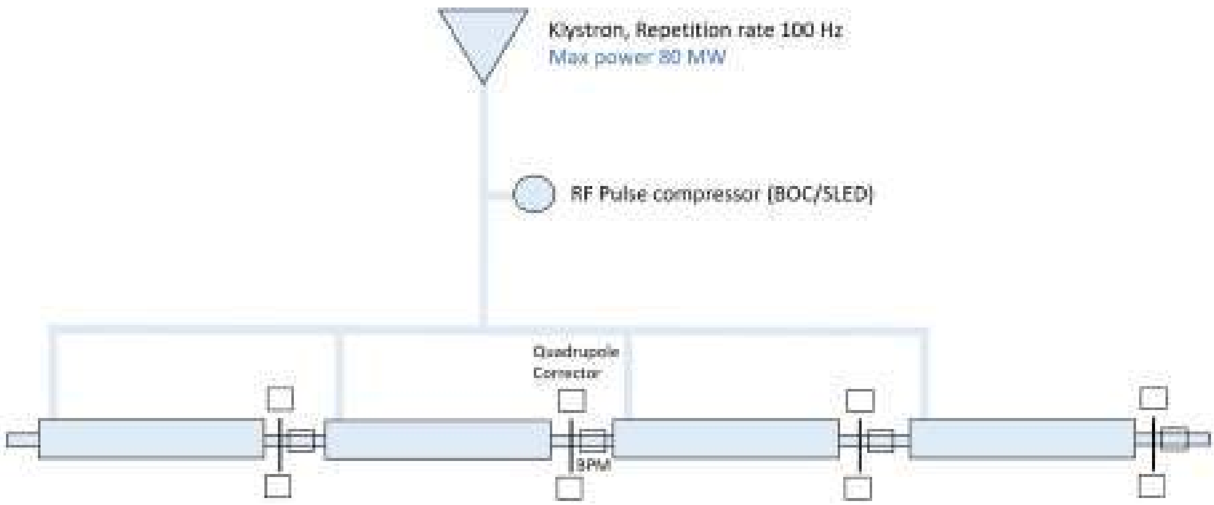

Fig. 7.31 Schematic layout of an RF module for the electron, S2 positron and high-energy linacs

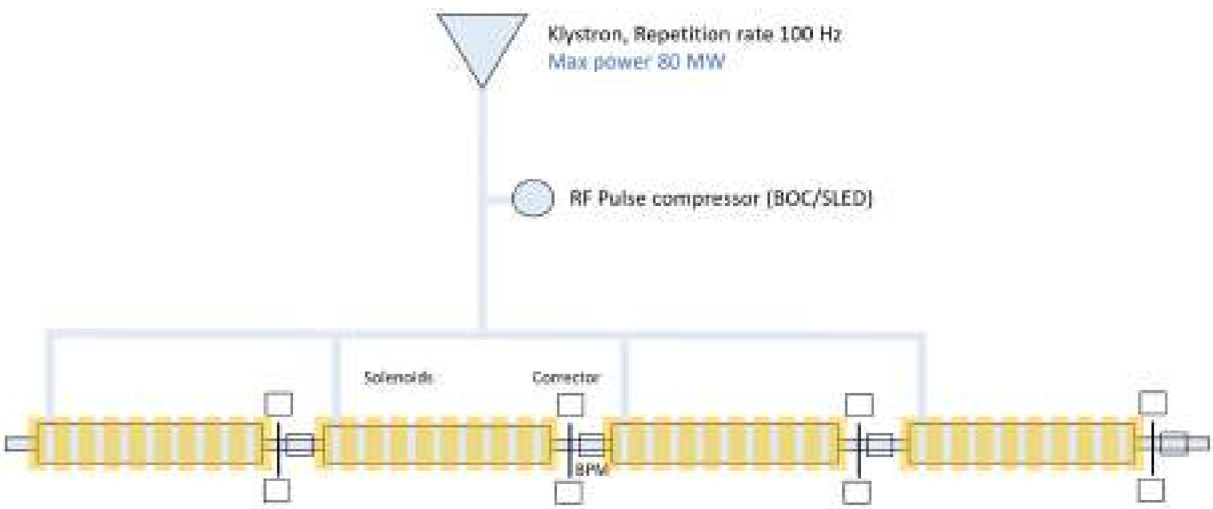

Fig. 7.32 Schematic layout of the RF module for the positron capture and S1 linacs

7.8.2 RF module and RF power

Each RF module of the electron and high-energy linacs consists of one high voltage modulator (HV), one klystron operating at 2806 MHz, one pulse compressor (Barrel-Open Cavity or SLED type) and four accelerating structures with one quadrupole, one corrector magnet and one BPM between each structure. Its total length is 15 m. The choice of an RF module consisting of four structures results from cost and power consumption optimisation. Figure 7.31 shows the schematic layout of such an RF module.

The positron linac has two types of RF modules. The first type equips the end part of the capture linac and the S1 linac. It is about 13 m long, since instead of 4 quadrupoles, it has 40 solenoids, i.e., 10 solenoids per structure for beam focusing. A schematic layout of this type of module is shown in Fig. 7.32. The second type of RF module in the p-linac is similar to the electron and high-energy linac module (see Fig. 7.31). The klystron operates at 2004 MHz in the p-linac.

For the electron and the high-energy linacs, the peak power specification of each klystron is 80 MW. Its repetition rate and RF pulse length are 100 Hz and 3 µs, respectively. For the positron linac, the power specification of the klystron and its repetition rate are also 80 MW and 100 Hz, respectively, but its RF pulse length is 5 µs. Although no klystron exists at the specific frequencies of 2806 MHz and 2004 MHz, many klystrons have demonstrated reliable performance at 2856 MHz with such a power specification and RF pulse length. The development of a conventional klystron at 2806 MHz with a 100 Hz repetition rate is straightforward by retuning its cavities and

Table 7.18 Klystron parameters

Linac	Freq. [MHz]	Peak power specification [MW]	Rep. rate [Hz]	RF pulse length [μs]	Duty factor [10^{-3}]	Average power [kW]	Number required
e-Linac	2806	80	100	3	0.3	24	15
p-Linac	2004	80	100	5	0.5	40	21
HE-Linac	2806	80	100	3	0.3	24	72

Table 7.19 RF module summary table for the injector linacs

	e-Linac	p-Linac	HE-Linac	Unit
RF frequency	2.8	2.0	2.8	GHz
Repetition rate	100	100	100	Hz
Modulator max. peak power	190	190	190	MW
Modulator max. average power	114	152	114	kW
Klystron max. RF power	80	80	80	MW
Klystron RF pulse length	3	5	3	μs
Structures per klystron	4	4	4	
Klystron power per structure	14.2	15.4	14.2	MW
Average loaded gradient	19.5	13.3	21.1	MV/m
Number of rf modules	1 + 14	1 + 6 + 14	72	
Module Length	15	13, 14.8	15	m
Length of all modules	215	304	1080	m

Table 7.20 Comparison of the plug power consumption for the injector linacs assuming 42% or 70% klystron efficiencies

Linac Klystron efficiency [%]	Plug power [MW]	
	42	70
e-Linac	2	1.2
p-Linac	8	6.5
HE-Linac	9.5	6

redesigning its collector. As for the design of a 2004 MHz klystron with such specifications, it would be a completely new development but presents no technical challenges. Several companies have indeed been contacted to assess the feasibility of such conventional klystrons and confirmed that such specifications are achievable. The RF efficiency of such klystrons would be 42%. Their parameters are summarised in Table 7.18.

Both types of klystron operate at 80% of their peak power specification, i.e., at 64 MW. For the electron and high-energy linacs, it is assumed that the RF waveguide system comprises S-band WR284 waveguides and is 25 m long. Taking into account the waveguide losses, the klystron power per structure is then 14.2 MW before pulse compression. For the positron linac, the RF waveguide system comprises the less lossy L-band WR510 waveguides. With a 25 m long waveguide system, the klystron power per structure is 15.4 MW before pulse compression. The specifications of each RF module for all linacs are summarised in Table 7.19.

In recent years, research and development have been conducted on pulsed high-efficiency klystrons, and it is conceivable that more of these klystrons will be available in the near future. A comparison of the plug power consumption for all linacs assuming 42% and 70% klystron efficiencies is shown in Table 7.20. The advantage of operating with high-efficiency klystrons is remarkable for the electron and high-energy linacs but less so for the positron linac since the power consumption of the structure solenoids in the capture and S1 linacs is a substantial fraction of the positron linac total power consumption.

7.9 Availability

This section details results from the enhanced Monte Carlo simulation environment for FCC-ee availability described in Sect. 2.4, focusing on systems specific to the injector complex.

7.9.1 Contributing systems

For availability modelling, the injector chain is divided into two top-level accelerators. The statistical failure rate and blocking duration from subsystems in each accelerator are taken from two representative machines with similar performance characteristics. These are simulated in the injector complex of the FCC-ee to gauge the effect of equivalent availability on global physics performance.

1. **Lower Energy Injectors:** The electron and positron source, linac and damping ring up to an energy 2.86 GeV are modelled from fault data from the SuperKEK-B e^-/e^+ source, injector linac and damping ring between 1998-2023, detailed in Ref. [369].
2. **High Energy (HE) Linac:** with an energy up to 20 GeV is modelled using fault data from the Linac Coherent Light Source (LCLS) at SLAC [370].

Subsystems within each accelerator have been re-categorised for illustration to preserve naming conventions in the CERN complex. These include the relevant supporting technical infrastructure for each accelerator. Only faults leading to downtime in each accelerator were considered, thereby assuming a similar degree of redundancy in the FCC-ee as exists in practice for each representative subsystem.

7.9.2 Inherent resilience to shorter fault types

In the event of an outage in the booster and injector complex, stable beams can be maintained in the main collider rings for a lifetime of 10-15 minutes, depending on energy mode (see Table 2.2). If top-up injection can be restored in this time, normal physics can resume. This significantly reduces the FCC-ee's sensitivity to short-duration fault types in the injector complex and leads to an inherent advantage in availability. The contribution for lost luminosity of subsystems in the injector complex is therefore biased towards those with longer-duration fault types.

7.9.3 Results

The overall contribution to downtime of each accelerator in the injector complex is compared with the booster systems in Fig. 5.14. The lost luminosity contributions in the Z mode from the low energy injectors and HE linac are significant, second only to the booster RF system. The availability of the injector complex will be a challenge for overall FCC-ee performance.

Lower energy injectors The contribution to unavailability and lost luminosity from each subsystem in the low energy injectors is shown in Fig. 7.33. These only contribute to downtime, as the relevant systems have high redundancy, meaning that faults generally block the beam for only short durations. The majority of faults are due to RF breakdowns, which contribute significantly to lost luminosity in Z and W modes, given the lengthy turnaround time required to recover from dumps.

High energy (HE) linac The contribution to unavailability and lost luminosity from systems in the HE linac are shown in Fig. 7.34. RF breakdowns are again the most problematic, representing contributions from S-band klystrons, high-power sub-boosters, waveguides and modulators. The control system is also a high contributor, composed of micros and CAMAC crates as well as the MCC/VMS computing and timing systems. The access system is represented by the Personnel Protection System (PPS). Contribution from the gun laser system is also significant.

7.9.4 R&D opportunities

Opportunities exist for exploiting the injector complex's natural resilience to shorter fault types. If a failed component can be brought back online before the beams in the main collider expire, a lengthy turnaround time may be avoided. This mirrors the opportunities already discussed for the booster in Sect. 5.3.4.

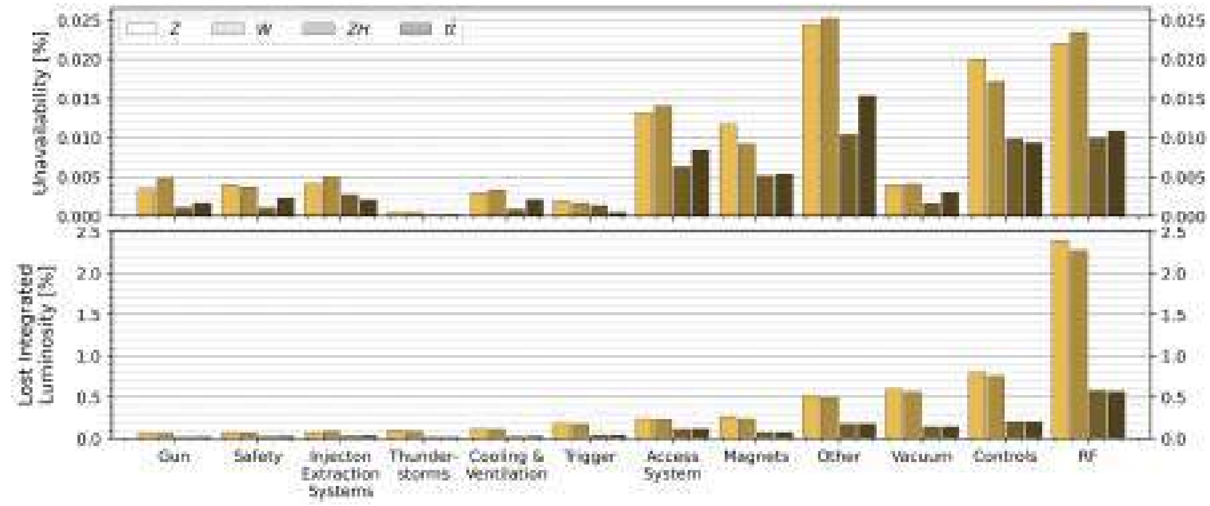

Fig. 7.33 FCC-ee unavailability and lost luminosity contribution of the low energy injectors (up to 6 GeV) determined by applying fault statistics from equivalent equipment at SuperKEK-B [369]. Systems are ordered according to Z mode lost luminosity contribution

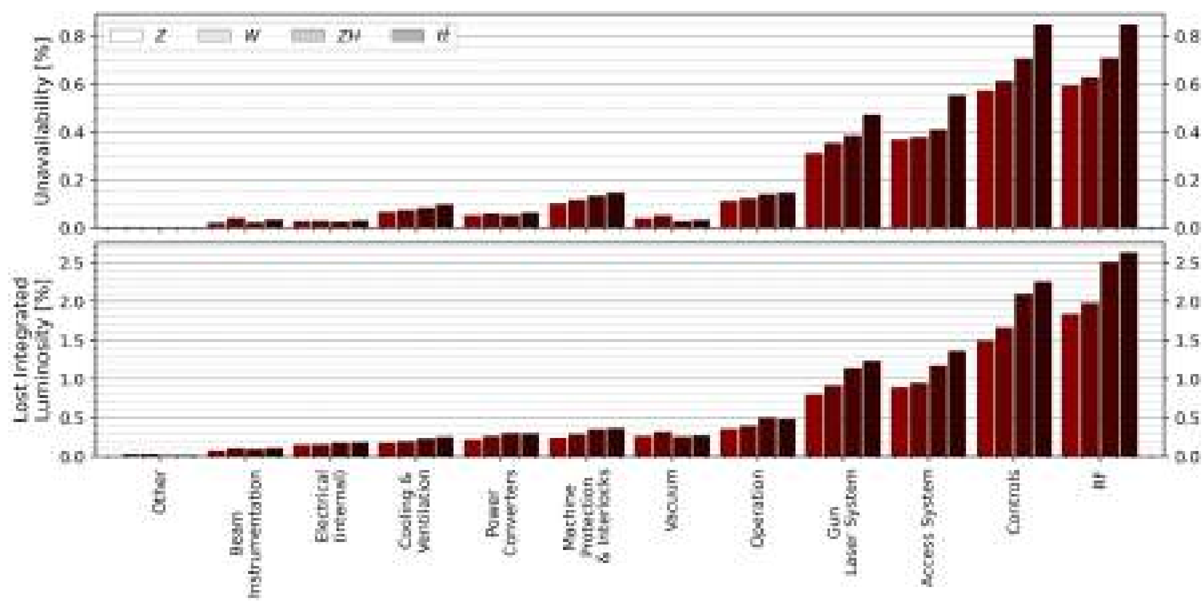

Fig. 7.34 FCC-ee unavailability and lost luminosity contribution of the HE Linac determined by applying fault statistics from the Linac Coherent Light Source (LCLS) at SLAC [370]. Systems are ordered according to Z mode lost luminosity contribution

The short beam lifetime is especially significant for Z mode operation, where the charge imbalance between electron and positron beams in the collider must be less than 5%. Assuming a lifetime of 10-15 minutes, the injection of electrons and positrons must alternate for top-up every 50 seconds. This places significant design constraints on the injector hardware and has profound implications for reliability and availability, as even short interruptions could impact the collider's performance. This requirement limits the breakdown (BD) rate in the injector's accelerating structures. The time required to bring an accelerating structure back into operation after a BD is on the order of a minute. This poses a problem with the injector's availability. An analysis of BDs in the SwissFEL linac is conducted in Ref. [371]. During regular user operation, the RF modules failure rate began to reduce thanks to RF conditioning incidental to nominal operation. This incidental conditioning followed a power law trend that saw the BD rate decrease by over three orders of magnitude in the first three years of user operation, from 10^{-6} to less than 10^{-9} BD per pulse per metre or about two BD per day in the entire linac. Nonetheless, RF BDs continue to account for about half of all broken interlocks in SwissFEL.

Fig. 7.35 Plan view of high-energy linac civil engineering

Given the number of RF structures planned for the FCC injector and scaling, the results obtained for SwissFEL, translate into a reduction of the BD rate from about 850 events per day to about eight events per day after the first four years of operation. The proposed solution, which is to be further investigated, to mitigate these events, is to use some additional RF modules during these BD events. The low probability of having more than two events simultaneously led to the adoption of one additional RF module for the positron and electron linacs and two additional RF modules in the HE linac. Thanks to this approach, the injector's availability due to the BDs could be greater than 99% after a few years of operation.

7.10 Civil engineering

7.10.1 Injector complex

The preferred location for the FCC-ee injector complex is on the existing CERN Prévessin site. Several options for the location of the high-energy linac were explored, with the preferred choice being near the northwest edge of the Prévessin site. A more detailed placement study considering also environmental aspects will be performed in the next phase before confirming the location. The envisaged layout of the facility is shown in Fig. 7.35.

The civil engineering for the high-energy linac will consist of four main elements, namely: the high-energy linac tunnel, the associated e^+ and e^- tunnels, the damping ring and the transfer tunnels/structures to connect the damping ring to the rest of the facility. All these structures will consist of reinforced concrete buried structures extending over a length of about 1.2 km. For shielding purposes, these structures will be built in a series of trenches up to 15 m below the ground level. These so-called 'cut-and-cover' tunnels will be backfilled using the excavated material from the trench formation, and then a surface hall will be constructed above the tunnels. A series of 6 m long vertical mini-shafts of about 0.8 m diameter will connect the tunnels to the surface hall for connecting the klystrons and to allow for the passage of services and cables. A schematic section of this arrangement is shown in Fig. 7.36.

Compared to the other options studied for the high energy linac, the preferred site has a number of significant advantages including:

- The proposed location is quite flat, with a total difference in ground level along the length of the HE-linac of about 5 m
- The proposed location has minimal existing infrastructure. A small number of underground networks will need to be rerouted before construction, and two or three older structures on the Prévessin site will be carefully dismantled or relocated as needed.
- The location and orientation are well suited for a potential future connection of beam lines to the North Area of Prévessin, where fixed-target physics research is conducted.

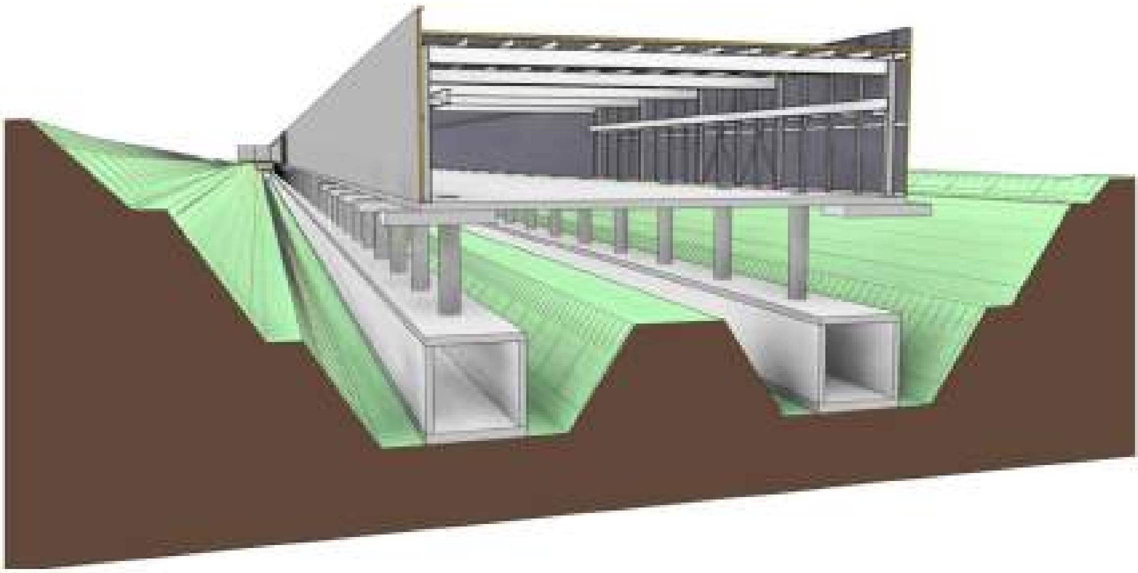

Fig. 7.36 Cross-section of high energy linac civil engineering

Fig. 7.37 Schematic view of transfer tunnels

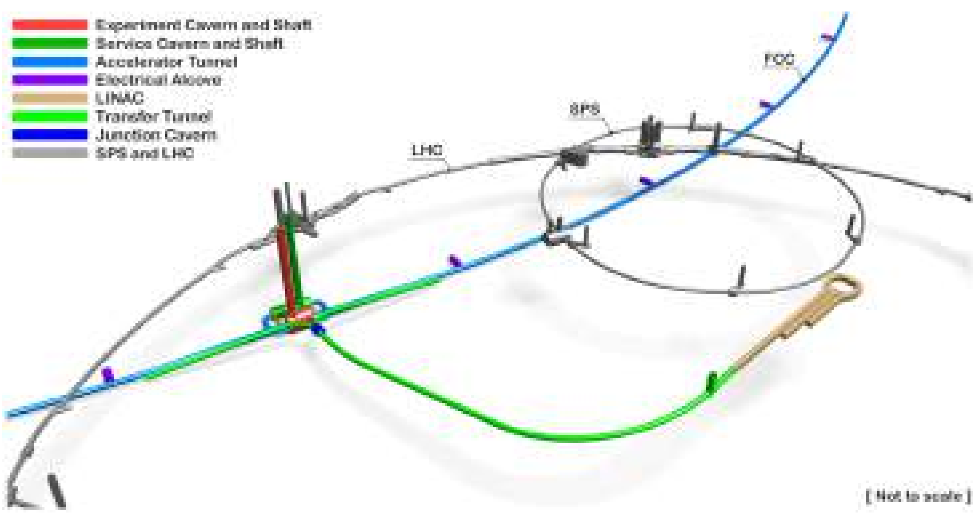

7.10.2 Transfer tunnel

The beam lines from the high energy linac will be connected to the FCC main accelerator tunnel through a transfer tunnel. This transfer tunnel will consist of a single tunnel of internal diameter 3 m and total length of 5560 m. As this tunnel approaches PA of the FCC, the tunnel will bifurcate to provide a clock-wise and anti-clockwise link to the FCC. These two link tunnels will be symmetrical and each 747 m in length. This arrangement is shown schematically in Fig. 7.37 and a plan view is given in Fig. 7.38.

The main characteristics of the transfer tunnel are:

- Three horizontal curves with a minimum radius of 300 m are required
- The tunnel will have a slope of 4.9%.
- Connection of the tunnel to the high energy linac will be made on the CERN Prévessin site at the end of the high energy linac.
- Connections to the FCC main tunnel would be created with 0.8 m diameter drilled horizontal passage for the clockwise and anti-clockwise beam lines. A small personnel access connection would also be created between the FCC and transfer tunnels for emergency access and ventilation. These connections would be constructed in the widened section of the accelerator tunnel either side of PA, where the span of the accelerator tunnel is 14.5 m.

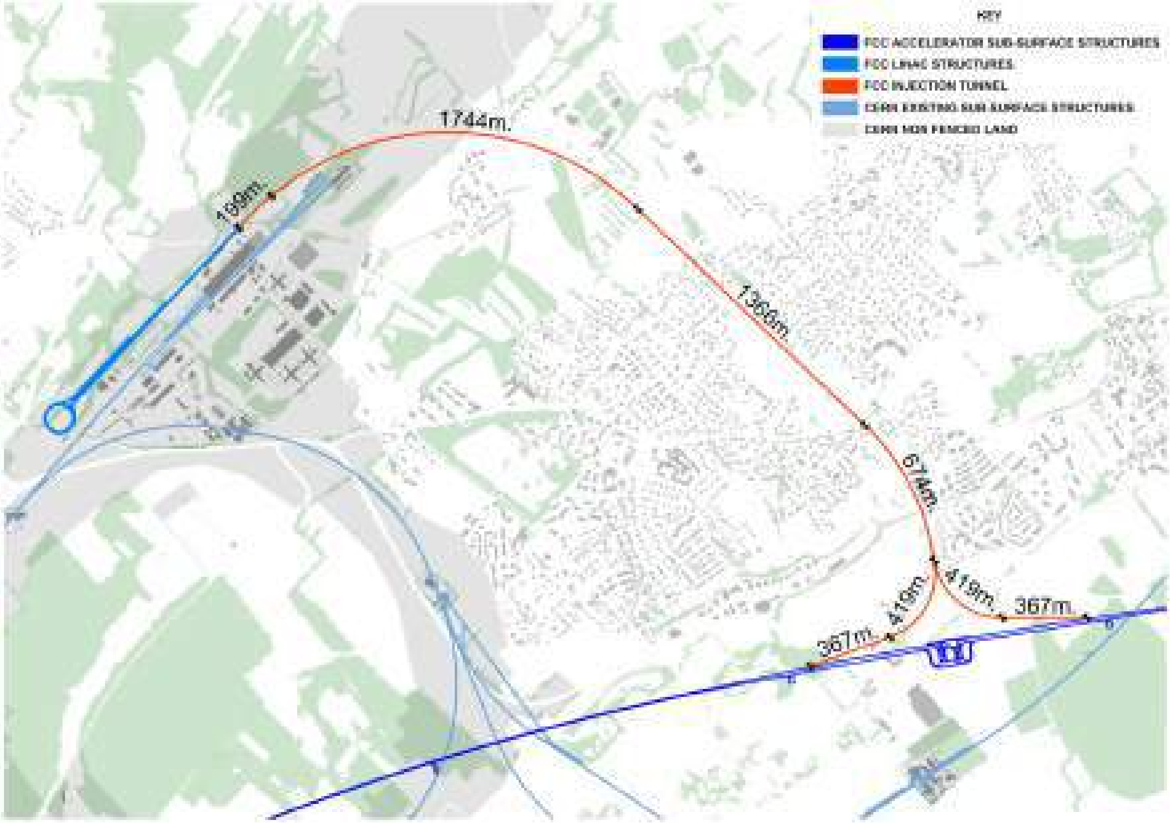

Fig. 7.38 Plan view of transfer tunnels

- A temporary shaft located within the existing Prévessin site would be built to provide access for the construction of the transfer tunnel. This shaft would have a depth of 30 m and an internal diameter of about 10 m to suit the contractor's plant and equipment. The shaft may not be needed for the operation of the FCC. The transfer tunnel will be excavated from this shaft using either a tunnel boring machine or roadheader or a combination of the two.
- A junction cavern of 30 m length and 9 m span will be necessary to accommodate the bifurcation of the tunnel for the clockwise and anti-clockwise injection into the FCC machine.

Geological conditions for tunnelling this small-diameter tunnel are expected to be favourable, with molasse strata serving as the tunnelling medium from the access shaft down to the FCC accelerator tunnel. The connections to the FCC tunnel will be made at a depth of approximately 200 m below ground level. Additional confidence in the feasibility of construction comes from CERN's extensive experience in underground civil engineering projects in this region, including the SPS, LHC, and CNGS, all of which were successfully constructed in the same general area. If a tunnel boring machine (TBM) is used for excavation, reinforced concrete segments will likely be employed for support, similar to the main FCC accelerator tunnel. Alternatively, if a roadheader is used, a two-phase approach will be followed for tunnel support, consisting of an initial lining with rock bolts and shotcrete, followed by a secondary cast in-situ reinforced concrete lining.

7.11 Technical infrastructure

The new injector complex will be integrated in CERN's Prévessin site, requiring additional energy and services. Initially constructed for the SPS accelerator and its fixed-target physics programme, the Prévessin site hosts the SPS North Area and serves as a critical hub for CERN's technical infrastructure. This includes the 400 kV power lines from RTE (France's Transmission System Operator) that supply power to the entire CERN complex, the CERN Control Centre (CCC) responsible for operating all CERN accelerators, the new data centre, and the Ethernet backbone hub. These infrastructures are regularly upgraded to support the evolving demands of CERN's programmes. The new injector complex will become a significant addition to the existing layout. The injector complex consists of five main areas: the e-linac, the p-linac, the damping ring, the HE-linac, and the transfer line to the booster. Each area includes an accelerator tunnel and its associated surface building. Dedicated

Table 7.21 Main electrical loads from the accelerators of the injector complex for the Z and WW modes of operation. Here, the RF numbers for the three linacs assume a commercially available klystron efficiency of 42%

Accelerator loads	Area	Power rating
RF	e-linac	2 MW
RF	p-linac	4 MW
Magnets	p-linac	4 MW
RF	HE-linac	9.5 MW
Magnets & RF	Damping ring	3.2 MW
Magnets	Transfer line	2 MW
Total		**24.7 MW**

Table 7.22 Additional loads of the injector complex

Other loads	Types	Power rating
Accelerator systems	Auxiliary magnets, vacuum, instrumentation, control...	2 MW
General services	AC plugs, lighting, safety systems...	2 MW
Cooling and ventilation	Pumps, motors, fan coils...	3 MW
Total		**7 MW**

technical infrastructures will be established to meet the needs of these areas, which can operate independently. For electricity and cooling, there will be a shared infrastructure. A new electrical substation will connect to the existing main substation to supply power to the complex. Cooling towers, grouped in a dedicated building near the end of the HE linac, will dissipate heat generated by the five areas. Each area will also have its own ventilation systems.

The tunnels will house accelerator system components such as RF cavities, magnets, instrumentation, and beam pipes. The surface buildings will accommodate RF klystrons, high voltage modulators, magnet power supplies, vacuum control systems, and beam instrumentation electronics. These buildings will require power distribution, water cooling, ventilation, control systems, and safety features, including fire detection and alarm systems. Services like electricity, cooling, and control will be distributed from the tunnels to the surface buildings.

Additional technical infrastructures will support the complex, including access systems, smoke extraction, environmental monitoring, radiation protection systems, handling and transport systems, and communication systems. These systems will be integrated into the surface buildings above the tunnels. The injector complex can be operated remotely from the existing CERN Control Centre.

The estimated main accelerator electrical loads for the injector complex are presented in Table 7.21. Complementing the main loads, the additional power demand of other systems is presented in Table 7.22. Considering instead of 42%, as in Table 7.21, a higher klystron efficiency of 55%, a value that seems reasonable given the developments in high-efficiency klystrons (which aim at S-band klystrons with 70% efficiency), it appears possible to save 3.2 MW on the electrical load for the linacs. This consideration would result in a reduced total electrical load for the injector accelerators of 21.5 MW for the Z and WW modes operation, instead of 24.7 MW. For the ZH and $t\bar{t}$ running, the reduction in energy consumption with the linacs operating at 50 Hz instead of 100 Hz is approximately 6.5 MW at a klystron efficiency of 55%, resulting in a total electrical power of 18.2 MW for the injector accelerators.

The injector complex will require a main electrical substation with a capacity of up to 40 MVA. For the Z and WW running with 42% S-band klystron efficiency and 10% margin, its annual energy consumption is estimated at 150 GWh. With a klystron efficiency of 55% and reduced margins, the injector annual energy consumption for Z and WW running decreases to 120 GWh (linac repetition rate of 100 Hz), and for the ZH and $t\bar{t}$ modes of operation to about 93 GWh (linac repetition rate of 50 Hz).

The cooling towers will have a capacity of approximately 25 MW, with an annual water consumption of 200,000 m^3. This water will be sourced from the existing distribution system, which uses water from Lake Geneva. From a technical infrastructure perspective, integrating the injector complex into the Prévessin site is feasible without affecting SPS operations.

7.12 Ongoing studies and possible upgrades

As the study advances there is strong support from Switzerland and PSI to continue and strengthen the CHART collaboration. The injector project team, consisting of PSI and CERN members and external partners, is preparing a comprehensive proposal to be included in the CHART programme for the financial period 2025-2028, complete with detailed resource and cost estimates, to be finalised in early 2025. In the next phase, several critical areas will require focused attention. The updated baseline design includes a 2.86 GeV damping ring, which must be integrated into the forthcoming technical design study.

The current baseline design assumes an RF frequency in the linacs compatible with the main rings to retain operational flexibility. However, the limited availability of suitable power sources on the market presents a challenge, prompting efforts to adopt a commercial S-band frequency for the RF system in the linacs. Additionally, the positron linac will undergo optimisation to shift from the current 2 GHz setup to a more widely available S-band frequency. Reliability and availability of the injector complex will be key factors in the injector's design, particularly for continuous 'top-up' operation, which requires a low-gradient injector configuration with an experimentally validated RF breakdown rate. Assessing the impact of short interruptions caused by RF breakdowns in top-up operations will also be critical for ensuring stable performance.

The involvement of international partners will remain crucial as the injector study progresses towards the technical design and construction stages. A comprehensive technical design report could follow the feasibility study phase, building on the SwissFEL linac technology for RF accelerating structures and related upgrade projects. This report will also benefit from the expertise of international partners who have experience in synchrotron light and positron source operations. Its primary objective will be to establish detailed specifications for the accelerator and technical infrastructure requirements necessary to initiate civil engineering design. These specifications will ensure that all system and subsystem requirements are addressed, making the initial construction phase and mass production of critical components smoother.

A comprehensive TDR for the accelerator and the associated technical infrastructure will be completed should the project move to its next phase. This will be pivotal, enabling further engineering design efforts and finalising all necessary specifications for civil engineering work. This phase is essential to confirm that all design elements undergo rigorous examination and are fully integrated into the project, ensuring a seamless transition to the construction phase. A prototyping phase will be critical in this context. During this phase, RF accelerator structures will undergo exhaustive testing to validate their performance and reliability. Additionally, based on a photo-cathode RF gun, the electron source concept will be demonstrated to support top-up operation for reliably injecting electrons into the collider ring. This demonstration is essential to confirm that the chosen technology can meet operational requirements and integrate smoothly into the overall system.

Furthermore, the P^3 positron production experiment at PSI will be completed and commissioned, with subsequent development focusing on a hybrid scheme expected to reduce the power dissipated on the target while keeping the efficiency of positron production. This development phase will refine the specifications for the positron source, ensuring that all components meet the operational criteria for integration into the injector complex.

Chapter 8

Technical infrastructure for FCCs

8.1 Requirements and design considerations

The infrastructure requirements and the proposed technical solutions for FCC-ee have been defined for the PA31-1.0 layout, which, as described above, features eight points with associated surface areas. Four of the points are experiment points, and four are technical points. The technical infrastructure systems described here are electricity and energy management, cooling and ventilation, integration, geodesy and survey, cryogenic systems, transport and logistics, and computing infrastructures and robotics. The present study focuses on the technical infrastructure related to FCC-ee. However, wherever design choices are made which may impact FCC-hh (in particular, the space requirements and dimensions), constraints from and possible synergies with the hadron collider are taken into account.

8.1.1 Assignment of points

Four of the eight FCC points are designated for experiments: PA, PD, PG, and PJ. Among these, PA and PG are considered as large experimental areas for FCC-hh, whereas PD and PJ are optional sites that may accommodate smaller hadron collider detectors requiring less infrastructure. All four points can accommodate the much smaller experiments of the FCC-ee collider.

The remaining four points are technical. Point PB, the only one located in Switzerland, has been chosen to house the beam dump system. Points PL and PH have been selected to house the booster and collider RF, respectively. Point PF was found less appropriate to house the RF due to difficult access conditions (the access shaft is displaced laterally w.r.t. the FCC ring by several hundred metres) [372], but it could house the collimation system.

The assignment of points PL and PH was made based on constraints from accelerator physics (a preference to concentrate the collider RF at a single point), constraints at the surface areas, and infrastructure constraints (accessibility, resources, electrical network connection, and powering). Since point PL features a relatively complicated surface site with many constraints, it was decided to install the booster RF 800 MHz cryomodules at this point. The Booster RF requires much less infrastructure than the collider RF and can be more easily integrated. Point PH was designed to house the collider RF (400 and 800 MHz cryomodules), which requires substantial infrastructure.

8.1.2 Electricity supply

Electrical power will be provided by the French network and fed into the FCC at three points (PA, PH, and PD). Further distribution is then accomplished via the FCC tunnel. The electrical infrastructure is designed to support all FCC-ee configurations seamlessly, eliminating the need for additional substations between different operational stages. The proposed setup also includes the possibility of operating the machine without one sub-station (PA or PD). The PH substation, which has the main RF loads (200 MW), is mandatory for beam operation. This setup will ease the maintenance and repairs as all substations will be connected together through the HV network. RTE (Réseau de Transport d'Électricité) has launched a study on how to connect the FCC to the French network. The requirements of the FCC project are not considered significant by RTE, and will not impact the French electrical network operation.

8.1.3 Cooling and ventilation

The potential sources of cooling water in the area are lake Geneva and the Rhône and Arve rivers. As a baseline, the required cooling water will be taken from Lake Geneva via the existing infrastructure, which has enough capacity to supply the FCC. Pipework within the tunnel will connect the remaining points to PA, PD, or PJ to ensure their respective water supply. The drainage flow rates correspond to around 30 m^3/h in the RF points and a maximum of 11 m^3/h in the remaining points.

A semi-transverse ventilation scheme has been adopted for the FCC tunnel, with air supplied through a dedicated duct running along the entire sector and extracted either via the tunnel itself or through an emergency extraction duct. To ensure continuous airflow in case of a duct failure, air is supplied to each sector from both endpoints, with the same configuration adopted for the extraction system.

8.1.4 Cryogenic systems

The cryogenic system design of FCC-ee follows the requirements of the superconducting devices, which are distributed throughout the machine. Whilst the technical points PB and PF do not feature any cryogenic needs, the technical points PH and PL are associated with the radiofrequency (RF) system, which needs to be operated at 2 K and at 4.5 K. These RF points have the largest cryogenic installations due to their high concentration of heat loads. Additionally, each experiment point – PA, PD, PG, and PJ – requires a dedicated cryoplant to support the cooling needs of the detector magnet and the magnets in the machine detector interface (MDI) region.

8.1.5 Transport and logistics

In the first phase of the analysis, an inventory was established detailing the type, quantity, dimensions, and weight of the components to be transported. Simultaneously, the number of personnel requiring transport to their workplace in the tunnel was determined, and evacuation studies were conducted.

Based on these input data, two vehicle concepts have been studied: the first for the transport of the equipment, including the accelerator components, and a second for the transport of personnel throughout the installation, operation and dismantling phases.

The vehicle for transporting materials will be electric, fed by batteries. Charging stations will be installed all along the tunnel. The design comprises a trailer carrying the material, pulled by a tractor hosting the batteries. The trailer is equipped with two robotic arms capable of handling and manoeuvring the components up to their final location.

As the market already offers valid solutions, the personnel vehicle will be based on an existing system. This will then be customised to meet the specific requirements and constraints of the FCC tunnel. The personnel vehicles will be electric and powered by batteries. The personnel transport will consist of a mixture of individual and scheduled transport systems. Its characteristics will be defined to ensure the safe evacuation of people present in a sector at the appropriate time.

For safety reasons, vehicle overtaking must be possible at any location in the tunnel, which imposes a constraint on the width of the vehicles.

In addition to technical solutions for material and personnel transport, a logistics study is being conducted. This study develops logistics scenarios based on various boundary conditions, such as the number of shafts available for material transfer and the number of vehicles used for underground transportation.

For each scenario, key performance indicators (KPIs) are generated, including the number of magnets that can be installed per day and the total installation time required for the accelerator. Potential bottlenecks in material flow are also identified. These indicators serve as an objective tool for evaluating and comparing different scenarios, enabling the selection of the most suitable approach for the overall project.

8.1.6 Geodesy

The size of the FCC requires a refined and extended geodetic infrastructure, including reference frames and a gravity field model. The geodetic infrastructure must be compatible with each phase of the project. This comprises the generation of a primary surface geodetic network. To this end, Swisstopo and IGN are increasing the density of their national geodetic networks. In order to meet the vertical alignment accuracy, a refined model of the gravity field is being prepared.

8.1.7 Communications, computing, and data services

Three different infrastructures will be deployed to enable data, telephone and radio networks. They are all built on top of a fibre optics infrastructure. Regarding the IT infrastructure, the FCC will feature two redundant data centres on the Meyrin and Prévessin sites.

8.1.8 Surface areas

Based on the design choices above and input from the infrastructure and equipment groups, the needs for infrastructure and buildings at the eight surface points have been compiled. The tables summarise the key elements (element, location, construction type, size, capacity) by domain (safety, electricity, and energy management, cooling and ventilation, geodesy and survey, cryogenic systems, transport and logistics, computing infrastructures). The contents of these inventory tables are the basis for the layout of the surface points [373].

8.1.9 Underground areas

Integration studies of the underground areas, including the tunnel, main caverns and service caverns, shafts and alcoves, have been performed. Equipment sensitive to radiation will be placed in alcoves. There are seven alcoves per arc. The alcoves are linked to transport lay-by zones, which allow transport vehicles to park, pass and overtake each other.

In addition to the alcoves, there are service caverns at the eight points. The current civil engineering design for the service caverns at technical areas is 60 m long, 25 m wide and 15 m high. These caverns will each be divided into three levels to provide additional floor area on the upper levels. The service caverns are mainly occupied by power supplies, cooling and ventilation equipment, as well as cryogenics equipment.

8.2 3D integration studies

The 3D integration studies of the FCC-ee have been detailed for all the areas of the underground tunnels and caverns, fitting the requirements from the work packages (e.g., civil engineering, infrastructure, general services, transport, safety, optics, accelerators requirement, etc.). This section presents the results of the configuration and layout of the accelerators and infrastructure systems that were studied for the feasibility study report. This is an evolution of the previous studies made for the conceptual design report [13, 306]. The 3D integration studies take into account the configurations of both the FCC-ee and the FCC-hh to ensure space compatibility.

8.2.1 General layout of the FCC

The FCC is a 90.6 km circumference tunnel including eight access points equally spaced above the accelerator tunnel and currently named as point PA, PB, PD, PF, PG, PH, PJ and PL (see Fig. 8.1). The points PA, PD, PG and PJ will host the detectors in dedicated civil engineering areas. They are mentioned as large experiment

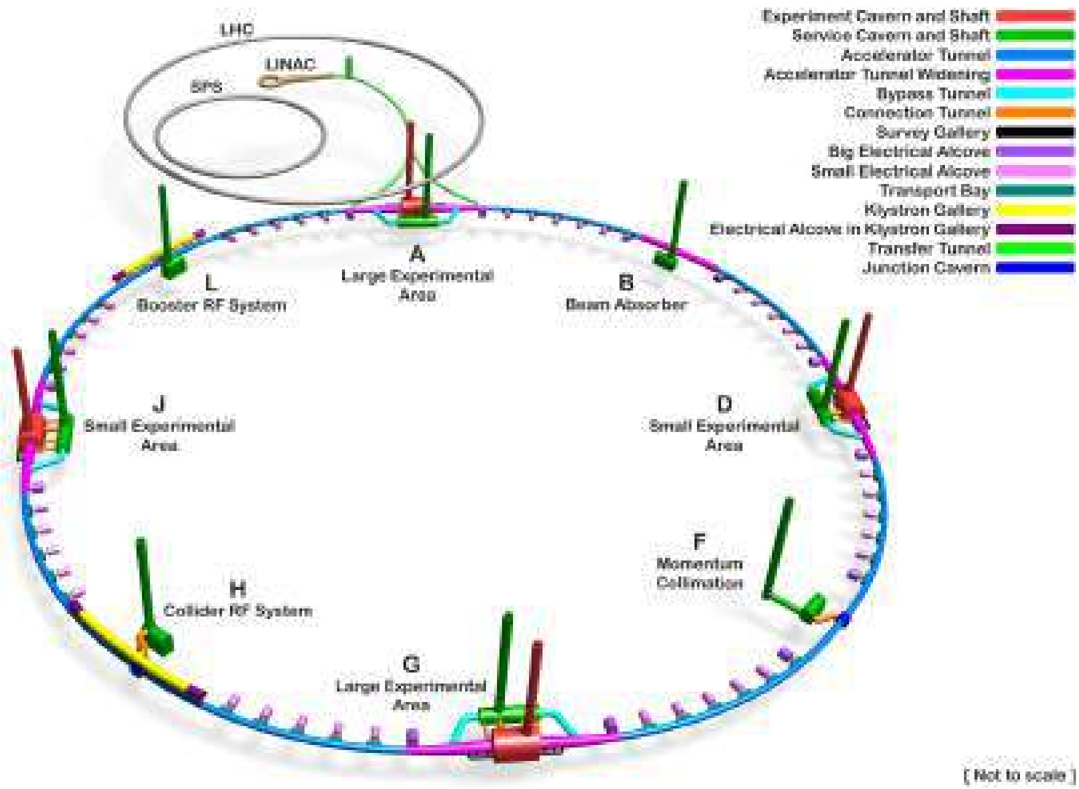

Fig. 8.1 FCC-ee schematic view

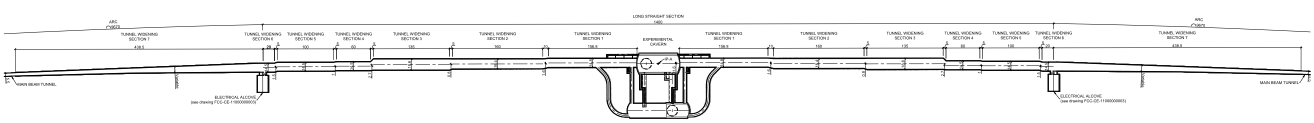

Fig. 8.2 FCC underground - civil engineering in point PA

points for points PA and PG and small experiment points for points PD and PJ. The points PB, PF, PH and PL are mentioned as technical points hosting different accelerator parts.

For the FCC-ee machine,

- The point PB will host the extraction system from the booster, transfer line and injection system to the collider, and the extraction systems and transfer lines to the dumps for both the collider and the booster,
- The point PF will host the collimation systems (betatron and momentum),
- The point PH will host the collider RF system,
- The point PL will host the booster RF system.

For the FCC-hh machine,

- The point PB will host the collider injection lines and the extraction lines to the dumps,
- The point PF will host the betatron collimation system,
- The point PH will host the momentum collimation system,
- The point PL will host the RF system.

8.2.2 Integration of point PA and point PG

Point PA and point PG will serve as large experimental points, hosting detectors in the cavern in both the FCC-ee and the FCC-hh phases of operation. The cavern size and extent meet the needs of the detectors for both FCC-ee and FCC-hh. In addition, for the FCC-ee, the long straight sections (LSS) on either side of point PA and point PG will host the beamstrahlung dumps and the polarimeter system (see Fig. 8.2 and Fig. 8.3). The LSS of point PA will also host the end of the transfer line from the injector linac, into the booster.

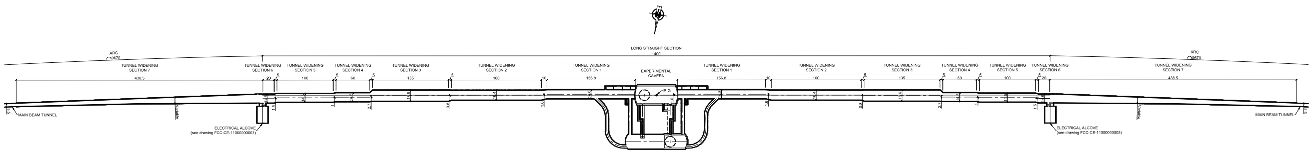

Fig. 8.3 FCC underground - civil engineering in point PG

Fig. 8.4 FCC-ee point PA and point PG - general overview

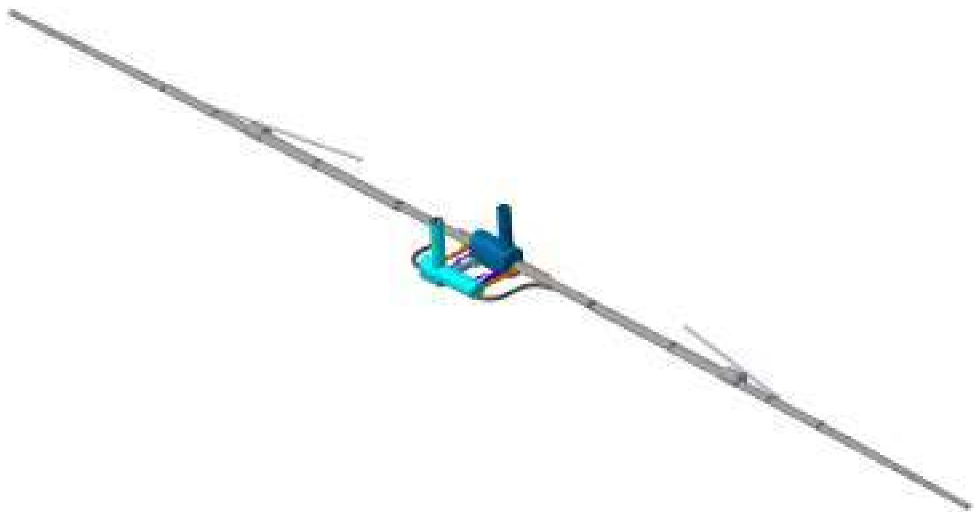

Fig. 8.5 FCC-ee point PA - top overview with optics

Fig. 8.6 FCC-ee point PA - experiment cavern cross-section

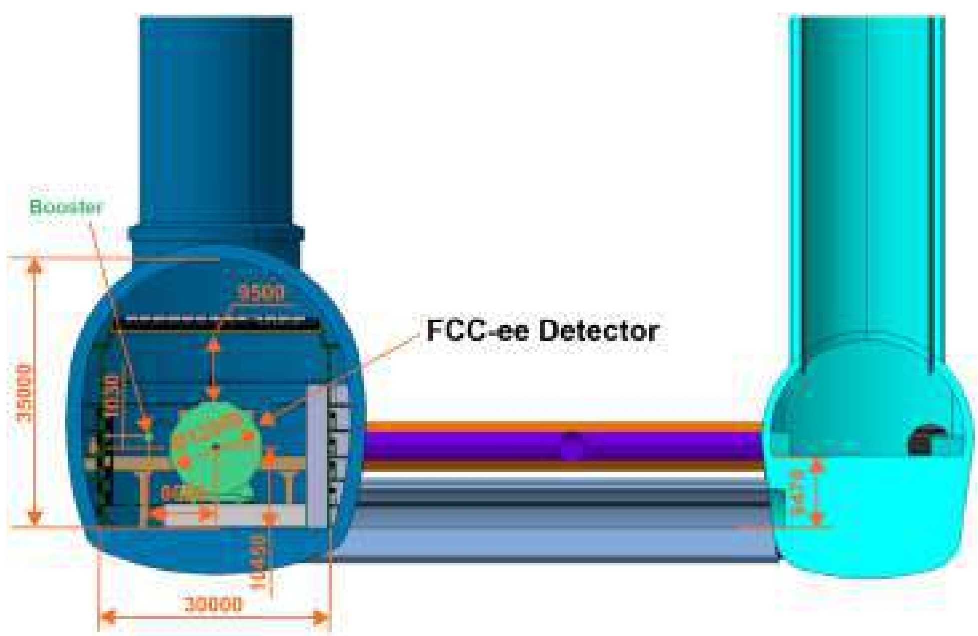

Figures 8.4 to Fig. 8.12 are the results of the 3D integration studies for the point PA and the point PG.

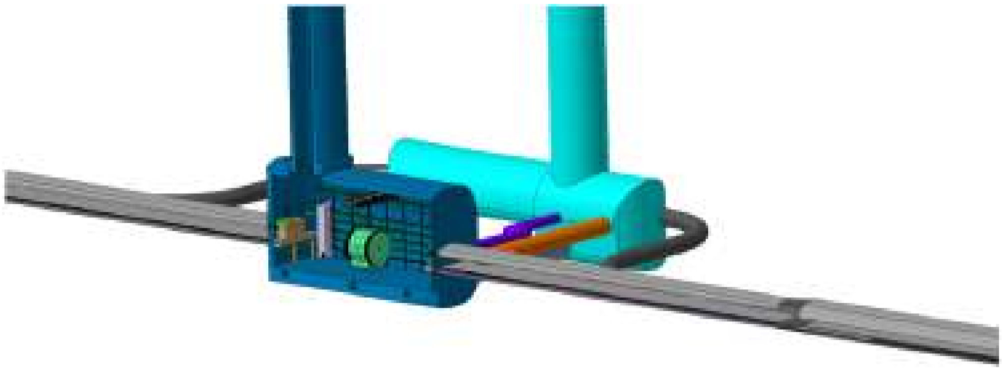

Fig. 8.7 FCC-ee point PA - experiment cavern iso view

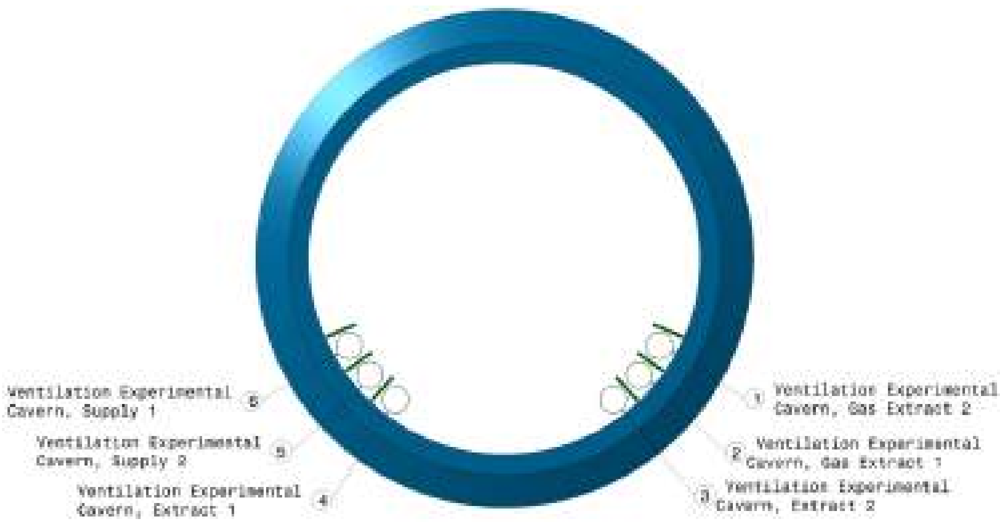

Fig. 8.8 FCC-ee point PA - shaft of the experiment cavern

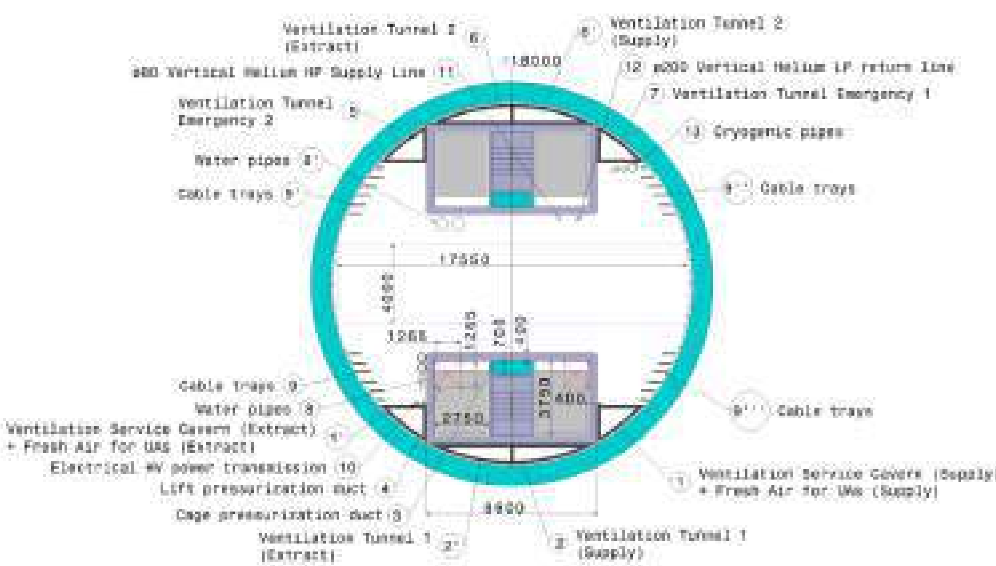

Fig. 8.9 FCC-ee point PA - shaft of the service cavern

Fig. 8.10 FCC-ee point PA - tunnel cross-section with booster

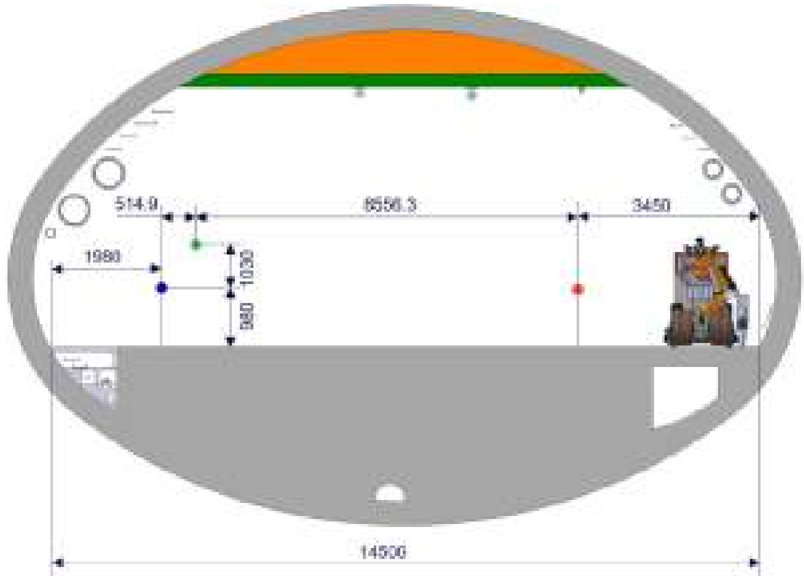

Fig. 8.11 FCC-ee point PA - tunnel cross-section with dump

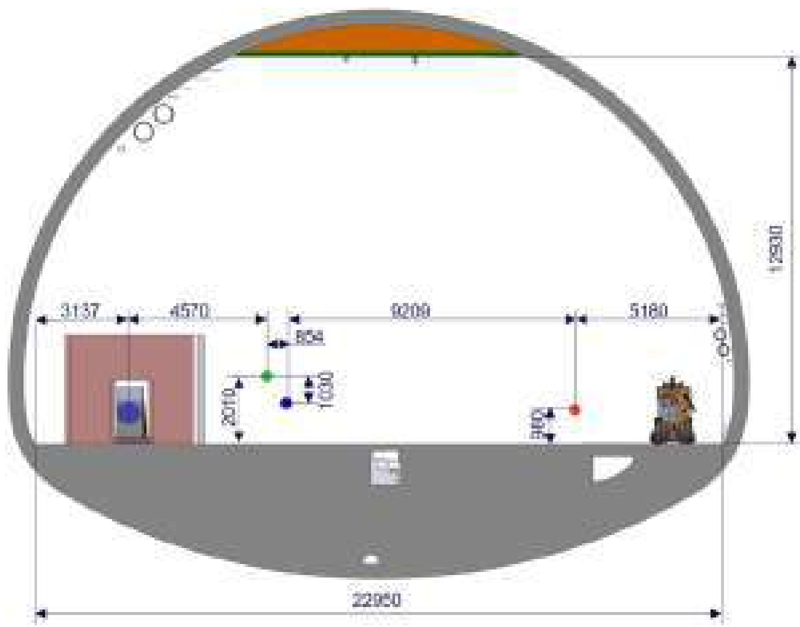

Fig. 8.12 FCC-ee point PA - booster injection tunnel

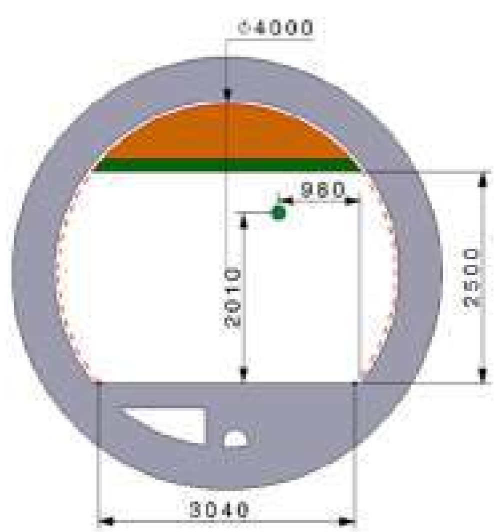

8.2.3 Integration of point PB

Point PB will house the FCC-ee beam dump and injection from the booster into the collider. In the next phase of operation, FCC-hh will house the beam dump system. The civil engineering volumes meet the needs of FCC-ee (see Fig. 8.13).

Figures 8.14 to Fig. 8.16 are the results of the 3D integration studies for the point PB.

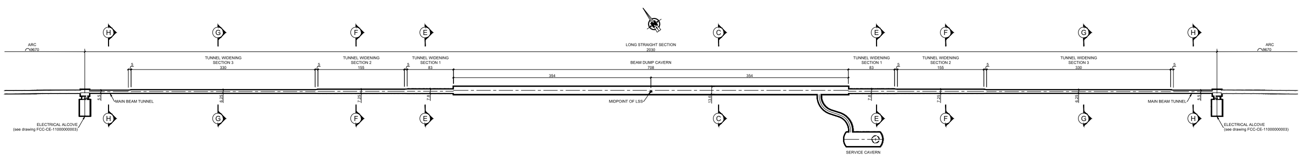

Fig. 8.13 FCC underground - civil engineering in point PB

Fig. 8.14 FCC-ee Point PB - general overview

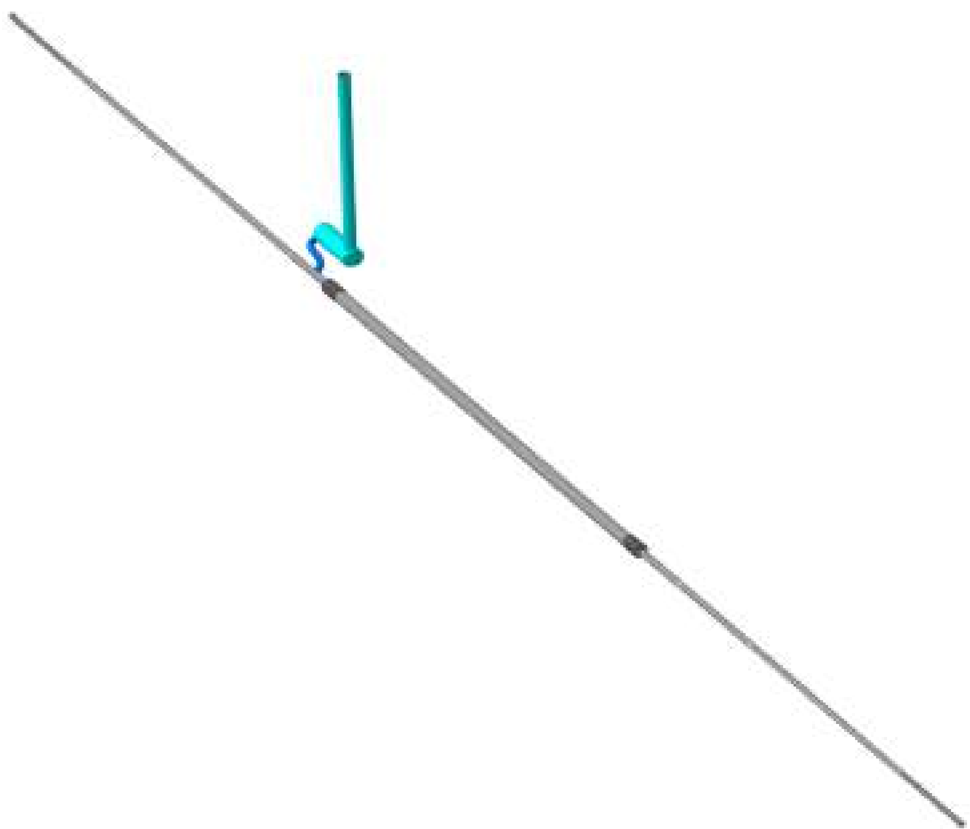

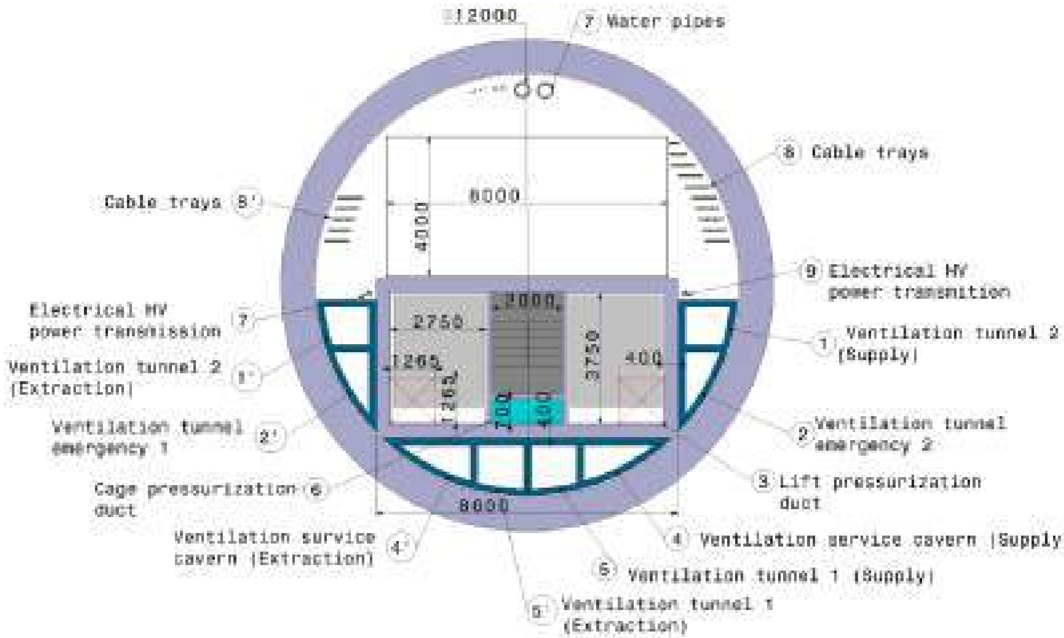

Fig. 8.15 FCC-ee Point PB - shaft of the service cavern

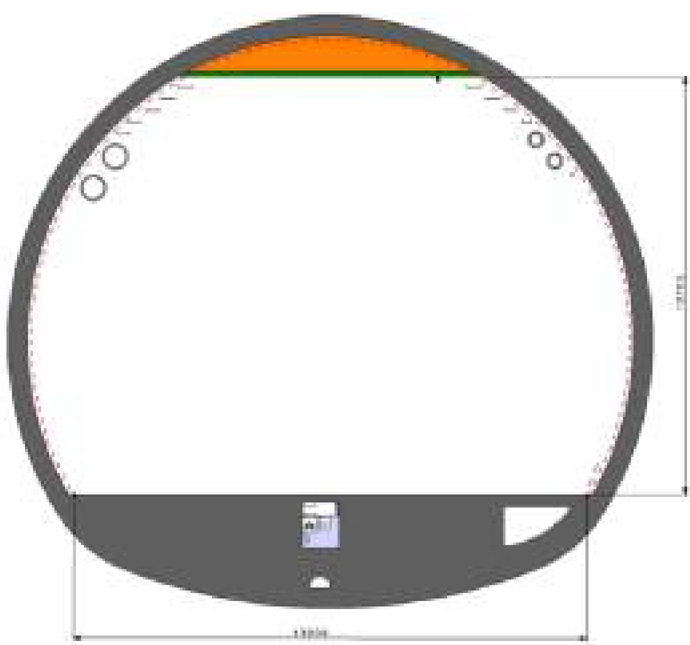

Fig. 8.16 FCC-ee Point PB - tunnel including the dump

8.2.4 Integration of point PD and point PJ

Point PD and point PJ will serve as small experimental points, hosting detectors in the cavern in both the FCC-ee and the FCC-hh phases of operation (see Fig. 8.17 and Fig. 8.18). The cavern size and extent meet the needs of the detectors for both FCC-ee and FCC-hh. In addition, for the FCC-ee, the long straight section (LSS) on either side of point PD and point PJ will host the beamstrahlung dumps.

Figures 8.19 to Fig. 8.23 are the results of the 3D integration studies for points PD and PJ.

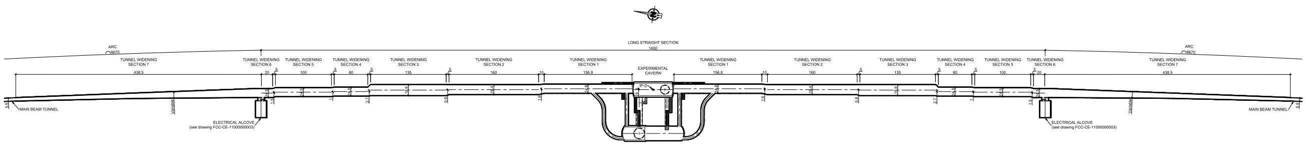

Fig. 8.17 FCC underground - civil engineering in point PD

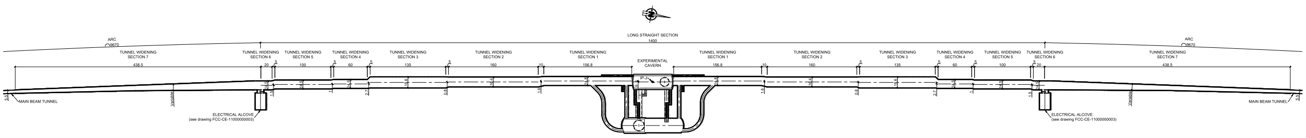

Fig. 8.18 FCC underground - civil engineering in point PJ

Fig. 8.19 FCC-ee point PD and PJ - general overview

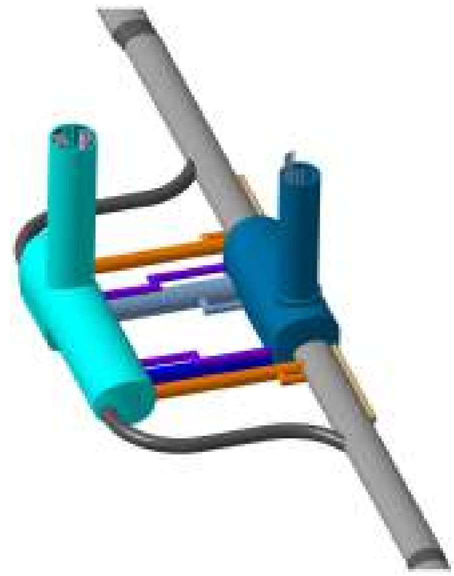

Fig. 8.20 FCC-ee point PD and PJ - shaft of the experiment cavern

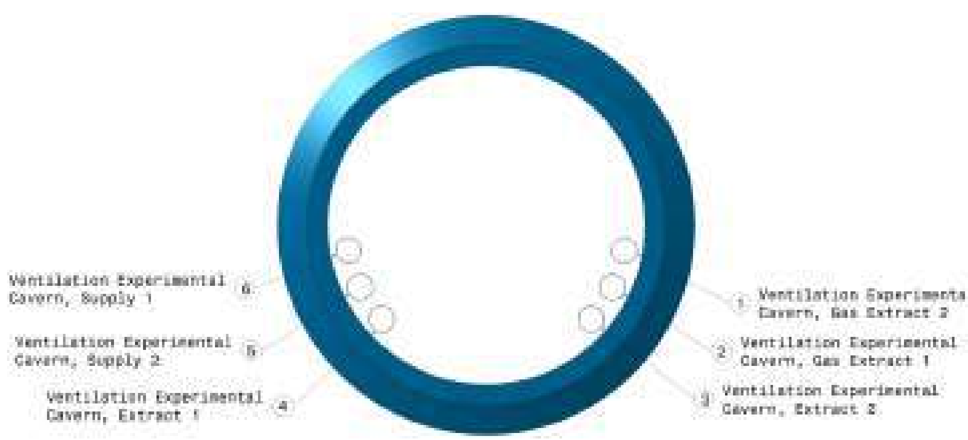

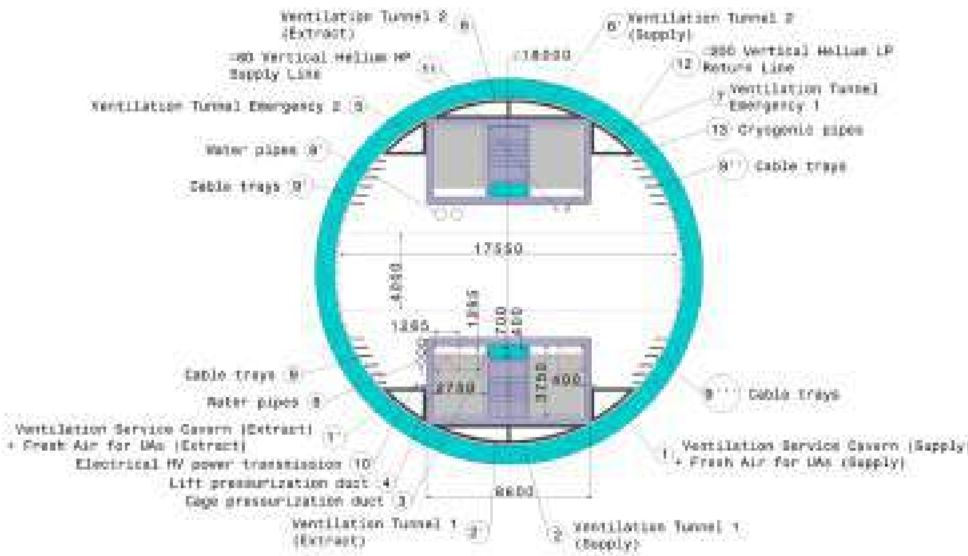

Fig. 8.21 FCC-ee point PD and PJ - shaft of the service cavern

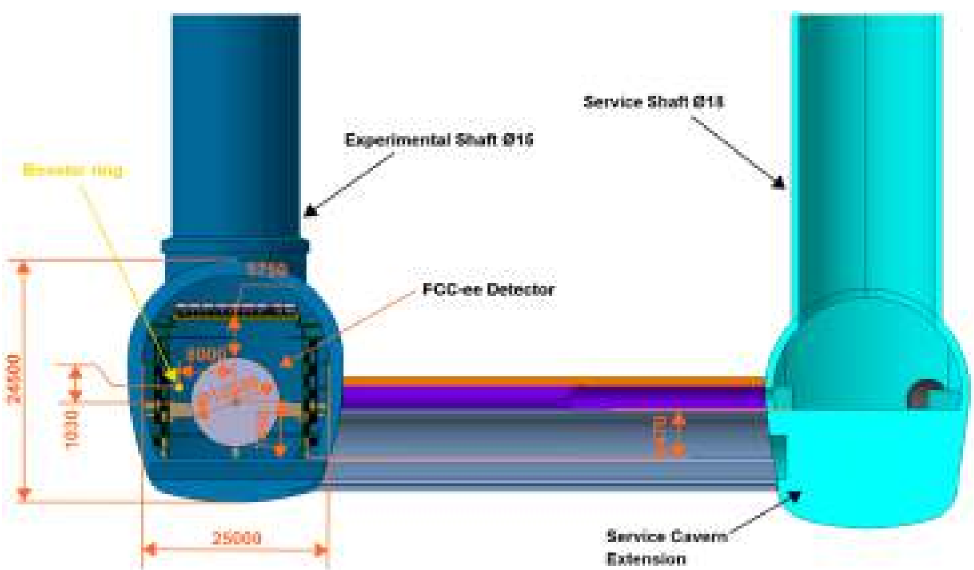

Fig. 8.22 FCC-ee point PD and PJ - experiment cavern cross-section

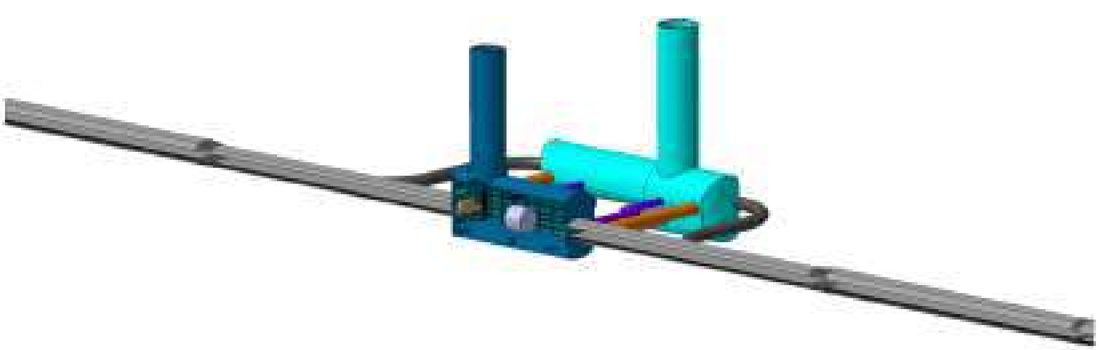

Fig. 8.23 FCC-ee point PD and PJ - experiment cavern iso view

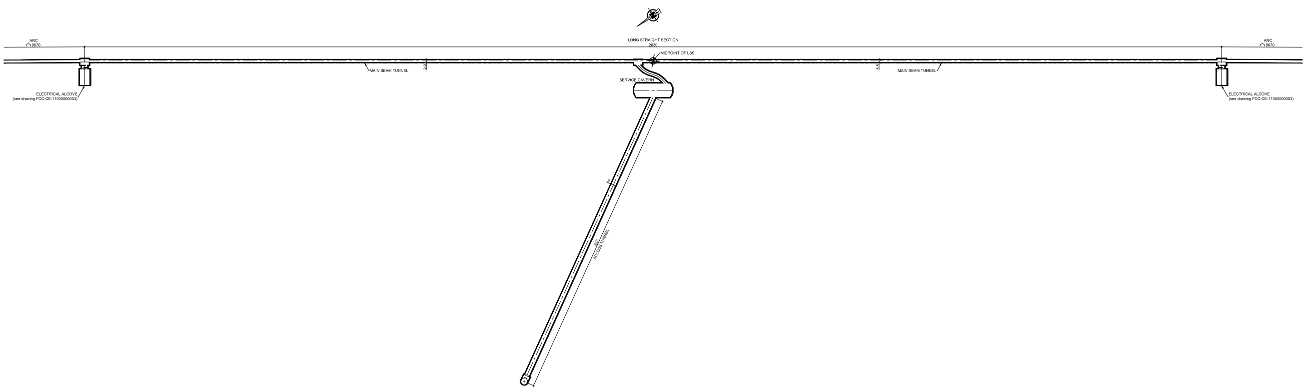

Fig. 8.24 FCC underground - civil engineering in point PF

Fig. 8.25 FCC-ee point PF - general overview

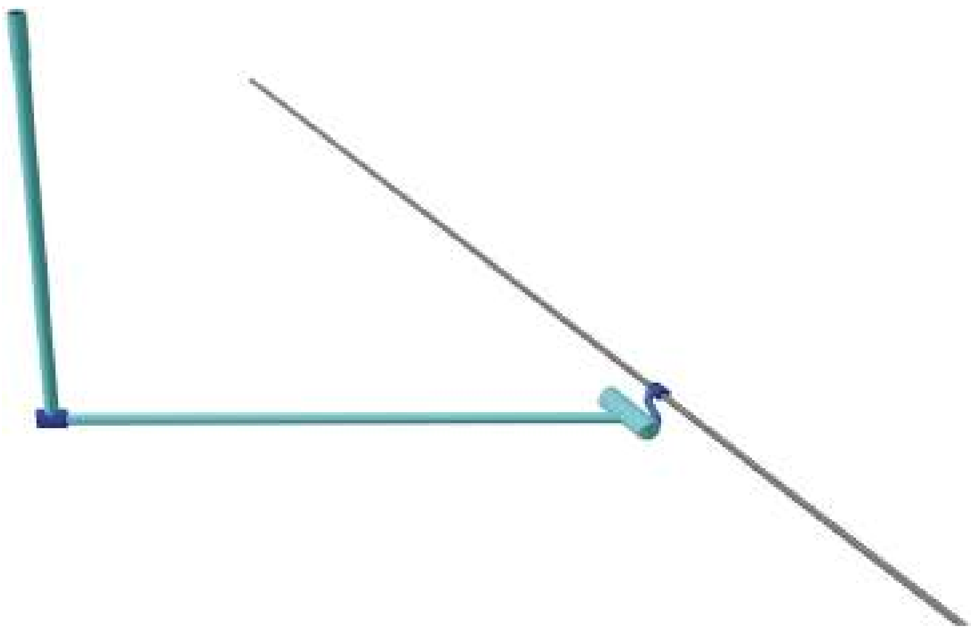

8.2.5 Integration of point PF

Point PF will house FCC-ee betatron and momentum collimation systems. In a next phase of operation, FCC-hh will house the beam dump systems. The civil engineering volume meet the needs of FCC-ee (see Fig. 8.24).

Figures 8.25 and 8.26 are the results of the 3D integration studies for the point PF.

8.2.6 Integration of point PH and point PL (RF systems)

The RF systems of the FCC-ee will be located in point PH for the collider and point PL for the booster (see Fig. 8.27 and Fig. 8.28).

Configuration and layout of collider RF systems - point PH Figures 8.29 to Fig. 8.33 are the results of the 3D integration studies for point PH.

For radiation safety, the distance between the klystron gallery and the machine tunnel is 10 m and shielding is installed in the klystron gallery. The vertical cores house the waveguides and electrical cables. For fire protection, there are partition walls every 400 m in the klystron gallery, and a smoke extraction system on the ceiling. There is a stairway connection between the klystron gallery and the machine tunnel every 280 m.

Configuration and layout of booster RF systems - point PL Figures 8.34 to Fig. 8.37 are the results of the 3D integration studies for point PL.

Fig. 8.26 FCC-ee point PF - shaft of the service cavern

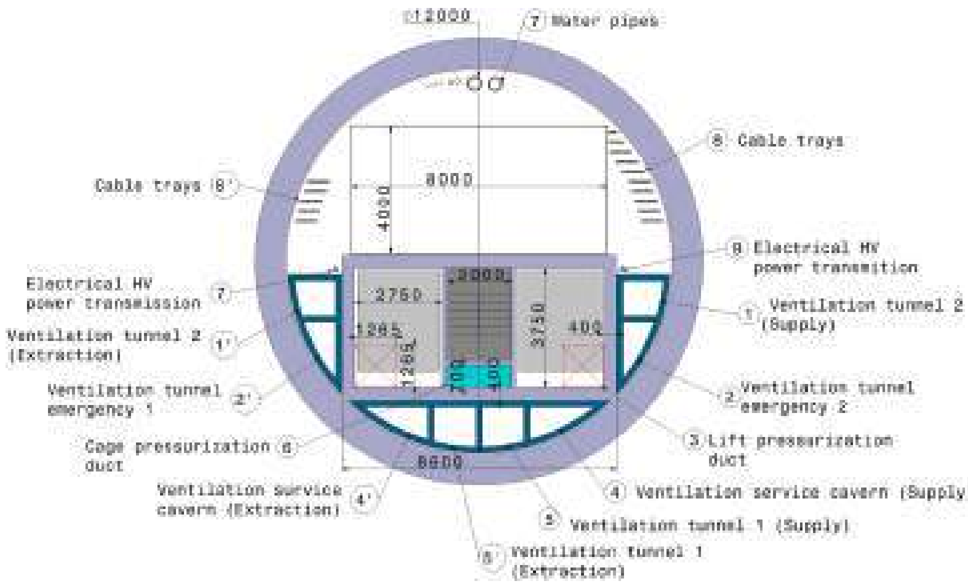

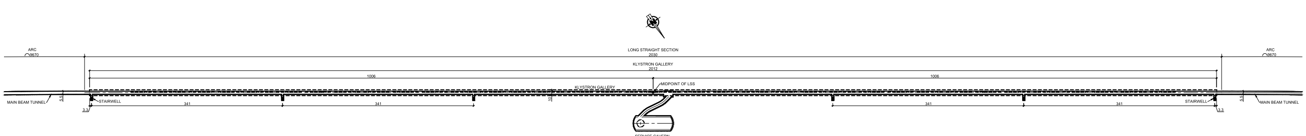

Fig. 8.27 FCC underground - civil engineering in point PH

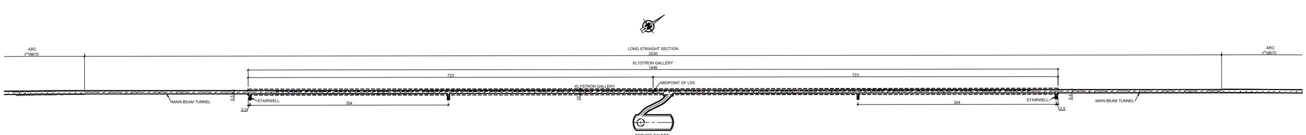

Fig. 8.28 FCC underground - civil engineering in point PL

Fig. 8.29 FCC-ee point PH - general overview

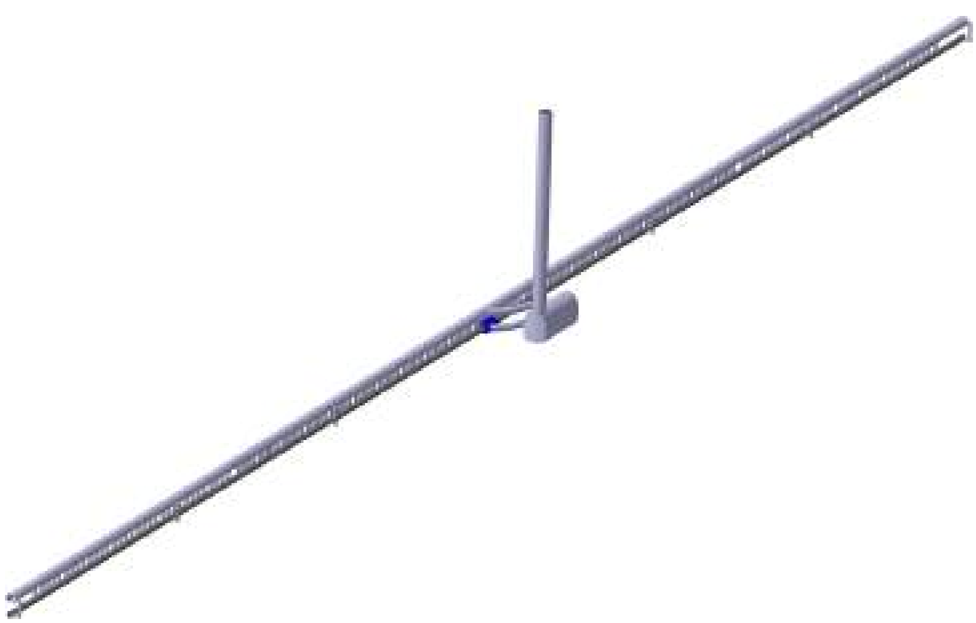

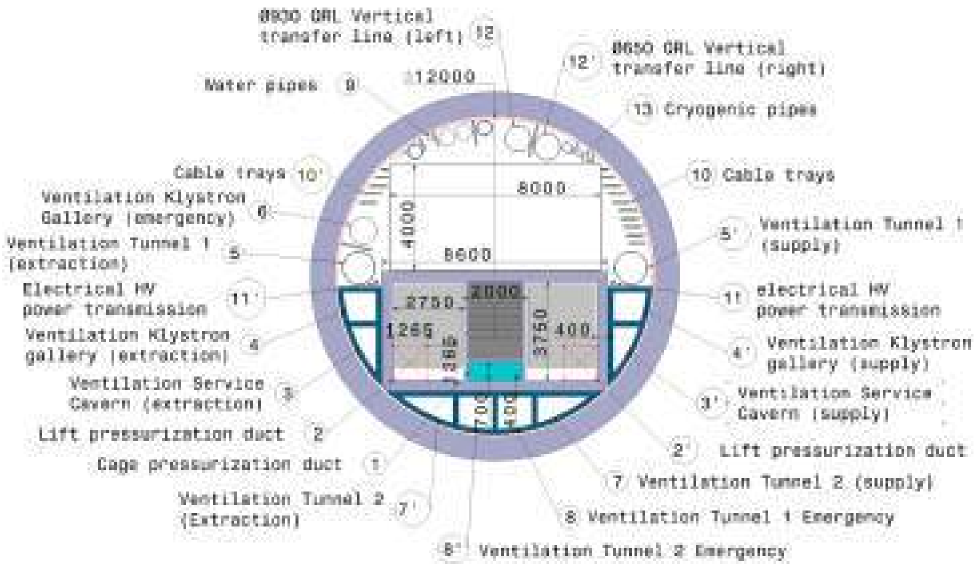

Fig. 8.30 FCC-ee point PH - shaft of the service cavern

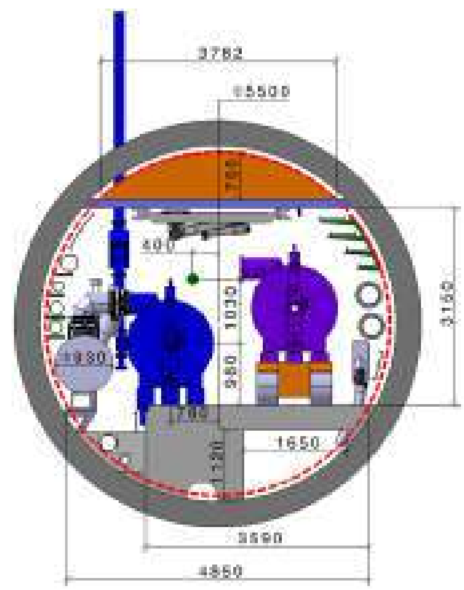

Fig. 8.31 FCC-ee point PH - tunnel cross-section with FCC 800 MHz cavity

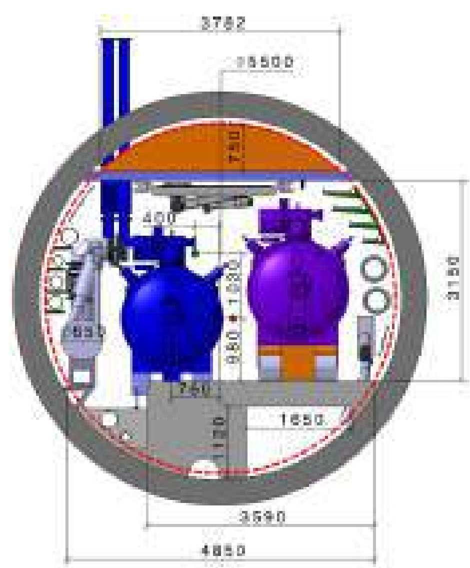

Fig. 8.32 FCC-ee point PH - tunnel cross-section with FCC 400 MHz cavity

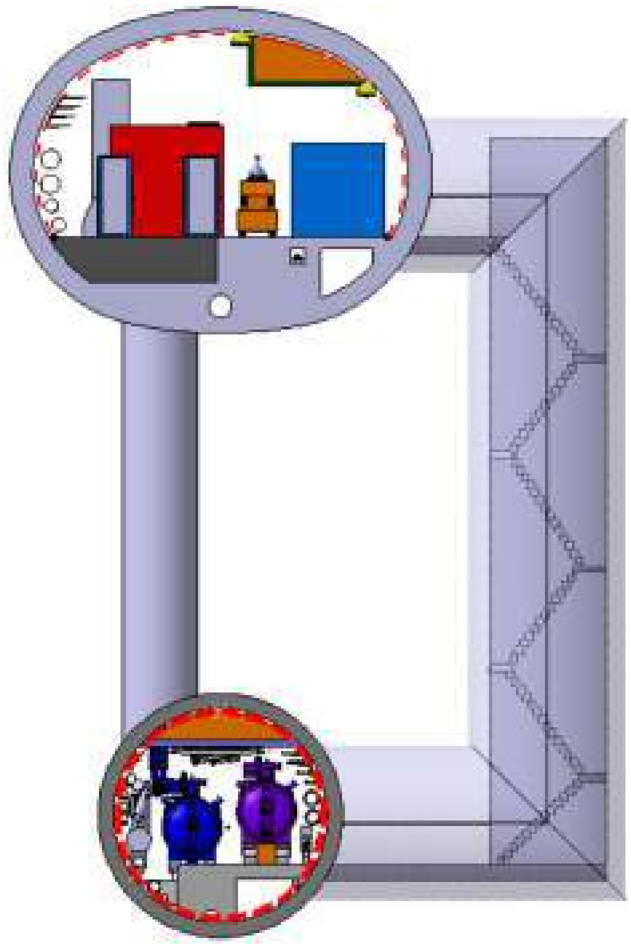

Fig. 8.33 FCC-ee point PH - tunnel and gallery cross-section

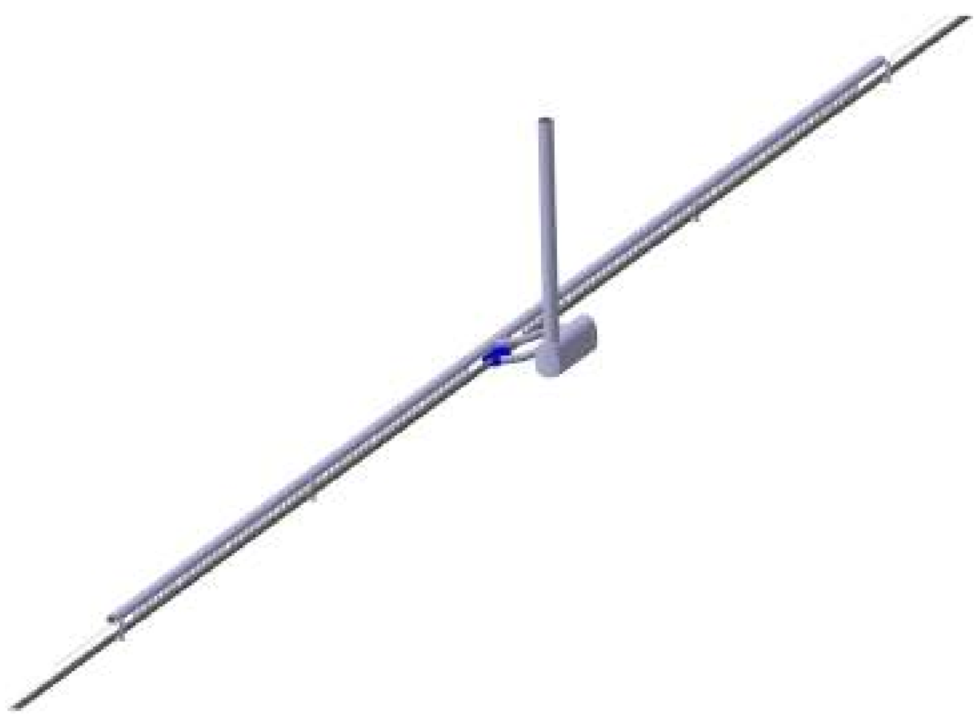

Fig. 8.34 FCC-ee point PL - general overview

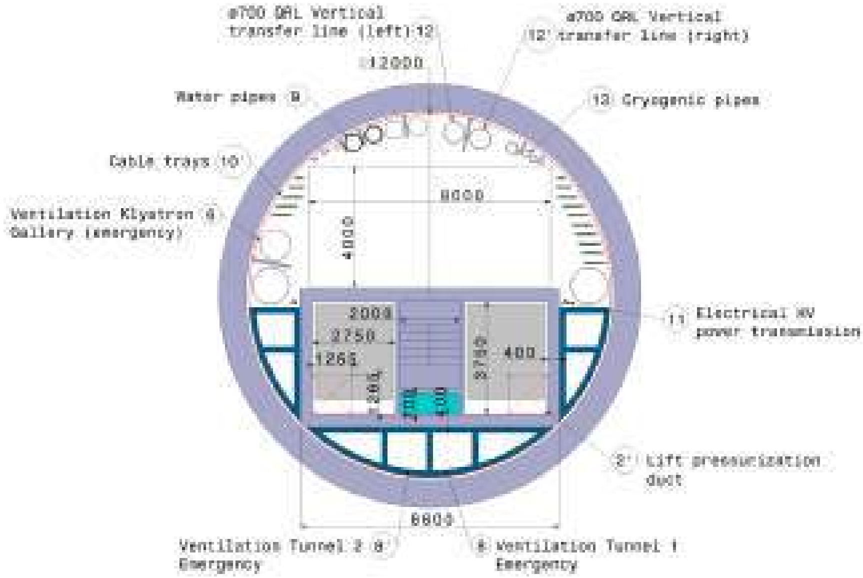

Fig. 8.35 FCC-ee point PL - shaft of the service cavern

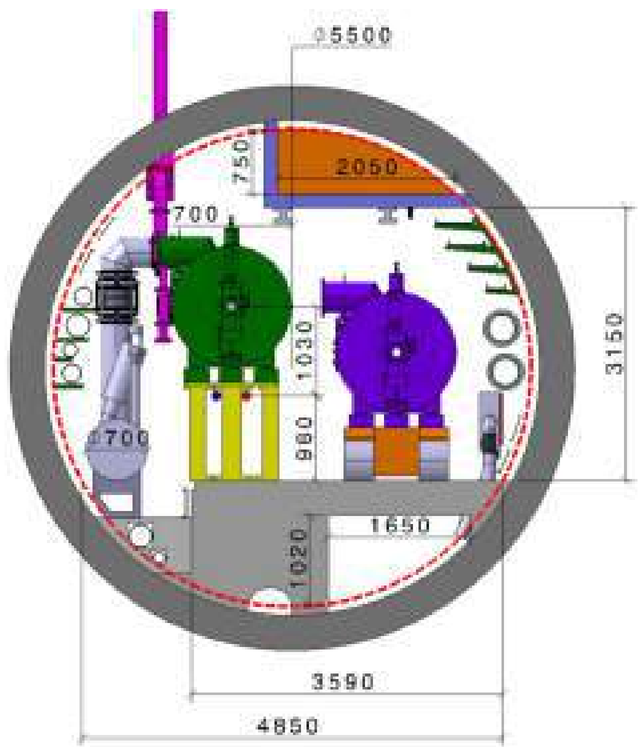

Fig. 8.36 FCC-ee point PL - tunnel cross-section with booster 800 MHz cavity

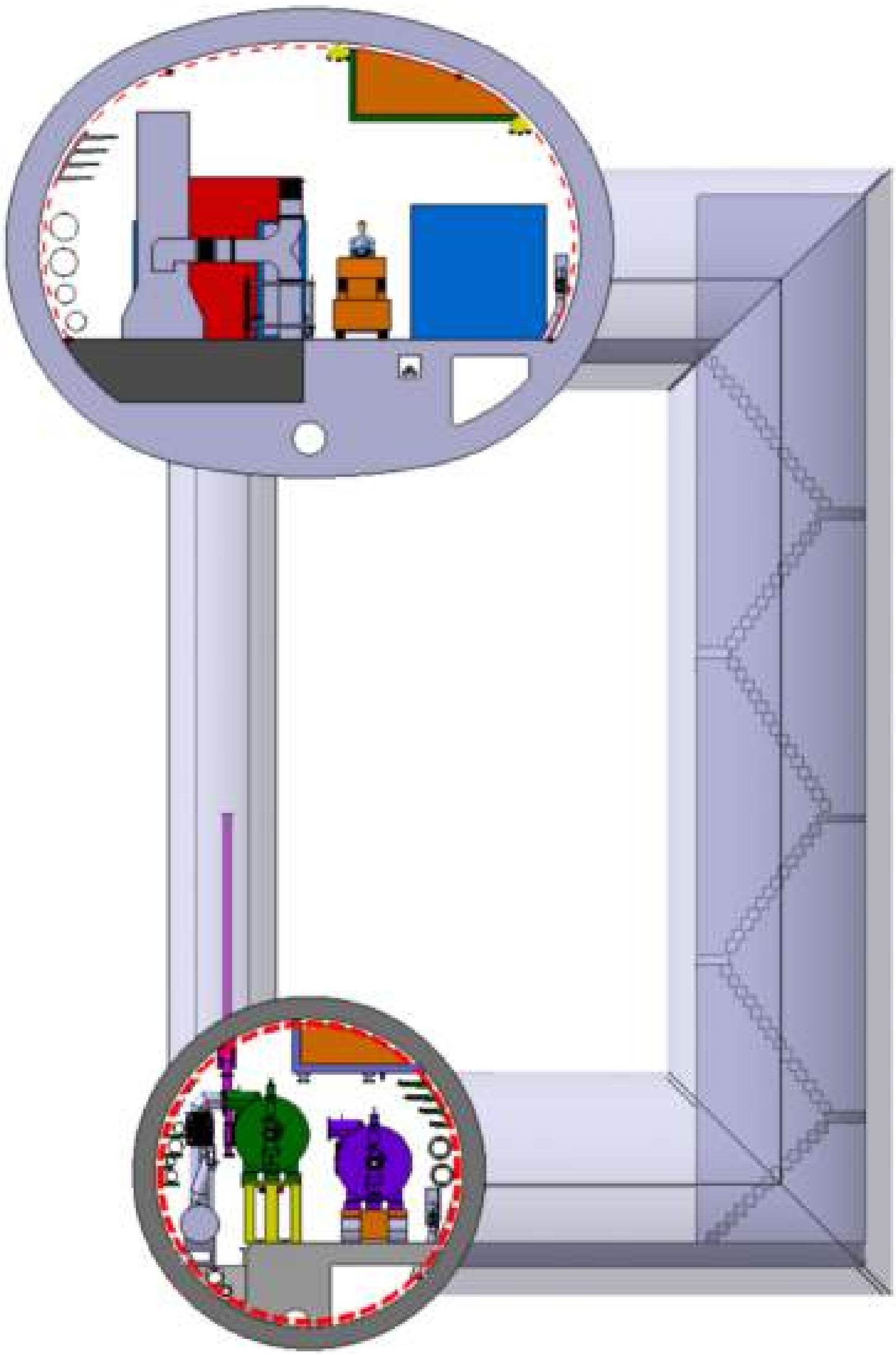

Fig. 8.37 FCC-ee point PL - tunnel and gallery cross-section

8.2.7 Integration of the arcs

The machine tunnels will house the FCC-ee accelerator and, in the following phase of operation, the FCC-hh accelerator. The civil engineering volume meet both accelerators needs.

Since the publication of the conceptual design report [13], the collider and booster have been lowered to give more space above the beam lines for safety requirements. After collecting updated requirements from all the stakeholders, the space requirements were reviewed with respect to installation and maintenance accessibility. A

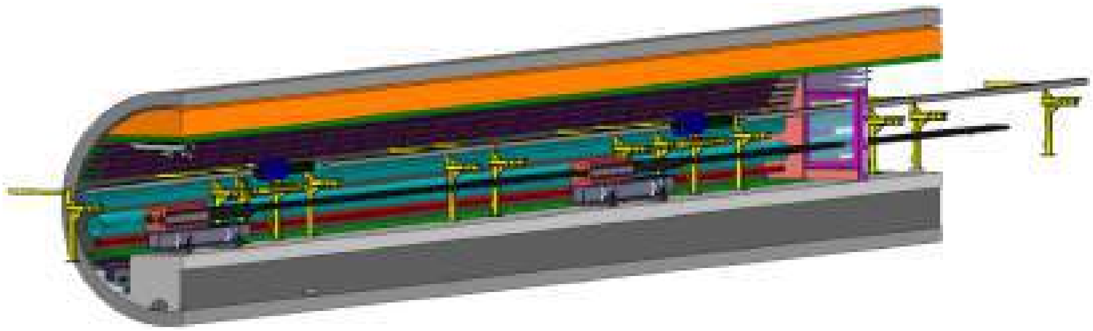

Fig. 8.38 FCC-ee layout in the arcs - longitudinal view

Fig. 8.39 FCC-ee layout in the arcs - cross-section view

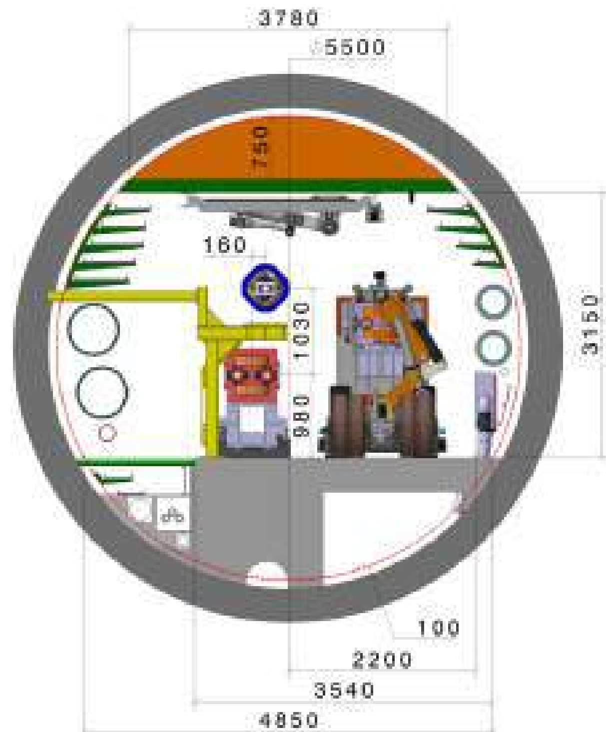

robot was added to the ceiling of the tunnel for better control of installation and maintenance of both magnets and support services.

Figures 8.38 and 8.39 are the results of the 3D integration studies for the arcs based on one of the baseline scenarios of a half-cell layout (see Fig. 3.71 and Fig. 3.72). The optimisation of the arc-supporting structures to maximise their performance, easing the installation and maintenance while minimising cost is facilitated by the FCC-ee Arc Half Cell Mock-up (see Sect. 3.10).

8.2.8 Integration of the alcoves

In addition to the technical and experiment points, there will be 56 alcoves distributed around the ring (7 per arc). These alcoves will mainly house electronics and power supplies, which need to be shielded from ionising radiation. The alcoves integrate the electrical equipment to supply a sector of the FCC, including systems installed in the alcoves themselves, plus the tunnel infrastructure like lighting, general services and a secured network. The entrance of the alcoves will also serve as a parking area for the transport vehicles (see Figs. 8.40 and 8.41). Figures 8.42 to Fig. 8.45 are the results of the 3D integration studies for the alcoves.

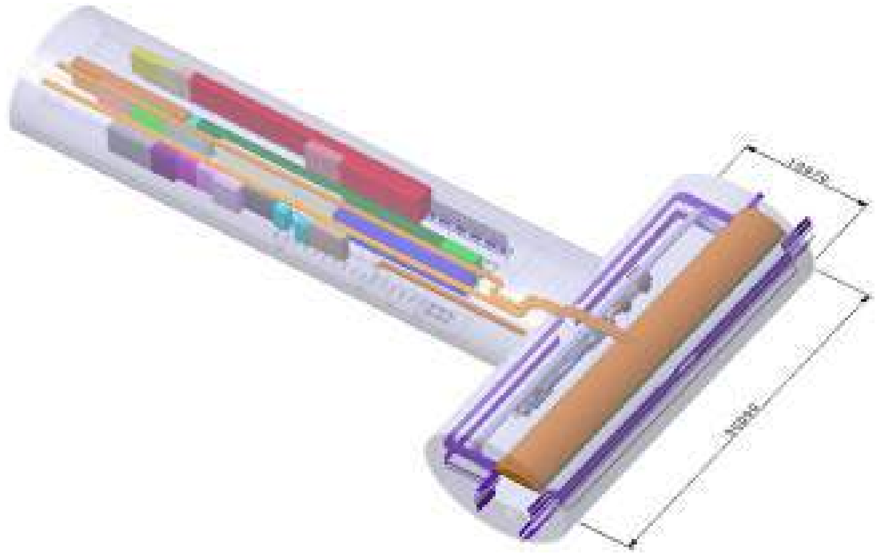

Fig. 8.40 FCC-ee alcove in the arcs with big parking area

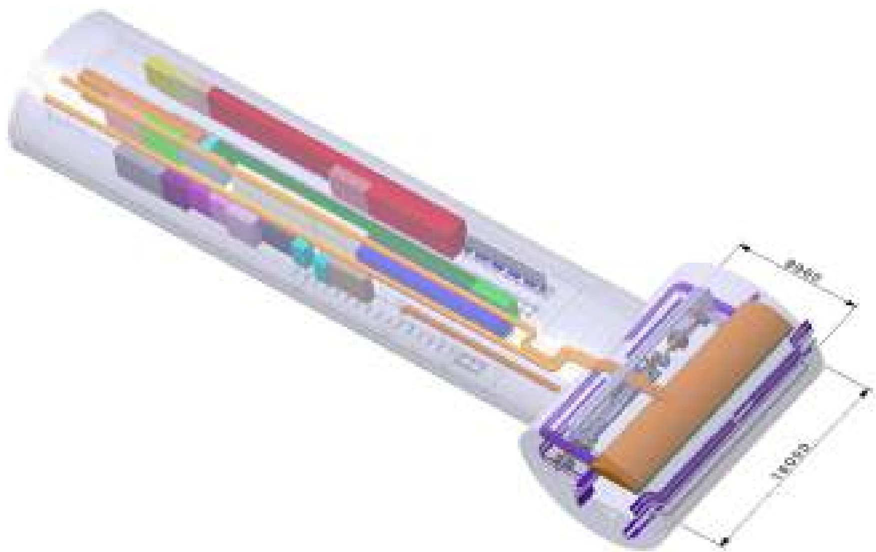

Fig. 8.41 FCC-ee alcove in the arcs with small parking area

The integration of power converters in the alcoves and the routing of cables in the machine tunnel present significant challenges due to space constraints and the high number of circuits involved. Power converters are installed in both small and big alcoves. Table 8.1 provides an overview of the number of converters in the alcoves and the number of cables in the cable trays.

There are five cables trays of varying sizes located above the booster supporting structure. The layout of the cables in the cable tray must respect the normal cabling rules. The proposed radiation shielding must reduce the radiation level to be low enough for the cables to survive for the entire lifetime of operation.

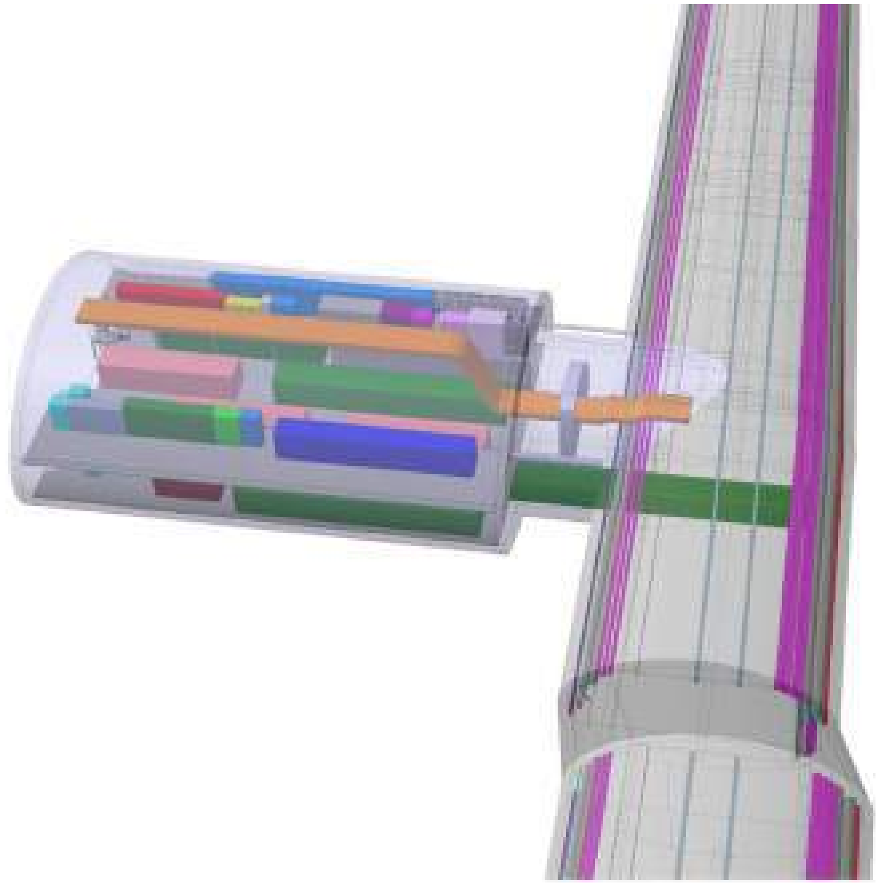

Fig. 8.42 FCC-ee alcove at point PA and PG

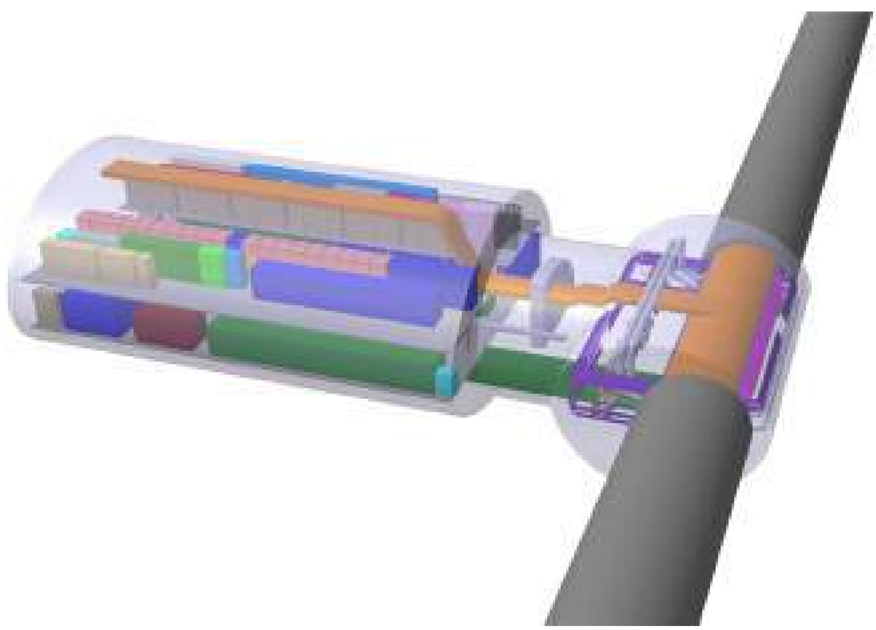

Fig. 8.43 FCC-ee alcove at point PB

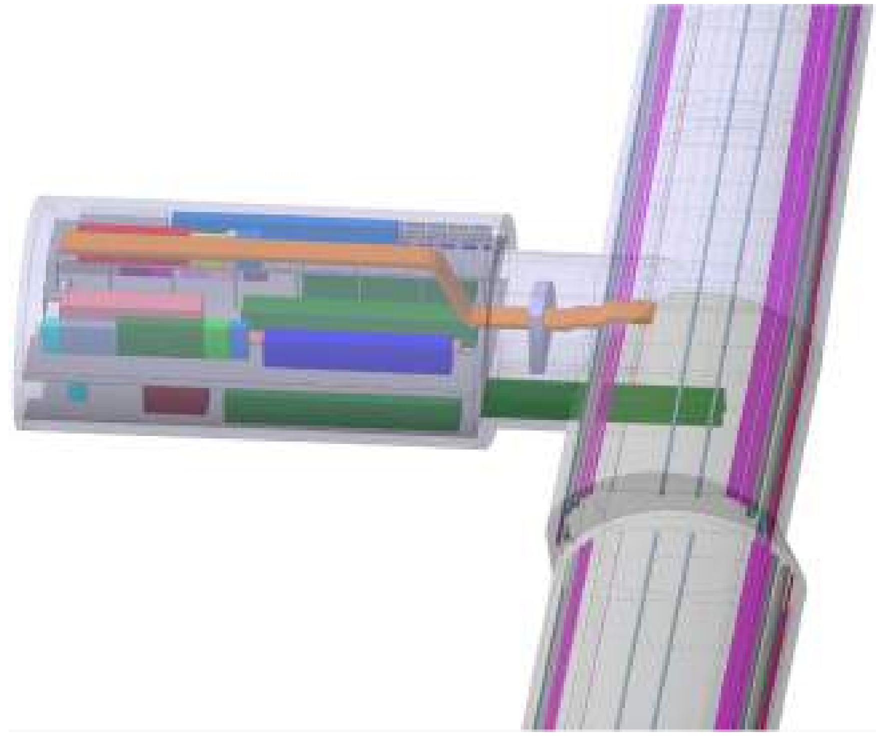

Fig. 8.44 FCC-ee alcove at points PD and PJ

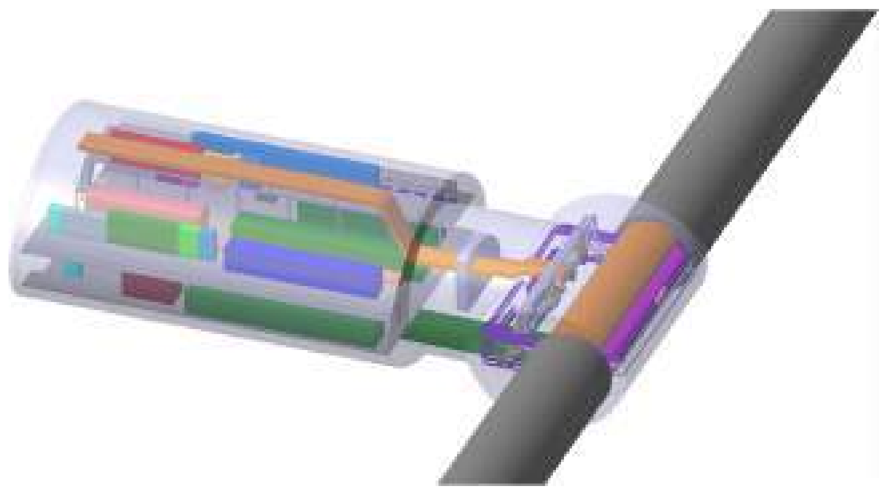

Fig. 8.45 FCC-ee alcove at point PF

8.2.9 Next phase for the integration studies

The integration studies have been made with the pre-design of volumes and will evolve with detailed technical design in the next phase of the FCC studies. Optimisation of the 3D integration studies with respect to the requirements from work packages will continue for all the areas following the identified technical and space needs:

- Optimisation of the large experiment points PA and PG [374, 375] and small experiment points PD and PJ [376], integrating more detailed detectors design in the experiment caverns,
- Optimisation of the technical point PB [377], integrating more detailed mechanical design of the accelerators and transfer lines,
- Optimisation of the technical point PF [378], integrating more detailed mechanical design of the collimation systems,
- Optimisation of the technical point PH and PL [379, 380], integrating the more detailed mechanical design of the radiofrequency and cryogenic systems and enlarging the space for transport and safety in the passage part of the tunnel,

Table 8.1 Quantities of converter racks in the alcoves and cables in cable trays at the exit of an alcove

Magnet	Quantity of racks in		Cables	
	Big alcove	Small alcove	Size (mm^2)	Quantity
Collider Dipole	27	-	1x500	2
Collider Quadrupole (F and D)	46	-	1x300	4
Collider Sextupole (F and D)	42	84	1x70	28
Collider Dipole Tapering	1	2	1x6	16
Collider Quadrupole Tapering	1	2	1x10	16
Collider Horizontal Corrector	2	3	1x10	60
Collider Vertical Corrector	2	3	1x16	60
Collider Skew Quadrupole	2	3	1x10	60
**Collider Straight Section*	*18*	-	-	-
**Collider Injection*	*n/a*	*n/a*	*n/a*	*n/a*
Booster Dipole	35	-	1x500	2
Booster Quadrupole (F and D)	86	-	1x185	8
Booster Sextupole Focusing	4	-	1x240	2
Booster Sextupole Defocusing	11	-	1x185	4
**Booster Dipole Tapering*	*1*	*2*	*1x4*	*8*
**Booster Quadrupole Tapering*	*1*	*2*	*1x6*	*8*
**Booster Horizontal Corrector*	*3*	*6*	*1x25*	*36*
**Booster Vertical Corrector*	*3*	*6*	*1x25*	*36*
**Booster Quadrupole Corrector*	*3*	*5*	*1x16*	*30*
**Booster Skew Quadrupole*	*3*	*5*	*1x16*	*30*
**Booster Straight Section*	*23*	-	-	-
**Booster Injection*	*n/a*	-	*n/a*	*n/a*
Total	**314**	**123**	-	***410***

*Magnet specifications not yet fully defined or inexistent – values extrapolated

- Optimisation of the arc half-cell [381], including the optimisation of the arc-supporting structures studied by the FCC-ee Arc Half Cell Mock-up (Sect. 3.10) to maximise their performance, ease the installation and maintenance while minimising cost.
- Optimisation of the alcoves [382], updating the control and powering racks layout with respect to technical specification evolutions.

8.3 Cooling and ventilation

8.3.1 Introduction

The cooling systems for the FCC mainly concern several water systems for the machine and its infrastructure, including accelerator and detector equipment (electronic racks, cryogenic plants, water-cooled magnets, RF equipment, etc.). Raw water will be used to fill the cooling circuits in some firefighting systems and as make-up water for the cooling towers. Chilled water is needed to extract the heat load from air in ventilation systems. Demineralised water would be employed to cool sensitive equipment like magnets, synchrotron radiation absorbers, and power converters.

The ventilation systems for the FCC should ensure the necessary conditions of humidity and temperature in the tunnel during operation, providing a supply of fresh air for personnel working within the facilities and heating for the working environment. The extraction systems must be capable of purging the air in the tunnel before access is allowed, as well as removing smoke and gases during an emergency.

Other systems comprise several and varied applications, some unrelated to cooling and ventilation. The compressed air systems for the FCC would provide compressed air to end clients requiring it, including the dampers

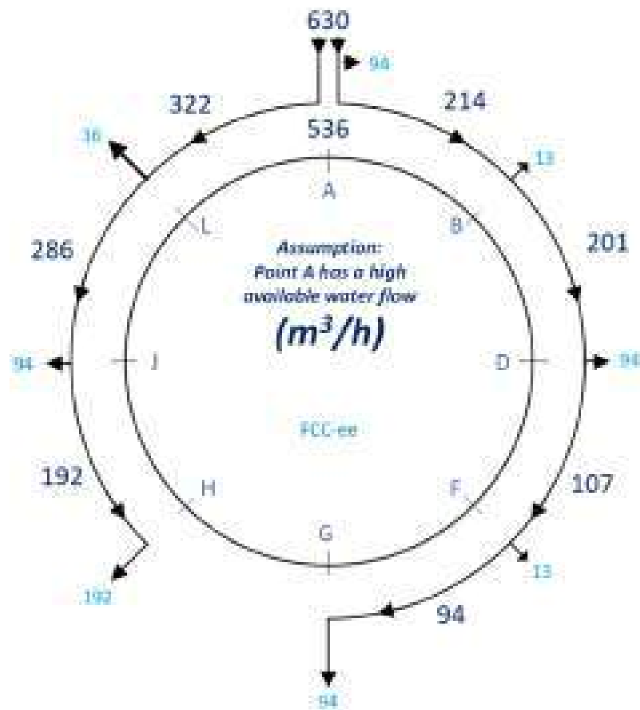

Fig. 8.46 Distribution of raw water coming from point PA, Lake Geneva

Table 8.2 Maximum make-up and effluent water of cooling towers (m^3/h)

Point	PA	PB	PD	PF	PG	PH	PJ	PL
Make-up water for cooling towers	94	13	94	13	94	192	94	36
Effluent water from cooling towers and filters	13	2	13	2	13	26	13	5

employed in the FCC tunnel. Effluent water from the cooling towers and filters would be concentrated in salts and returned to a water treatment plant. Drinking water would be needed for sanitary purposes. Finally, a drainage network would evacuate the water drained from the surface facilities and underground areas.

Cooling systems

Water supply The FCC accelerator would need to be supplied with water at the eight surface points. The main water consumers are the cooling towers, but water is also needed for the fire-fighting systems, the demineralised water production plant and all the cooling plants in the surface buildings as well as in the tunnels and caverns.

As a baseline, raw water is supplied from point PA to the rest of the accelerator, as represented in Fig. 8.46. Lake Geneva, located near PA, also serves as a water source for other accelerators within the CERN complex. Pipes running through the FCC tunnel sectors distribute water to one or more contiguous points: one branch supplies water from point PA to points PB, PD, PF, and PG, while another branch supplies water from point PA to points PL, PJ, and PH. Table 8.2 presents the approximate maximum raw water flow rates required, along with the effluent water generated at the cooling towers and filters.

An alternative design to this baseline could include the Rhône and Arve rivers as potential water sources for the FCC. In that case, point PA would feed points PL and PB with water from Lake Geneva, point PD would feed points PF and PG with water from the Arve river and point PJ would feed point PH with water from the Rhone river. This would effectively decrease the piping and pumping system sizes.

Firefighting water is available across each surface site, as well as in the service and experiment caverns. An additional flow rate of 240 m^3/h per point is allocated for firefighting purposes. Each surface site is equipped with water tanks capable of storing the estimated water supply needed for one hour.

In addition to the cooling towers and firefighting systems, the demineralised and chilled water circuits also require periodic refilling, with an estimated maximum demand of 0.5 m^3/h.

Water transfer between points is managed through a pumping station at point PA and booster pumps positioned at the bottom of the shaft at point PF, as illustrated in Fig. 8.47, which also depicts the approximate surface and underground elevations, along with shaft depths.

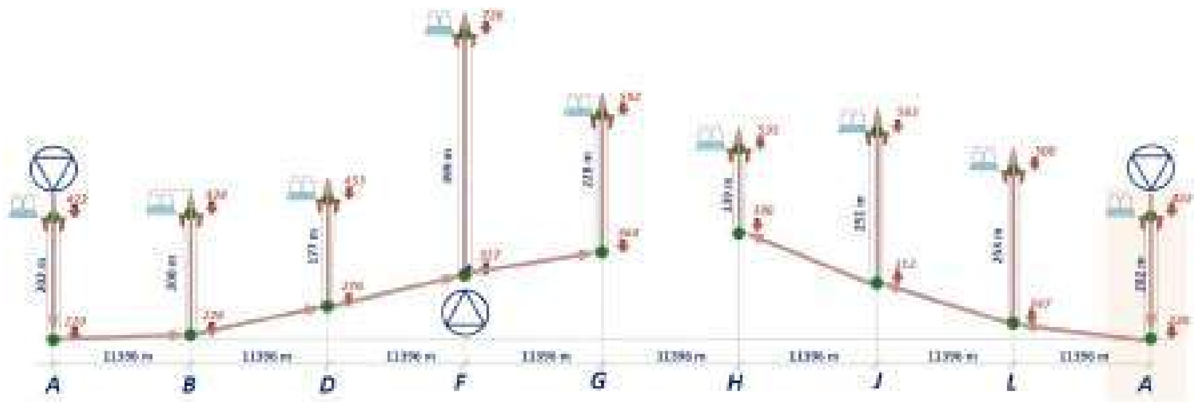

Fig. 8.47 Pumping stations and booster pumps of the raw water system

Table 8.3 Cooling demands (MW) of the primary circuit

Point	PA	PB	PD	PF	PG	PH	PJ	PL
Cryogenics						34.0		10.0
Experiments	0.5		0.5		0.5		0.5	
General Services	2.0	2.0	2.0	2.0	2.0	2.0	2.0	2.0
Power Converters						4.5		0.1
Chilled Water	5.8	5.2	5.8	5.2	5.8	11.3	5.8	5.8
Underground	42.5	1.0	42.5	1.0	42.5	48.9	42.5	2.7
Total power required	50.8	8.2	50.8	8.2	50.8	100.7	50.8	20.6

Table 8.4 Cooling capacity (MW) of the primary circuit

Point	PA	PB	PD	PF	PG	PH	PJ	PL
Number of cells per cooling tower	6	2	6	2	6	8	6	3
Cooling capacity per cell	10.0	10.0	10.0	10.0	10.0	15.0	10.0	11.0
Total cooling capacity	60.0	20.0	60.0	20.0	60.0	120.0	60.0	33.0

Primary cooling circuits The cooling towers will remove most of the heat generated by the accelerator equipment, the detectors and the technical areas. There will be a set of field erected, open wet cooling towers per surface site.

The evaporative cooling towers are of the mechanical-induced draft counter-flow type. Ventilation fans are positioned at the top of the cells, ensuring easy access for maintenance. Each tower consists of multiple cells with identical cooling capacity, with one cell per tower reserved for backup purposes (N + 1 redundancy). The towers are designed to operate with water treated with anti-corrosion and biocide chemicals. The cooling towers comply with the following parameters and conditions:

- Outside air wet bulb temperature: 21 °C.
- Cooling tower inlet temperature: 40 °C.
- Cooling tower outlet maximum temperature: 25 °C.

The cooling power to be installed at each point has been determined based on the users' cooling requirements. Certain equipment, particularly cryogenic systems, will be cooled directly by the primary circuit, while other equipment will be connected to the primary systems via heat exchangers (secondary circuits). In most cases, the secondary circuits will operate in a closed loop using demineralised water.

Table 8.3 gives an overview of the cooling requirements by type of equipment: each row represents a different type of equipment, except for the 'Underground' row, which groups all equipment cooled from the same primary circuit and is located underground. In addition, Table 8.4 provides the cooling tower complex capacity per point, including the backup cells. Figure 8.48 shows the cooling tower complexes per point, including the backup cells.

The cooling towers operate continuously in open air with the ambient conditions present in Geneva and its surrounding area, with only a short stoppage each year to carry out maintenance. The baseline strategy implemented

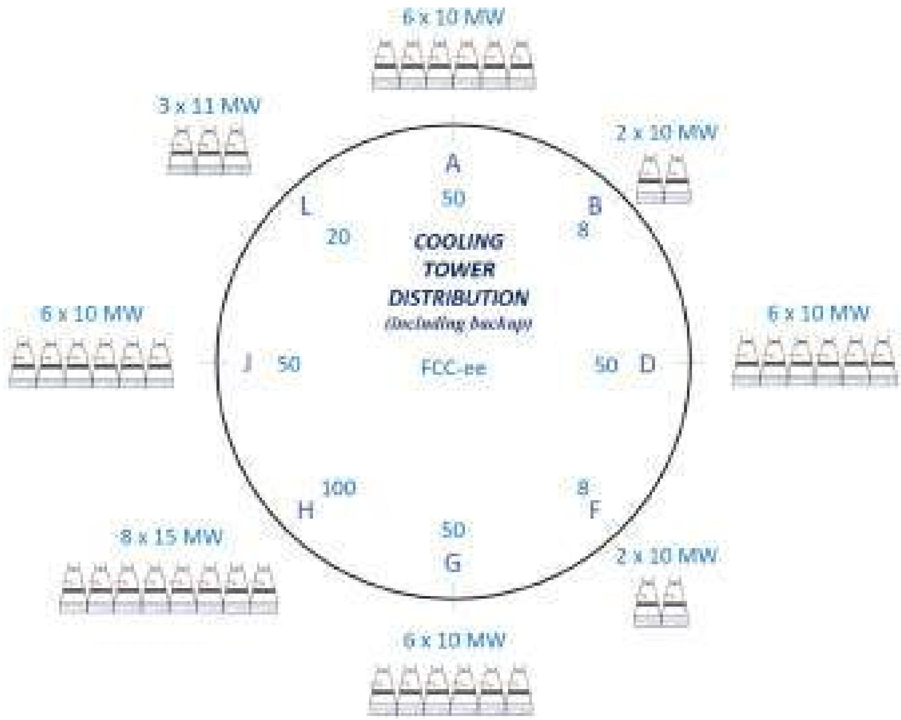

Fig. 8.48 Cooling tower complex for FCC-ee, including the backup cells

to reduce water consumption in the cooling tower is the recycling of its blowdown water. To do so, its conductivity is first reduced to values of around 20 µS/cm. The resulting water is then mixed with normal raw water, which is eventually used as a low-conductivity make-up water for the cooling towers.

An alternative to the baseline design is the adoption of hybrid cooling tower technology, which combines the advantages of both wet and dry cooling methods to enhance performance and reduce the environmental impact. In this system, the wet cooling tower - similar to the baseline design - uses water to absorb heat from the process, releasing it through evaporation. Dry air-water heat exchangers supplement this. The airflows from the wet and dry sections are mixed before reaching the fan stack, helping to reduce or eliminate the visible water vapour plume typically observed in wet cooling towers, particularly under certain weather conditions. However, hybrid cooling towers require a larger surface area and entail higher costs.

Demineralised water cooling circuits The secondary circuits are connected to the primary system through heat exchangers. In most cases, the secondary circuits use demineralised water in a closed loop. Demineralised water cooling circuits are grouped according to the typology of the equipment to be cooled and to the equipment pressure ratings. Since the underground areas are up to 400 m below ground level (case of point PF), it is necessary to install an underground cooling station in the service cavern at all points. Here, heat exchangers separate the circuit coming from the surface (with a static pressure of up to 40 bar) from the underground distribution circuit. For operability and maintenance purposes, both surface and underground cooling stations are accessible during accelerator running. Figure 8.49 shows the demineralised water distribution in the FCC tunnel, the water being supplied at the experiment points. The types of underground equipment cooled by demineralised water are listed in Table 8.5. The magnets, alcoves and SR absorbers rows correspond to equipment located in the tunnel. The other four columns refer to equipment located close to the access points.

The heat loads from the accelerator's radio frequency system come directly from the RF equipment. Furthermore, the cryogenic installation, which cools part of the equipment to cryogenic temperatures, is cooled by primary water, not demineralised water. The first fill of the demineralised water circuits can be done by a CERN-owned on-truck demineralised water production station and leave the topping up of the circuits to smaller local demineralisers at each point. Alternatives include renting an on-truck production station or designing the local demineralisers to carry out the first fill too. In this case, the production station would be underutilised, operating at reduced capacity most of the time.

Chilled water cooling circuits Chilled water at 6 °C is needed for air dehumidification and cooling purposes and for the cooling of electrical equipment with specific temperature requirements.

The water is cooled by industrial air-cooled or water-cooled chillers. The maximum heat load to be removed by chilled water per point is given in Table 8.6, together with the flow needed for a temperature difference of 6 K

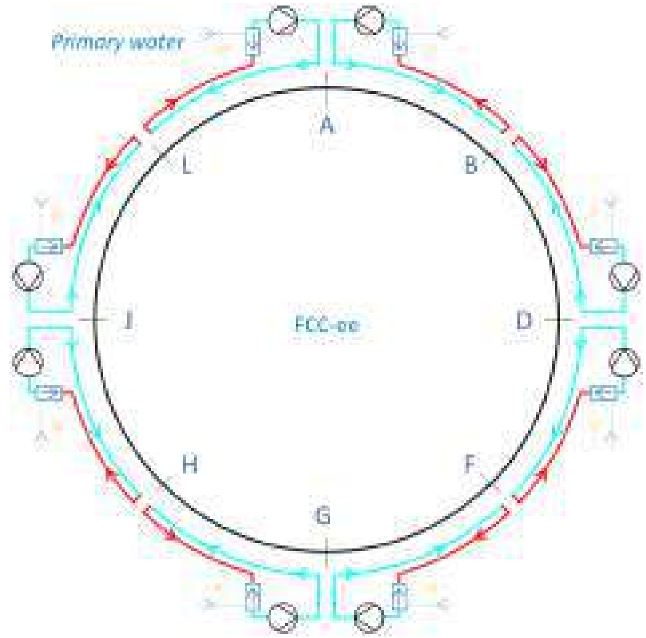

Fig. 8.49 Demineralised water distribution in the FCC tunnel

Table 8.5 Demineralised water cooling demands (MW) per underground user

Point / Sector	PA / PL-PA PA-PB	PB	PD / PB-PD PD-PF	PF	PG / PH-PJ PJ-PL	PH	PJ / PH-PJ PJ-PL	PL
Magnets	2×7.1		2×7.1		2×7.1		2×7.1	
Alcoves	2×0.9		2×0.9		2×0.9		2×0.9	
SR Absorbers	2×12.5		2×12.5		2×12.5		2×12.5	
Experiment Area	0.5		0.5		0.5		0.5	
Power Converters	1.0	1.0	1.0	1.0	1.0	1.0	1.0	1.0
RF						45.7		0.7
Cryogenics*	0.01*		0.01*		0.01*	2.2*	0.01*	1.0*
Total power	42.5	1.0	42.5	1.0	42.5	48.9	42.5	2.7

* Cryogenic equipment uses primary water quality in its secondary circuit.

Table 8.6 Chilled water cooling demands (kW) and supply water flow rate (m^3/h) per point

Point	PA	PB	PD	PF	PG	PH	PJ	PL
Cooling power	4895	4322	4875	4322	4895	9367	4875	4757
Flow rate	703	620	700	620	703	1345	700	683

between the supply and return chilled water temperature. The number of chillers and power per chiller is shown in Table 8.7: all of them have similar cooling demands except for point PH, which has a higher demand due to hosting the most power-intensive RF section.

The distribution of chilled water in the tunnel is designed as shown in Fig. 8.50. The selection of refrigerant for the chillers will be guided by both technological compatibility and environmental sustainability, with careful consideration of ongoing research developments. This decision will be made at a later stage, ensuring it reflects the latest advances and best practices. Additionally, the potential integration of mixed water production at 12 °C, which is not currently planned, will be assessed based on user requirements and implemented if deemed necessary to optimise efficiency and performance.

Table 8.7 Chilled water cooling capacity (kW) per point

Point	PA	PB	PD	PF	PG	PH	PJ	PL
Number of chillers	6	6	6	6	6	7	6	6
Cooling power of chiller	1000	900	1000	900	1000	1800	1000	1000
Total cooling power	6000	5400	6000	5400	6000	12,600	6000	6000

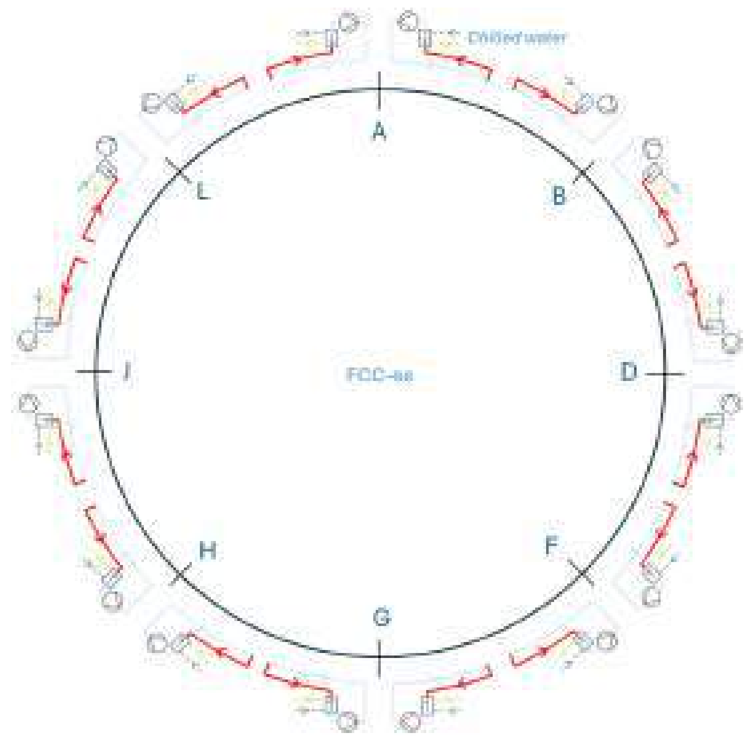

Fig. 8.50 Chilled water distribution in the FCC tunnel

8.3.2 Ventilation systems

Design principles and heat loads The FCC ventilation systems supply a sufficient amount of fresh air to meet the air quality and thermal requirements: the ambient temperature is suitable for the accelerator and auxiliary technical equipment. In addition, the air supplied is dehumidified to prevent condensation on equipment and structures.

In the current design, the underground areas are generally ventilated by air-handling units located on the surface, accessible at all times. Redundant units (N + 1) are planned everywhere to avoid affecting accelerator operation in case of breakdown. Additionally, fan coils provide local cooling wherever necessary. Tables 8.8, 8.9 and 8.10 present the air heat loads in all surface sites, in the underground areas and for each sector of the tunnel, respectively.

Tunnel ventilation For the FCC tunnel, a semi-transverse ventilation scheme has been adopted. The air is supplied through a specific duct running throughout the sector and extracted either through the tunnel itself or by an emergency extraction duct. Air is supplied to each sector from both endpoints to ensure air supply even in case of a duct failure; the same configuration has been adopted for the extraction (Fig. 8.51).

The air supply duct runs in the concrete floor slab and supplies air to the tunnel about every 100 m via diffusers at floor level. A closed circular segment in the upper part of the tunnel is used for emergency extraction. The structure consists of 70 mm thick steel panels, secured to the tunnel lining using post-drilled anchors, and is equipped with passive fire protection on both sides. Inlet diffusers and extraction grills are strategically offset to ensure optimal air distribution within the tunnel and to prevent direct airflow shortcuts between supply and extraction points.

Fire-resistant dampers are installed at every connection between diffusers and extraction grills, enhancing ventilation control in the event of a fire or helium release. These dampers help manage airflow within the affected tunnel compartment, improving safety and containment.

Table 8.8 Heat loads on air (kW) on the surface, per point

Point	PA	PB	PD	PF	PG	PH	PJ	PL
Cryogenics*	13		13		13	1400*	13	402*
Experiment Areas	50		40		50		40	
General Services	500	500	500	500	500	500	500	500
Power Converters*						2250*		35*
Shaft pressurisation	300	150	300	150	300	150	300	150
Fresh air for Underground	150	50	150	50	150	150	150	150
Total heat load to Chilled water	1013	700	1003	700	1013	800	1003	800

* Cryogenics and power converters heat loads that are extracted without chilled water.

Table 8.9 Heat loads on air (kW) underground, per point

Point	PA	PB	PD	PF	PG	PH	PJ	PL
Cryogenics	10		10		10	145	10	60
RF						4600		75
Experiment Areas	50		40		50		40	
Power Converters	220	220	220	220	220	220	220	220
CV Zone Underground	200		200		200	200	200	200
Total heat load to Chilled water	480	220	470	220	480	5165	470	555

Table 8.10 Heat loads on air (kW) for each arc of the tunnel

Magnets	Cables*	Synchrotron radiation absorbers	Alcoves	Total heat load to Chilled water
352	2500*	250	300	3402

* Heat load from the cables extracted without chilled water.

To further control the spread of smoke and helium gas, each tunnel sector is divided into 28 compartments, separated by fixed fireproof panels and automatic doors. This design prevents smoke propagation in case of fire and mitigates the spread of helium gas in the event of an accidental leak from accelerator equipment.

Under normal conditions, there are four different working modes for tunnel ventilation.

- *Run mode*: the accelerator is in operation, and most of the electrical systems are powered; a high heat load is transferred to the air in this mode. Additionally, radiation protection aspects are taken into consideration.
- *Access mode*: technical personnel can work in the tunnel, and therefore, occupational safety requirements are considered.
- *Economy mode*: a minimum airflow is employed in situations without personnel access, reducing the airflow. In this mode, the dew point of the air is controlled, but wider ranges of dry temperature are accepted to save energy.
- *Flushing mode*: used to renew the air underground completely and takes place when moving from Run to Access modes. The extracted volumes are filtered before release.

The airflow requirements under normal and emergency conditions are presented in Table 8.11. When the accelerator is in operation with full heat loads, the maximum dry temperature is limited to 32 °C and the maximum dew point is limited to 12 °C, inside the tunnel. In this mode, the nominal supply temperature is of 17 °C. In flushing mode, the minimum supply temperature is 15 °C. If the external temperature is below 0 °C, the airflow will be reduced to maintain the 15 °C supply temperature. For the access mode, the temperature inside the tunnel is set between a minimum of 18 °C and a maximum of 26 °C, while respecting the regulations regarding air renewal. In all operating modes, environmental sustainability and energy efficiency are key priorities. As a general

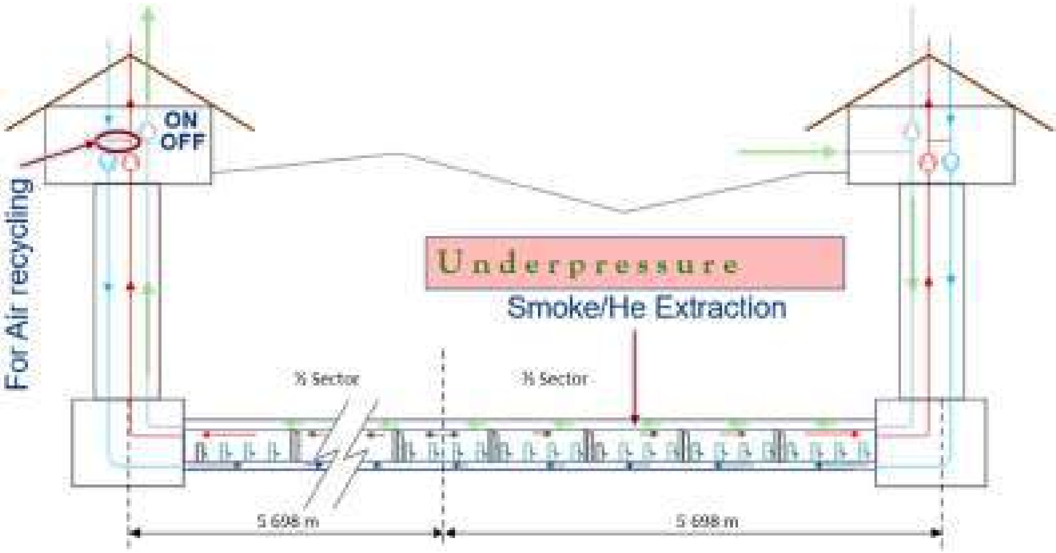

Fig. 8.51 Operation of the ventilation elements in one sector of the tunnel during normal operation. Smoke and helium extraction in green, general extraction in red and air supply in blue

Table 8.11 Airflow conditions for the tunnel ventilation

	Air supply	Regular extraction	Emergency extraction
Run and Access mode	2×27,000 m^3/h per sector.	2×27,000 m^3/h per sector.	Standby under pressure operation, no extraction.
Flushing mode	100,000 m^3/h per sector.	100,000 m^3/h per sector.	Standby under pressure operation, no extraction.
Emergency conditions	10,000 m^3/h in affected compartments (max. 2). 3500 m^3/h in adjacent compartments (max. 2). 2160 m^3/h in the rest of the compartments.	Max. 54,000 m^3/h Sharing between the two shafts depends on affected compartment location.	10,000 m^3/h in affected compartments (max. 2). 3500 m^3/h in adjacent compartments (max. 2).

principle, the ventilation system is designed to minimise electrical consumption by incorporating free cooling and air recycling strategies.

In run and access modes, airflow is supplied through an inlet duct integrated into the tunnel floor slab. In flushing mode, however, air is not delivered via this duct but is distributed longitudinally across the entire tunnel cross-section.

An alternative approach to tunnel ventilation would be to extend the longitudinal airflow concept of flushing mode to both run and access modes, resulting in a fully longitudinal ventilation scheme. This solution would simplify system controls, enhance robustness, and free up space required for the integration of the inlet duct. However, before implementation, the system's performance under degraded conditions and emergency scenarios must be carefully assessed to ensure full compliance with safety standards.

Experiment areas ventilation The ventilation system for the experiment areas (experiment caverns at points PA, PD, PG, and PJ) consists of a ventilation system on the surface with a supply and extraction unit and the possibility of recycling 100% of the air or the option to supply a controlled percentage of fresh air. The ventilation principle for the experiment caverns is represented in Fig. 8.52. No additional local cooling systems are planned.

The nominal airflow conditions are presented in Table 8.12. During operation, the experiment areas will have a temperature distribution of 18/32 °C from floor to ceiling. The same parameters as for the FCC tunnel are applicable in flushing and access modes.

RF areas ventilation The RF system is cooled mainly by the demineralised water circuits in the underground klystron galleries of points PH and PL. A considerable heat load nevertheless remains to be extracted: 4600 kW in point PH and 75 kW in point PL.

Table 8.12 Airflow conditions for the experiment areas ventilation

	Air supply	Regular extraction	Gas extraction
Run and Access mode	50,000 m^3/h to 70,000 m^3/h	50,000 m^3/h to 70,000 m^3/h	Switched off
Flushing mode	50,000 m^3/h to 70,000 m^3/h	50,000 m^3/h to 70,000 m^3/h	Switched off
Fire emergency (gas extraction)	Up to 70,000 m^3/h	Up to 70,000 m^3/h	Switched off
Gas emergency (gas extraction)	20,000 m^3/h	Switched off	20,000 m^3/h

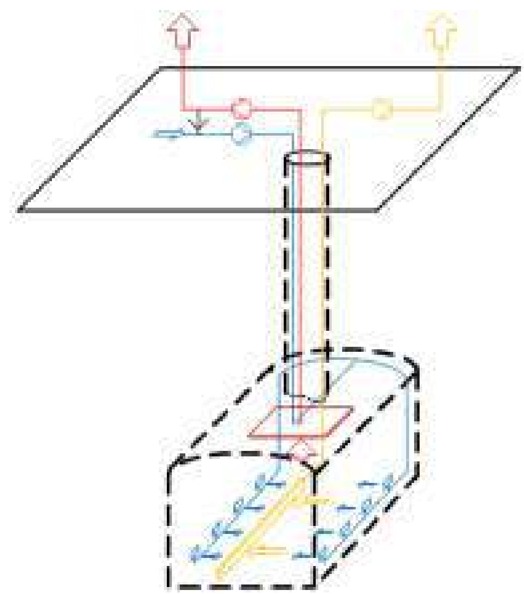

Fig. 8.52 Ventilation systems of the experiment cavern. Smoke and helium extraction in orange, general extraction in red and air supply in blue

Table 8.13 Airflow conditions for the RF areas ventilation

	Air supply	Regular extraction	Emergency extraction
Run and Access mode	30,000 m^3/h	30,000 m^3/h	Switched off
Emergency conditions	<30,000 m^3/h	<30,000 m^3/h	10,000 m^3/h in affected compartments (max. 2). 3500 m^3/h in adjacent compartments (max. 2).

The ventilation design features main ventilation from the surface, supplemented by a fresh air supply, and local cooling with fan coils cooled by chilled water. Table 8.13 presents the airflow requirements for each of the modes; flushing is not needed because contaminants are not present in the klystron gallery equipment.

Technical areas ventilation Dedicated ventilation systems serve the technical zones around each point and the connecting galleries between areas. These areas comprise the service caverns and connecting galleries at all points.

The design of each ventilation system differs because the general demands and heat loads vary significantly between the points. A difference is made between the technical areas in experiment points (points PA, PD, PG, PJ), the technical areas in technical points (points PB and PF), and the technical areas in RF points (points PH and PL). The ventilation solutions proposed under normal and emergency conditions are presented in Table 8.14. Finally, other ventilation systems pressurise airlocks to create pressure cascades for safety purposes.

Surface buildings ventilation Each surface building will be ventilated by a dedicated air-handling unit. Where the building size requires it, it is planned to have several units in the same building, each of them taking care of a part of the building. At present, it is not considered necessary to have redundant units in these buildings. Should this be needed, it can easily be implemented. All surface buildings will be equipped with a mechanical system on the roof to extract smoke, designed and certified for operation at 400 °C for a minimum period of 2 h.

Table 8.14 Airflow conditions for ventilation of the technical areas

	Air supply	Extraction	Emergency extraction
Technical Areas in Experiment points	Fresh air for UAs, 20,000 m^3/h. Ventilation for Service Cavern, 40,000 m^3/h.	Extraction through the Service Cavern, 60,000 m^3/h.	Emergency extraction through the Ventilation system for Service Cavern, 60,000 m^3/h.
Technical Areas in Technical points	Ventilation for Service Cavern, 40,000 m^3/h.	Extraction through the Service Cavern, 40,000 m^3/h.	Emergency extraction through the Ventilation system for Service Cavern, 40,000 m^3/h.
Technical Areas in RF points	Ventilation for Service Cavern, 40,000 m^3/h.	Extraction through the Service Cavern, 40,000 m^3/h.	Emergency extraction through the Ventilation system for Service Cavern, 40,000 m^3/h.

8.3.3 Other systems

Drinking water Drinking water will be used by personnel. It is planned that this will be provided by the local water network at each point.

Reject water and sumps Discharging effluent water into local disposal networks or small water bodies presents challenges due to its high salinity levels. To address this, a centralised treatment system is proposed, in which all effluent water is transported through the tunnel to a treatment plant at point PA.

An alternative approach would involve local treatment of effluent water at each point. Implementing minimum or zero liquid discharge (ZLD) technologies could significantly reduce the volume of effluent by concentrating the salts into solid pellets. However, this solution would introduce higher costs and increased surface area requirements due to the complexity of these treatment systems.

Compressed air The compressed air for all equipment and actuators will be provided by compressed air stations located on the surface at each point. These will supply both surface and underground areas. A level of redundancy of N + 1 is planned to ensure the reliability and maintainability of the plant.

Sumps and clear water Two separate pump systems to lift clear water and sewage will be installed underground at each point. They will be connected to the point's local drainage network. All underground equipment (tunnel and caverns) must have redundancy in order to avoid affecting operation in case of a breakdown. The sump pumping capacities for the tunnel at the points are 30 m^3/h, and the experiment caverns have an additional 30 m^3/h of sump pumping capacity. Alarms for 'high level' and 'level too high' will be implemented in all basins.

The key parameters of the clear water, including temperature and pH, will be systematically monitored prior to discharge. If the clear water fails to meet the required quality standards or poses a risk of environmental contamination, appropriate mitigation measures will be implemented. These measures may include the activation of retention basins at designated discharge points to ensure compliance with environmental regulations.

8.4 Power consumption and electricity distribution

8.4.1 Energy consumption of the FCC-ee machine

Overall power demand Since FCC-ee is a large-scale accelerator, accurately identifying and understanding its electrical loads is essential for designing a robust electricity infrastructure and assessing overall energy consumption. The accelerator's main electrical loads include the radiofrequency (RF) systems, magnets, cryogenic systems, cooling and ventilation, experiments, and general services, which cover all general-purpose energy needs. The total power demand varies depending on the operation mode of the machine (Z, WW, H, and $t\bar{t}$).

The collider radiofrequency system represents the largest electrical load, requiring 146 MW across all operation modes. It consistently supplies 50 MW per beam to compensate for synchrotron radiation losses. The global efficiency of the RF chain is 68%, with the goal of having klystron amplifiers operating at 80% efficiency. The power demand for the magnets and their powering chains depends on the beam energy, starting from 6 MW in Z mode, increasing to 39 MW in H mode, and reaching 89 MW in $t\bar{t}$ mode.

The cryogenic power demand remains relatively low at 13 MW up to H mode but becomes significant at 35 MW in $t\bar{t}$ mode. The cooling and ventilation systems require between 25 MW and 33 MW, while the power demand of the experiments and data centres is estimated to be 10 MW for all four experiments, with an additional 4 MW

Table 8.15 Power demand by technical system, in MW

Beam energy, GeV	Z	W	H	$t\bar{t}$
	45.6	80	120	182.5
Collider radiofrequency	146	146	146	146
Booster radiofrequency	2	2	2	2
Collider cryogenics	1.2	11.5	11.5	27.6
Booster cryogenics	0.35	0.8	1.5	7.4
Cooling and ventilation	25	26	28	33
Collider magnets	6	17	39	89
Booster magnets	1	3	5	11
4 experiments, PA, PD, PG, PJ	10	10	10	10
4 datacentres, PA, PD, PG, PJ	4	4	4	4
General services	26	26	26	26
Total power during beam operation	222	247	273	357

Table 8.16 Power demand by operation mode, in MW

Beam energy mode	Z	W	H	$t\bar{t}$
Shutdown	30	33	34	41
Technical stop	67	78	81	108
Short downtime	74	98	125	209
Commissioning	144	163	177	233
Machine Development	96	121	147	231
Beam operation	222	247	273	357

allocated for local data centres, given that detailed technical designs are not yet available. Finally, general services are expected to require up to 26 MW, based on scaling from LHC consumption.

These estimates will form the basis for the development of the FCC-ee's electrical infrastructure, ensuring it can accommodate the varying power demands while optimising efficiency and sustainability. Table 8.15 shows the estimate of the maximum power demand for the four different modes of operation.

Operational model The energy consumption is estimated based on the accelerator operational model. The power demand depends on the time of year and the machine's state. The machine schedule defines the different periods during the year, and the power demand varies from the minimum during the shutdown to the maximum during beam operation.

The schedule consists of six distinct periods: shutdown, commissioning, physics operation, short downtime (without access to the machine), technical stops (or long downtime), and machine developments. The power demand calculated for each period is shown in Table 8.16.

The machine schedule comprises 120 days of shutdown, 30 days of commissioning, 20 days of machine development, 10 days of technical stops and 185 days for physics, see Table 8.17.

The machine availability is expected to be at least 80%. Unlike other accelerators, FCC-ee does not lose time for acceleration, meaning that its operational efficiency is determined solely by technical downtime and the associated time required for beam refilling and recovery. Based on empirical data from similar machines, the effective efficiency factor is estimated to be approximately equal to the hardware availability (80%), with an additional 5% reduction to account for beam recovery after a failure.

Of the 185 days allocated for physics operation, an estimated 46 days are lost due to downtime, leaving 139 days for colliding beams.

The downtime is categorised into three types: long stops due to major failures, such as the loss of cryogenic conditions or RF cavity conditioning; downtime with machine access, allowing repairs and maintenance; and downtime between cycles, which includes beam dumps and refilling that do not require machine access.

Table 8.17 Distribution of operating modes in time

Period type	Duration
Shutdown	120 days
Commissioning	30 days
Physics Operation	185 days
Beam colliding	139 days
Downtime	46 days
Machine development	20 days
Technical Stops	10 days

Table 8.18 Power demand by point, $t\bar{t}$ mode

Point	Type	Max power [MW]
Point PA	Experiment	23
Point PB		20
Point PD	Experiment	23
Point PF		20
Point PG	Experiment	23
Point PH	Collider RF	194
Point PJ	Experiment	23
Point PL	Booster RF	30

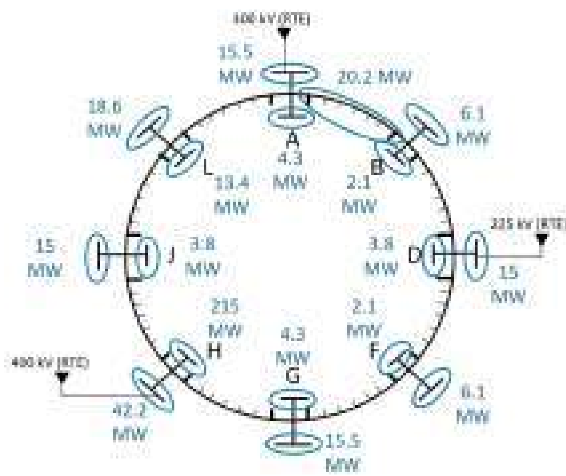

Fig. 8.53 Load mapping of the FCC-ee machine

Power demand by points As the distribution of the power demand is not uniform across the points (see Table 8.18), the installed power and its position need to be known to be able to design the electrical infrastructure. The load survey performed in the first phase of the study provided the following localised power requirements:

- Surface at each point: between 6.1 and 42.2 MW,
- Underground at each point: between 2.1 and 215 MW,
- Tunnel between points: around 20.2 MW.

This first analysis allowed the creation of a load mapping of the FCC-ee machine for the design of its electrical network, see Fig. 8.53.

Energy consumption With the schedule and the expected power demand for the various periods, the annual energy consumption can be calculated, see Tables 8.19 and 8.20 for Z and $t\bar{t}$ operation respectively. The energy consumption varies from 1.07 TWh/year for Z mode operation to 1.77 TWh/year for $t\bar{t}$ mode operation. For comparison, the complete CERN complex energy consumption in 2024 was 1.3 TWh/year. This yearly consumption is expected to increase after the completion of the HL-LHC project.

Table 8.19 Energy Consumption, Z mode

Z mode	Duration, days	Power, MW	Energy, GWh
Beam colliding	139	222	740
Downtime	46	67	75
Commissioning	30	144	103
Machine development	20	96	46
Technical Stops	10	67	16
Shutdown	120	30	86
Total Z mode operation			1070

Table 8.20 Energy consumption, $t\bar{t}$ mode

TT mode	Duration, days	Power, MW	Energy, GWh
Beam colliding	139	357	1200
Downtime	46	108	157
Commissioning	30	233	168
Machine development	20	231	111
Technical Stops	10	108	26
Shutdown	120	41	117
Total $t\bar{t}$ mode operation			1770

Grid connections To provide power to the machine which is spread over many points, the strategy is to connect three points to the high-voltage European grid and to create an internal transmission network through the tunnel to distribute it to the other points. These connections will be rated at the same level of 220 MVA at each point. These points are PH, PA, and PD (see Fig. 8.54) and will be connected to the French grid, operated by RTE. RTE confirmed that, beside a minimum additional infrastructure to connect the new FCC points, no further upgrades or power stations are required in the existing French grid.

PH needs a dedicated substation for the collider RF systems. PA can be powered through an existing CERN substation. PD is needed to cover the other parts of the machine, for redundancy with PA and for the future operation of FCC-hh.

In addition to that, all the points will be connected at much lower power to the local distribution grids: SIG (Services Industriels de Genève) for the point in Switzerland (PB), and ENEDIS for points located in France, except for point PG which will be connected to Energie et Services de Seyssel. These connections are needed for the civil engineering works, and later they will be used as backup sources. The voltage level of these connections will be at medium voltage (20 kV in France, 18 kV in Switzerland), and they will be in general rated at 14 MW, to cover the TBM loads in the civil engineering works phase.

8.4.2 FCC electrical grid

Transmission network The FCC can be powered from the French national grid, operated by RTE (France's Transmission System Operator, Réseau de Transport d'Électricité), through three access points (PA, PD, and PH) at two possible voltage levels (400 kV or 225 kV). Power will be distributed to the other access points via an internal high-voltage (HV) transmission network, which will be implemented using HV cables installed within the accelerator tunnel. These cables will link all access points, ensuring power transmission from one point to the adjacent ones.

Following verification with RTE, it has been confirmed that operating two or three high-voltage supplies of the FCC in parallel will not be permitted by the grid operator, as this would introduce the risk of uncontrolled or unwanted power transfers between connection points.

As a result, the option of operating the HV grid of the FCC as a closed loop, initially considered feasible, has been discarded at this stage of the study. Instead, the three high-voltage supplies will be operated in an antenna configuration, with each connection radially supplying other points in the accelerator. In the normal configuration, three distinct sectors have been defined, each powered by a single RTE connection: PA will supply PB, PJ, and PL; PD will supply PF and PG; while PH will operate standalone, as the RF systems at this location represent the largest power load of the machine.

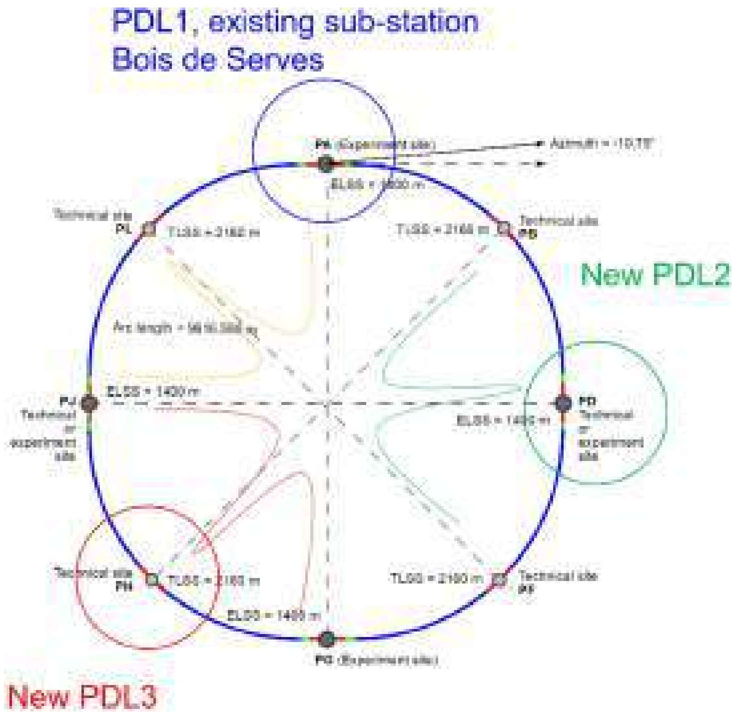

Fig. 8.54 High Voltage grid connections, PDL as delivery points

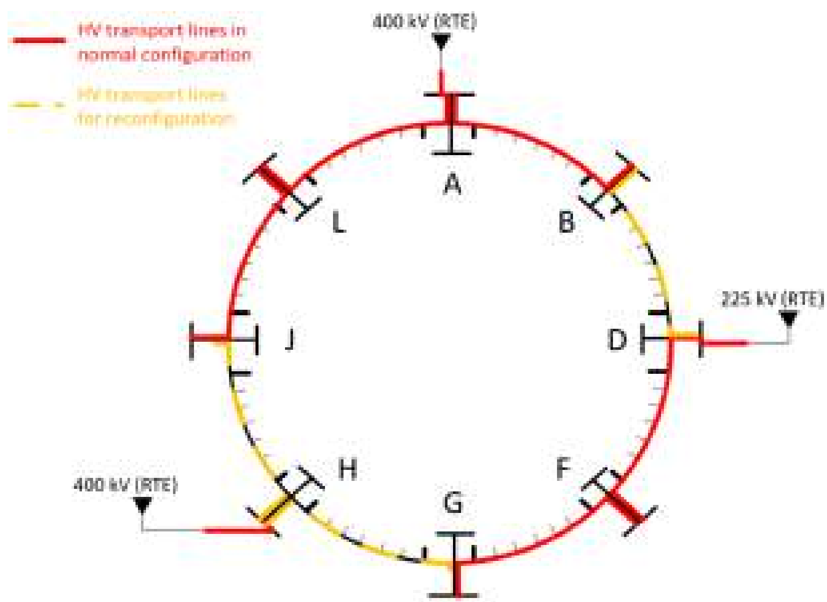

Fig. 8.55 General single line diagram of the transmission network of FCC

Even if the HV cables between PB and PD, between PG and PH, and between PH and PG will not be loaded during normal operation, they can be used as a backup supply in case part of the HV network is unavailable. The possible continuity of service based on the [N-1] principle has been analysed by simulating different failures in the network and reconfigurations to overcome these failures have been determined. The only scenario in which the machine will cease operation without the possibility of network reconfiguration is the loss of supply from PH, as the RF loads at this location are too high to be compensated by other power sources. Apart from this case, the network is designed to allow reconfiguration, ensuring that the accelerator can continue normal operation in the event of a failure of one HV source or one HV branch. The list of possible HV network failures that the system can withstand, along with the corresponding reconfiguration strategies, is summarised in Table 8.21.

This analysis also provides the minimum criteria for dimensioning the sources and lines of the HV network, in addition to the load requirements. Finally, to also cope with the objective of keeping the same HV grid for the

Table 8.21 Transmission network configuration modes to overcome failures

	PA - PB	PB - PD	PD - PF	PF - PG	PG - PH	PH - PJ	PJ - PL	PL - PA
Normal configuration	ON	OFF	ON	ON	OFF	OFF	ON	ON
Loss of PA	ON	ON	ON	OFF	ON	ON	OFF	ON
Loss of PD	ON	ON	ON	OFF	ON	ON	OFF	ON
Loss of PA - PB	OFF	ON	ON	ON	OFF	OFF	ON	ON
Loss of PD - PF	ON	OFF	OFF	ON	ON	OFF	ON	ON
Loss of PF - PG	ON	OFF	ON	OFF	ON	OFF	ON	ON
Loss of PJ - PL	ON	OFF	ON	ON	OFF	ON	OFF	ON
Loss of PL - PA	ON	OFF	ON	ON	OFF	ON	ON	OFF

future FCC-hh, it was decided that all the HV cables will be sized equally to a nominal rating of 115 MVA, to allow the infrastructure to be compatible with the FCC-hh load.

Selection of the voltage level, the location and the technology of the HV transmission network The selection of the operating voltage of the transmission network has been based on a study aimed at optimising infrastructure and operational costs. As a result, the voltage will be stepped down from 400 or 225 kV, to a lower level, see Fig. 8.55.

For the radiofrequency (RF) systems, the voltage will be stepped down to the required level for the main RF power conversion system, which is currently planned to be 40 kV. While adopting 40 kV for the entire transmission network would offer some benefits in terms of material uniformity, an initial analysis clearly indicated that this voltage level is not optimal due to the large cable cross-sections required, leading to high space occupancy in the tunnel and significant power losses. For these reasons, 40 kV was discarded from the beginning of the study.

To determine the most suitable internal transmission voltage, the analysis considered three reference voltages, selected from standard values used by European Grid Operators: 63 kV, 90 kV, and 132 kV. The study was conducted for these three voltage levels, allowing extrapolation to evaluate performance trends across different voltage ranges. For each voltage level, two options have been considered: i) substations installed on the surface or underground (in the technical galleries of the accelerator); ii) air-insulated substations (AIS) or gas-insulated substations (GIS).

The following parameters were included in the analysis, with the aim of evaluating the impact of the different alternatives on all the main aspects of the total lifetime cost of the network:

- OPEX[10] of the HV lines: electrical losses of the lines depending on their operation over the full FCC machine (based on the operating models of the phases of FCC-ee, and on a simplified estimation of the same models for FCC-hh).
- CAPEX[11] of the HV lines: initial cost of the cables, the accessories and the installation works required.
- OPEX of the HV substations: electrical losses of the transformers depending on their operation over the full FCC machine programme and the cost of the maintenance of the substations.
- CAPEX of the HV substations: initial cost of the substations, and equivalent financial value of their space occupation.

The values of CAPEX and OPEX of each case have been assessed based on detailed studies of the substations and the lines at the different voltage levels, but also with estimated financial values of the space occupied and energy cost.

This comprehensive analysis gave the total lifetime cost for each scenario, with the variation trends illustrated in Fig. 8.56. The study concludes that selecting a 63 kV transmission voltage and using GIS substations installed on the surface are the optimal choices within the range analysed. Additionally, manufacturers are demonstrating a clear trend toward reducing the greenhouse gases used in GIS mixtures, significantly improving the environmental sustainability of this technology. The final technical solution was developed based on these findings.

This analysis will be kept running in the future phases of the FCC study, as some parameters have a significant impact and can change the conclusions.

Main high voltage substations The design of the HV substations has been developed according to the results of the analysis shown on Fig. 8.56.

[10] Operational expenditure.

[11] Capital expenditure.

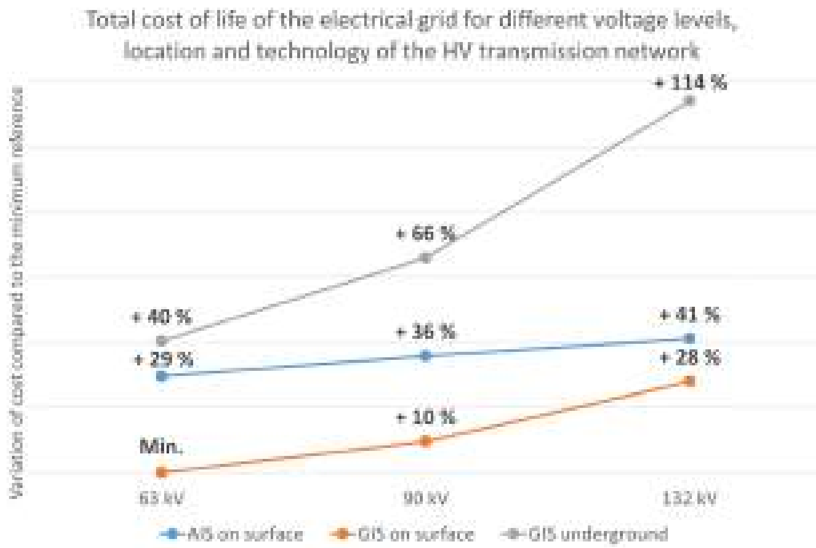

Fig. 8.56 Trend of the variation of the total lifetime cost of the electrical grid for different voltage levels, locations and technologies of the HV transmission network

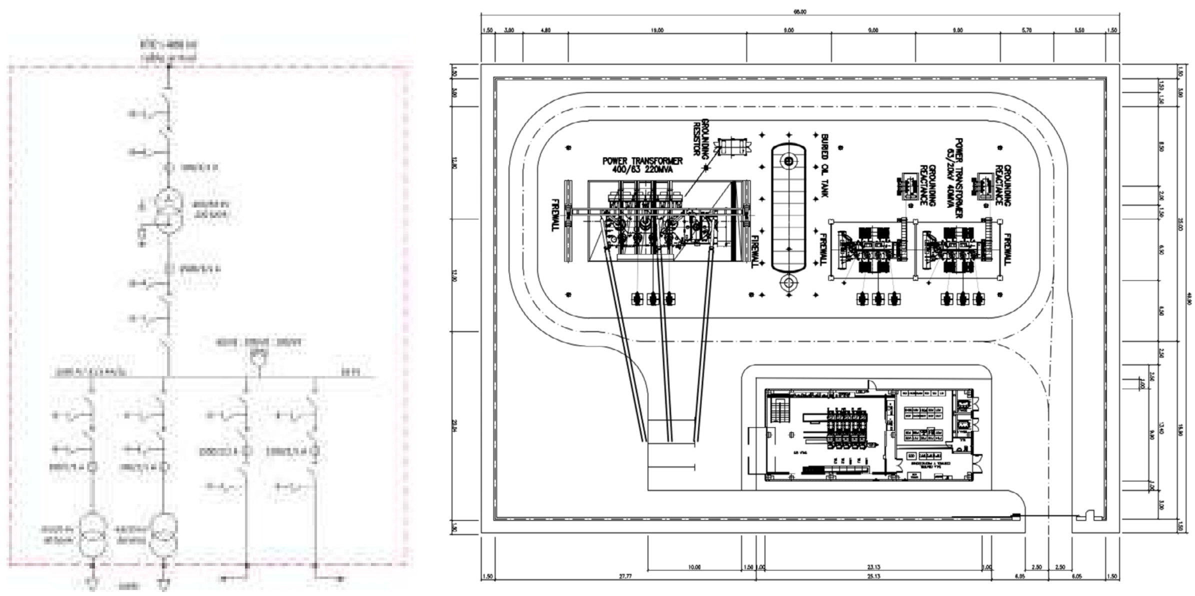

(a) Single line diagram. (b) Layout.

Fig. 8.57 Typical 400/63 kV substation

A 400/63 or 225/63 kV GIS substation (Fig. 8.57) will be installed with a main stepdown transformer of 220 MVA in the three points connected to the European grid. The main switchgears and auxiliary systems will be housed inside a dedicated building, while the transformer will be installed nearby, protected by firewalls and equipped with all necessary safety systems to manage potential oil spills. These include a containment pit, oil separator, retention basin, and fire protection measures, ensuring safe operation and environmental compliance. It is worth noting that in PH an additional bay will be available in the 400 kV switchgear, to supply an additional 150 MVA 400/40 kV transformer that will be dedicated to the power conversion system for the FCC-ee RF system.

A 63 kV GIS substation (Fig. 8.58) will be installed at all the other access points, as shown in the single line diagram of the transmission network in Fig. 8.58a. Also, in this case, the main switchgear will be housed with the auxiliary systems in a building. At each point, the 63 kV GIS substation will supply two 40 MVA 63/20 kV transformers that will be the sources of the distribution networks for each point.

In each access point connected to the grid, the total surface area of the HV substation will be approximately 10,000 m^2; in each of the other points, it will be approximately 4000 m^2, these requirements are already included

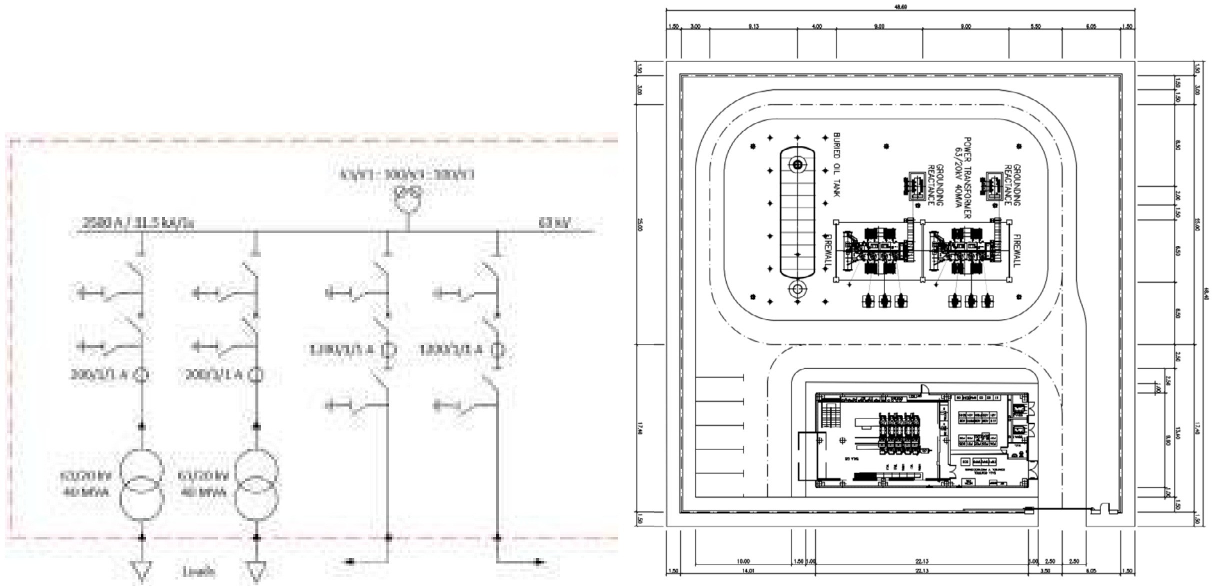

(a) Single line diagram. (b) Layout.

Fig. 8.58 Typical 63 kV substation

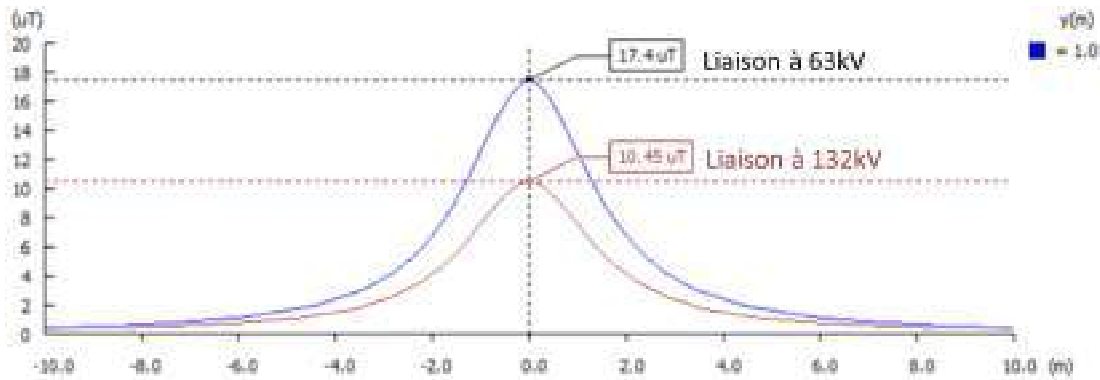

Fig. 8.59 Comparison of magnetic field simulations for cables (63 kV in blue, 132 kV in red)

in those considered by the civil engineering team for the surface occupation and the layouts of the different sites.

Installation of HV cables in the accelerator tunnel As the installation of HV transmission networks rated at tens or hundreds of MVA (Fig. 8.60) is not a standard solution adopted in the underground accelerator facilities (e.g., in LHC today only cables of up to 18 kV and rated at 15 MVA are installed for the electrical distribution), a detailed and specific feasibility analysis has been performed, in order to confirm the absence of showstoppers and to provide requirements for civil engineering.

The final report of this analysis confirms the feasibility of installing such cables in the underground areas of the accelerator. It provides models and datasheets of cables with their related losses, different installation methods with their constraints and the required space and civil engineering works to install and house the cables. It also includes a cost estimate and a tentative schedule for the installation. All the details can be found in Ref. [383], but a summary is presented in Table 8.22.

Two important points deserve to be mentioned: the cable runs in a concrete duct of 520×500 mm in the machine tunnel requiring a specific volume, as can be seen in Fig. 8.61; and the cables along a tunnel sector need junction chambers every approximately 1-1.5 km, requiring a significant space in the tunnel of approximately 1200×500×16,000(length) mm as shown in Fig. 8.62. This second point is important, as it was decided to create the junction chambers corresponding to each alcove (in the current baseline, every 1.6 km), housing them in the transport parking areas to ease their construction and future accessibility.

Fig. 8.60 Specification of the proposed 63 kV cable

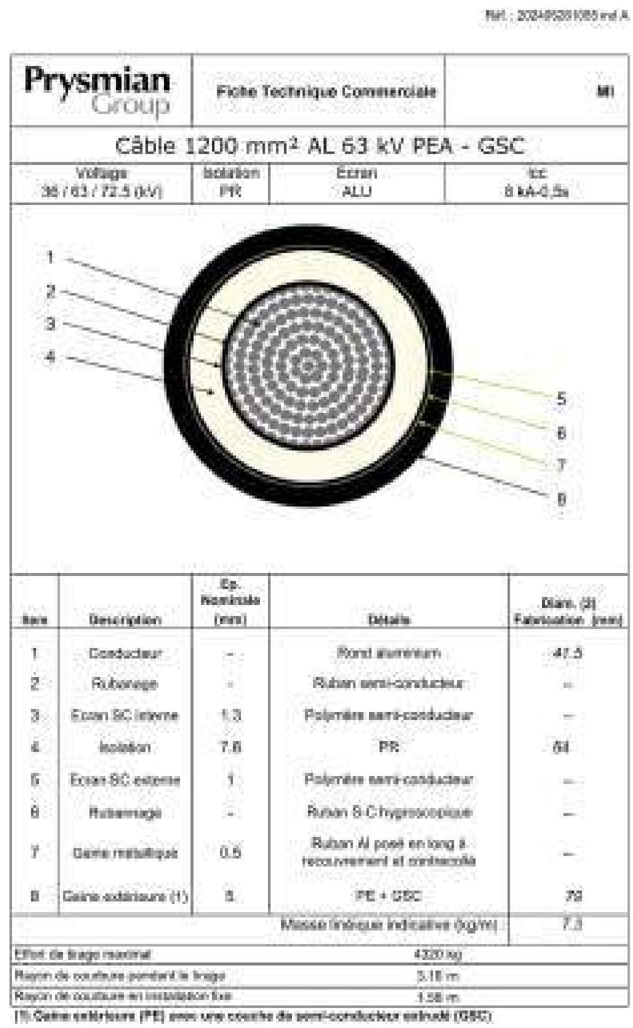

Table 8.22 Summary table of the requirements of the HV lines

	63 kV	132 kV
Proposed cable	3× 1200 mm^2, Aluminium cable	3× 630 mm^2, Aluminium cable
Proposed space occupation in the tunnel	Concrete duct of 520×500 mm.	
Proposed quantity of junction chambers	13 junction chambers (including 1 earthing junction chamber)	
Proposed space occupation of junction chambers	With earthing of screens: duct of 1500×500 mm with a length of 9.5 m.	With earthing of screens: duct of 1800×500 mm with a length of 12 m.
Preferred installation method	Within PEHD ducts with the so-called cable train pulling method.	
Cost of installation	Lower cost	+ 4% compared to 63 kV
Schedule estimation of installation (per line between two points)	160 days	170 days
Level of magnetic field in the tunnel	See magnetic field graphs on Fig. 8.59.	

Distribution networks The power is locally dispatched to the electrical loads of the surface and underground facilities by the medium and low voltage distribution networks available at each point.

The various loads can be classified based on their function and criticality, and each category has a dedicated distribution network with specific features, as shown in Table 8.23. The functional separation of the networks was one of the criteria in the study of the distribution at each point. This was to ensure users' power quality (in

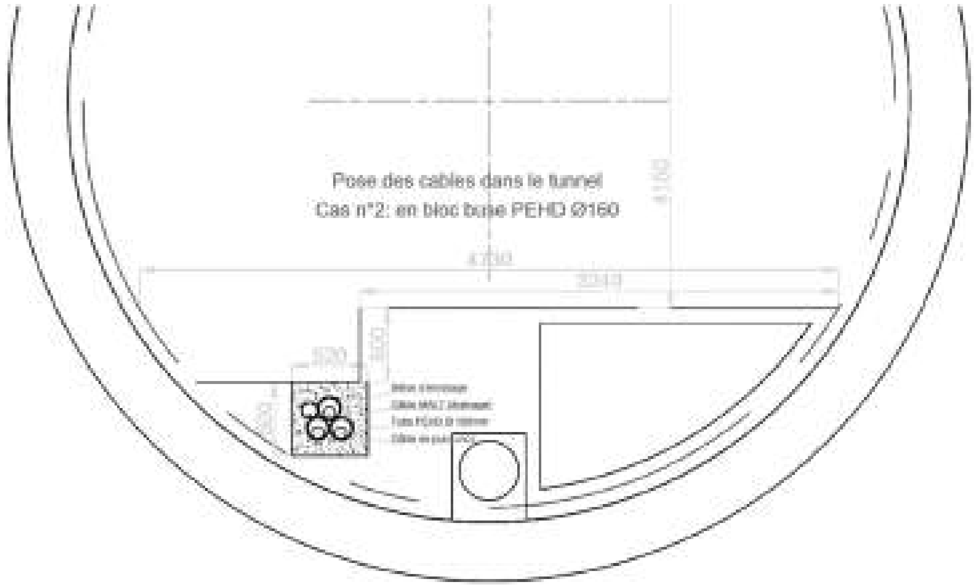

Fig. 8.61 Proposed space occupation of the cables in the machine tunnel

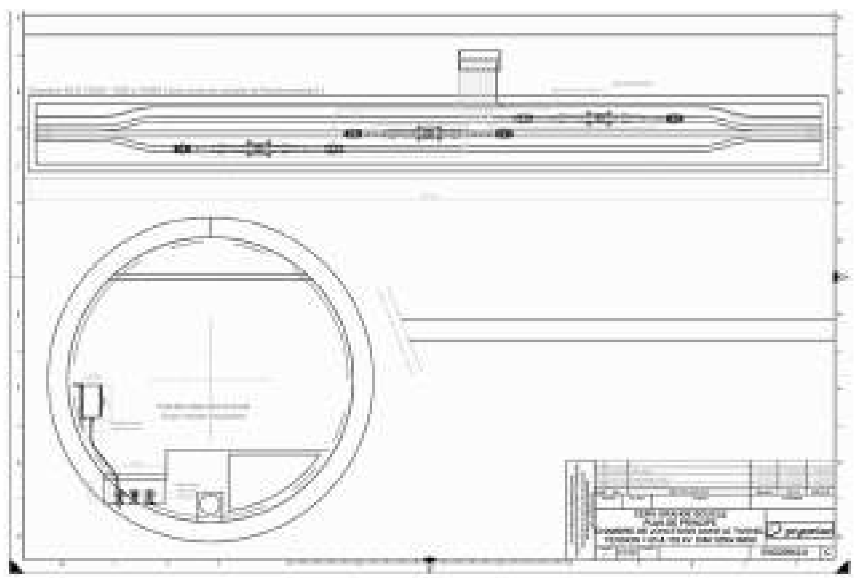

Fig. 8.62 Proposed space occupation of the junction chambers in the machine tunnel

particular, to minimise potential disturbances from power electronics) and to enhance reliability, operability, and maintainability of the grid.

The distribution network concept is the same for all points. The HV transmission network supplies two 63/20 kV transformers to create two main types of networks at 20 kV: General Services (GS) and Machine. The power is dispatched through two medium voltage substations (one in a surface building, the other in the underground service cavern) to 20/0.4 kV transformers that supply the low voltage switchboards in charge of local distribution to the terminal loads.

The GS and machine networks can be coupled at the 20 kV substations to allow a backup supply: the size of the main 20 kV transformers, busbars and links (primary and backup) has been set to allow full reconfiguration and nominal operation in case one element of the network is unavailable as a result of maintenance or failure. For these reasons, and also to cope with the load forecast of the FCC-hh, the two main transformers of each point have been sized at 40 MVA, and the main 20 kV links at 20 MVA.

An example is shown in the single line diagram of the distribution network of point PA shown in Fig. 8.63, and the layout of the 20 kV substations on the surface at the same point is shown on Fig. 8.64.

Secured and uninterruptible networks Based on the load categories of Table 8.23, there is a secured network (Fig. 8.65) with backup sources available at each point to power critical loads within a few seconds of the main

Table 8.23 Network types and characteristics

Network type	Loads type (non-exhaustive list)	Power unavailability duration in case of degraded scenario
Machine	Power converters, RF, cooling pumps, fan motors, etc.	Until return of main supply
General Services	Lighting, outlets	Until return of main or secondary supply
Secured	Personnel safety-related loads (lighting, pumps, elevators)	10-30 s
Uninterruptible	Personnel safety (evacuation and anti-panic lighting, fire-fighting system, oxygen deficiency, evacuation)	Interruptions are not allowed; continuous service is mandatory
	Machine safety (sensitive processing and monitoring, beam loss, beam monitoring, machine protection)	

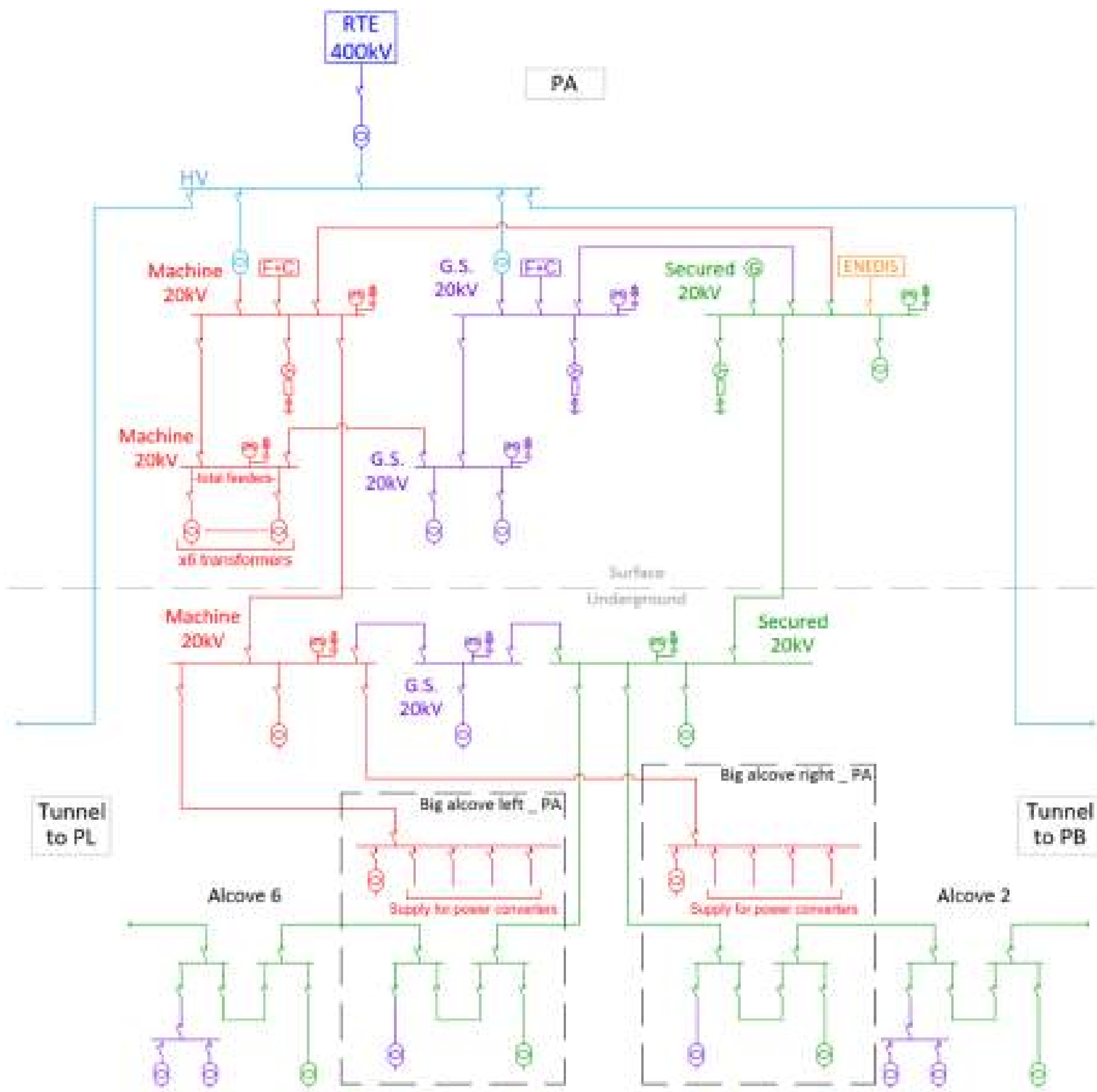

Fig. 8.63 Conceptual electrical distribution for point PA

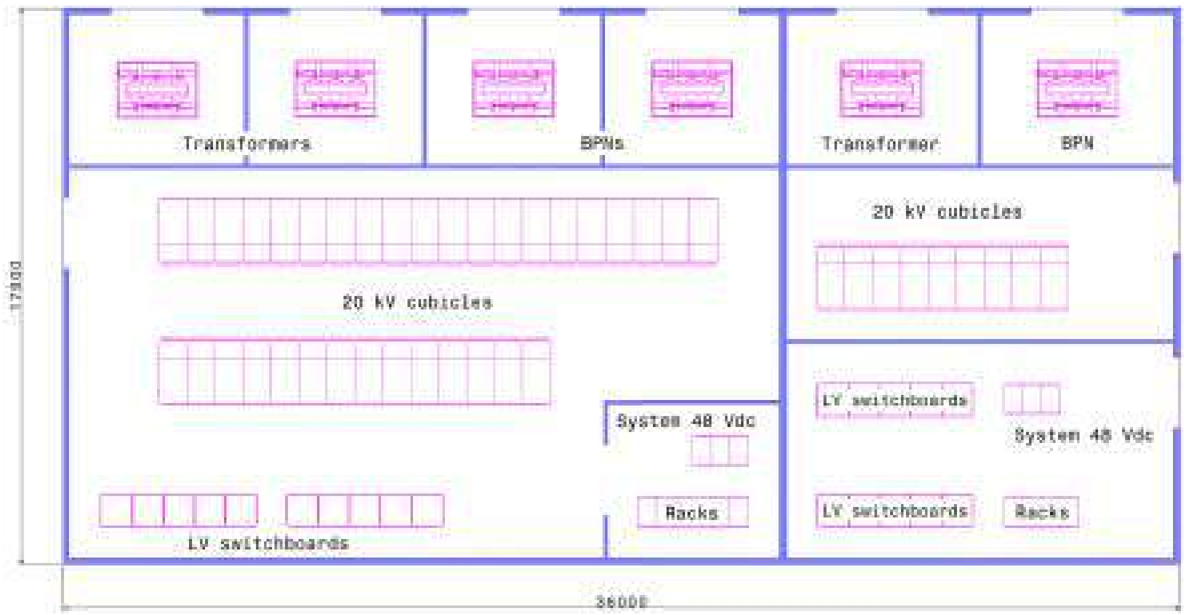

Fig. 8.64 Layout of the 20 kV substation of point PA

supply becoming unavailable. The first priority backup sources have an emergency power station installed on the surface close to the substation (the baseline is a diesel generator, alternatives like hydrogen-based groups are under evaluation). As an alternative, there will be a connection to the medium voltage utility deployed during the construction phase which will be kept available.

The backup sources will be at 20 kV and will be connected to the surface substation, on a busbar where only critical loads are hosted; from there, a cable running down the shaft will connect to the equivalent in the underground substation. From the underground substation, the secured network will be distributed to each alcove through a 20 kV line, and each secured load in the tunnel will be powered from its closest alcove.

The distribution from the secured substation in the tunnel must be done at medium voltage, as stepping down to low voltage would result in excessive voltage drop in the circuits running along the sector. In this sense, a possibility for optimisation was identified during the study, and to avoid duplicating the 20 kV cables in the tunnel (one for the normal network, one for the secured power), it is proposed to use the same link deployed for the general services, applying a load shedding logic in case of power outage. The aim is to minimise the space occupation and ease integration in this tight area.

In all the substations (surface, underground, alcoves) there will be a coupling between the critical loads 20 kV busbar and the general services busbar; in normal operation, the coupling will be closed, and the link between the substations will serve both critical and not-critical loads. In case of a failure, maintenance or any other unavailability of the main source, the electrical network will be supplied using the backup power sources: in this case, the couplings between the secured network and the general services network will be automatically disconnected, and in the tunnel the same 20 kV link will only keep the loads related to the safety of people live.

The secured network of one access point covers all the facilities of the point itself at medium voltage and extends up to half a sector to the left and right in the tunnel. To enhance the reliability of the system, there is an MV coupling to the last alcoves of each half sector: this stays open during normal operations. If a part of the network connected to one point is not operational, all the secured network busbars can be powered from the adjacent points through the tunnels by closing this coupling.

The secured network described so far is specifically designed to support electrical loads related to personnel safety. If a similar level of backup is required for systems associated with the accelerator or experiments, a parallel infrastructure with equivalent characteristics will need to be developed and implemented. For loads that cannot accept a brief interruption of a few seconds, whether they are safety-related or critical to operation, an uninterruptible power supply (UPS) system supported by batteries will be made available. This system will be strategically installed in buildings, service caverns and alcoves, to ensure a continuous power supply with the necessary autonomy. This infrastructure will serve critical loads of systems like vacuum, machine protection, cryogenics, RF, control, IT.

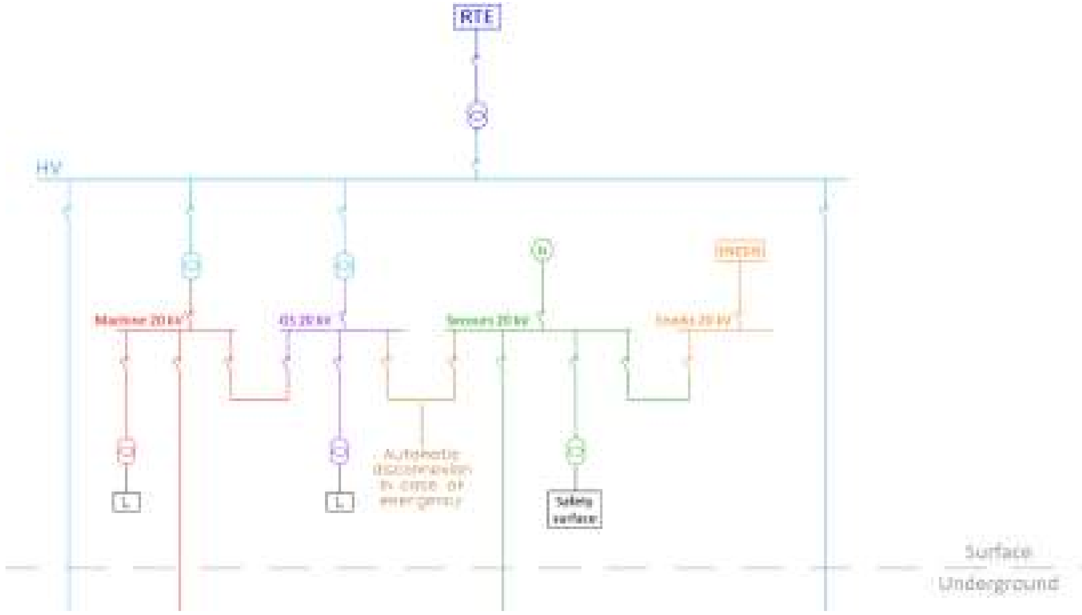

(a) On surface,

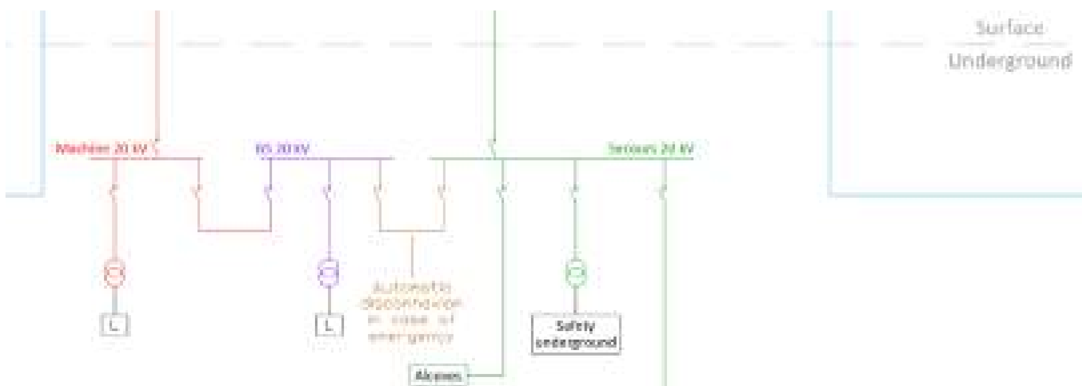

(b) underground,

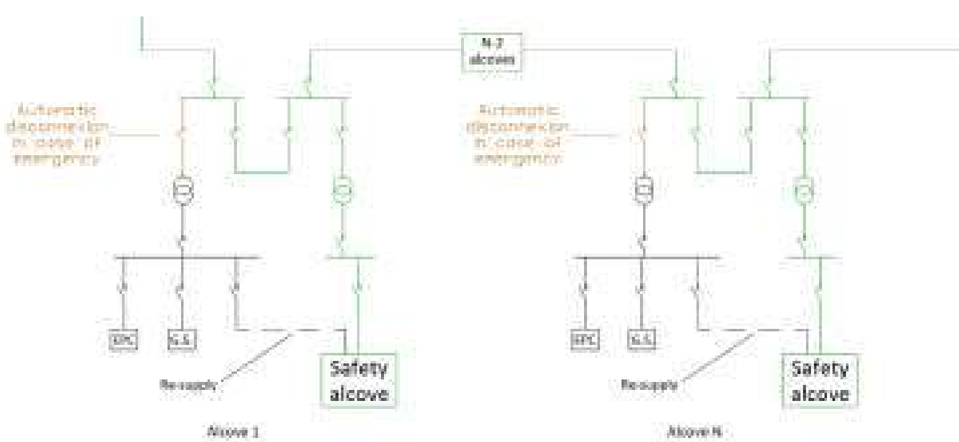

(c) in the tunnel.

Fig. 8.65 Conceptual electrical distribution for the secured network

8.4.3 RF powering

The RF system requires a power source capable of delivering a stable, high-quality DC high voltage. In existing implementations, such as the LHC and other accelerators, this is typically achieved by supplying a small group of RF amplifiers with a power converter operating in the MW range. However, for FCC-ee, this approach has been deemed economically unfeasible due to the large number of power converters and the extensive surface infrastructure that would be required at point PH. To address this challenge, a centralised power conversion strategy has been adopted, utilising a modular multilevel converter (MMC) to efficiently meet the system's power requirements.

Given that the RF system's power demand exceeds 100 MW, a thyristor-based converter was considered but ultimately found to be impractical due to power quality issues. If such a converter were implemented, a large-scale reactive power and harmonic compensation system would be required to maintain acceptable power quality. In contrast, the MMC solution offers significant advantages: it requires minimal or no harmonic filtering on the AC side and provides flexible reactive power control. This capability could potentially be leveraged to partially compensate for the reactive power consumption of the accelerator, further optimising energy efficiency.

8.4.4 Arc powering and alcoves

Power is distributed through the alcoves along the tunnel from the underground 20 kV substations. The alcoves serve multiple functions: they house equipment that must be protected from radiation, as well as local distribution systems for the arc, including accelerator systems, cooling and ventilation, safety systems, lighting, and power boxes. Additionally, they accommodate the power converters responsible for supplying the magnets in the arc.

The current baseline design includes seven alcoves per arc, with two larger alcoves positioned at the ends of the LSS (long straight section) of each point. These larger alcoves will host the power converters for the main arc magnets (dipoles and quadrupoles), as they require more space. The remaining alcoves will be spaced every 1600 m, each covering a sector extending 800 m on either side, distributing power accordingly.

The machine and general service networks will be separately available only in the first alcoves at the LSS ends, as the power converters in these locations have significantly higher loads and must be powered using dedicated transformers connected to a separate machine network. However, for the other alcoves, where power requirements for converters and other accelerator systems are much lower, it has been decided to supply them only from the general service network to avoid installing two separate 20 kV links in the tunnel.

To achieve this optimisation, the functional separation criteria outlined in Table 8.23 have been suspended for the alcoves. Instead, the choice is based on the assumption that the electrical parameters of the installed systems, particularly the power converters, will comply with specific requirements for connection to the network, including resilience to voltage and frequency variations and low total harmonic distortion (THD).

A similar synergy has been adopted for the safety-related loads and the secured network in the alcoves. These will be supplied through the same 20 kV link running through the tunnel, using a load-shedding logic to prioritise general services when necessary.

Following these technical choices, one 20 kV cable will run through the tunnel to the first smaller alcove from the alcoves at the end of the LSS at each access point, connecting it and continuing to the next, up to the end of the arc at the next access point (see Fig. 8.66. In the nominal configuration, each access point will supply the alcoves of half sectors to the left and to the right, with the one in the middle having an open coupling between the two sides. Closing this coupling, and having the 20 kV cable running from one point to the other, will allow re-supplying all the alcoves from only one point if the other is unavailable.

Electrical equipment in the alcoves The power distribution of the alcoves has been studied and sized based on the load requirements identified for the FCC-ee arc. The 20 kV cable coming from the arc will arrive at a switchgear divided into two busbars for secured and other loads. The switchgear will be connected to 20/0.4 kV transformers powering various low voltage switchboards, from where all the circuits going to the alcove and the tunnel are supplied. A redundant UPS will provide the required backup to create an uninterruptible network for the critical loads, and a redundant power supply will be dedicated to the emergency lighting.

In addition to the power converters, a certain number of racks will be installed, supplied through ad-hoc busbar trunking systems, and hosting the systems required for the accelerator and the services in a sector. Today, the number of these racks is estimated at 13 units, but could evolve in accordance with the evolution of the systems' requirements. Figure 8.67 shows the typical single-line diagram of the power distribution of an alcove.

A preliminary study has been conducted for the so-called big alcoves at the end of the LSS, concerning the powering of the power converters and of the loads of the half sector. The principles that have been applied are the same as used for the other alcoves, and the single line diagram is shown on Fig. 8.68.

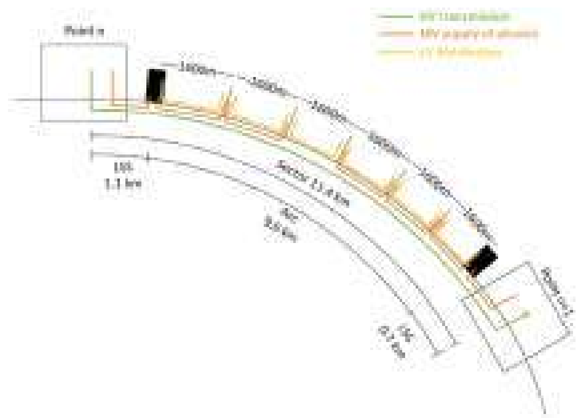

Fig. 8.66 Arc and alcoves powering layout concept

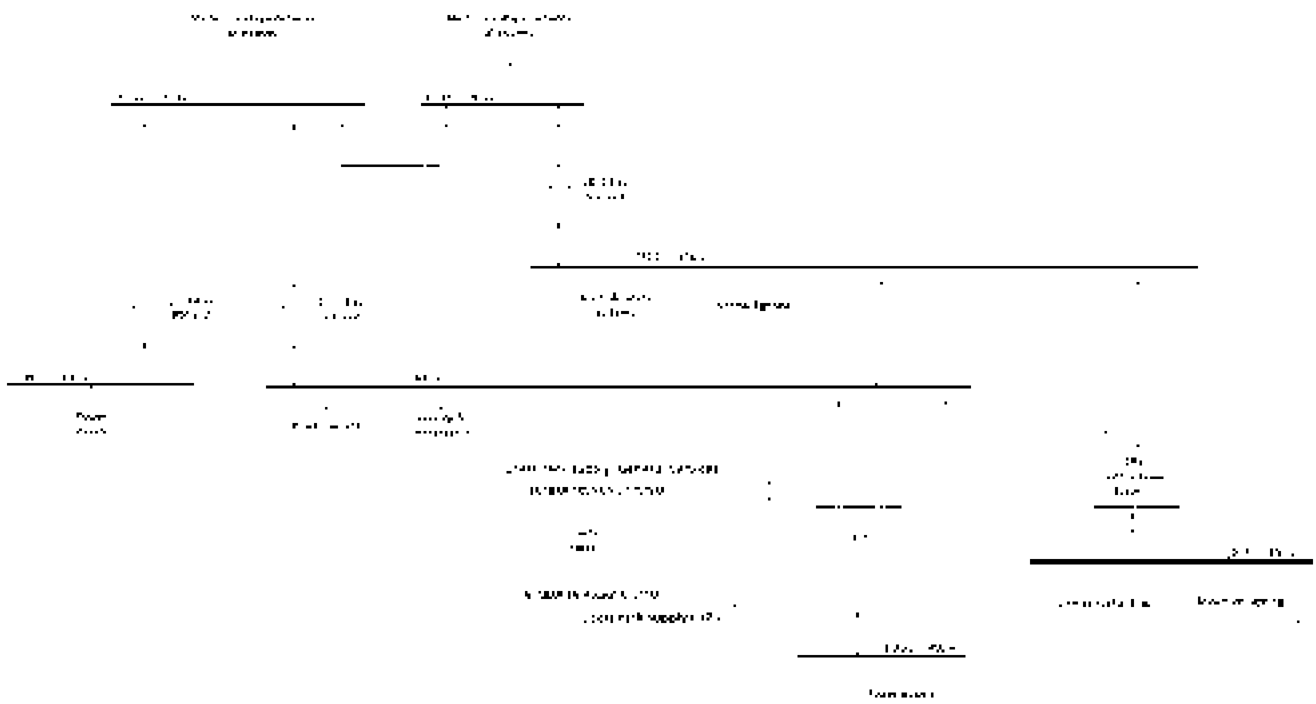

Fig. 8.67 Typical single line diagram of the power distribution of an alcove

Electrical equipment in the arc The list of equipment and circuits for powering the arc (see Fig. 8.69) includes:

- One power outlet box on the general service network every 50 m, powered from only the closest alcove (maximum length of the circuit: 800 m), without redundancy.
- One power outlet box on UPS network every 50 m, with secured redundant powering from both alcoves to the right and left (maximum length of the circuit: 1600 m).
- One normal light every 5 m, powered from only the general service network of the closest alcove (maximum length of the circuit: 800 m), with a circuit connected in parallel to the secured switchboard of the same alcove supplying 1 light out of 5 (to create a set of minimum lighting every 20 m).

In addition, the list of electrical equipment related to safety in the arc includes:

- One electrical emergency button (AU) every 50 m.
- One emergency light every 14 m, with secured redundant powering from both alcoves on the right and left (maximum length of the circuit: 1600 m).

The list of the cables composing these circuits is given in Table 8.24.

The quantification of these cables is of great importance in the assessment of the space required for the cable trays and other containment systems (e.g., cablofil, duct) that need to be installed in the arc.

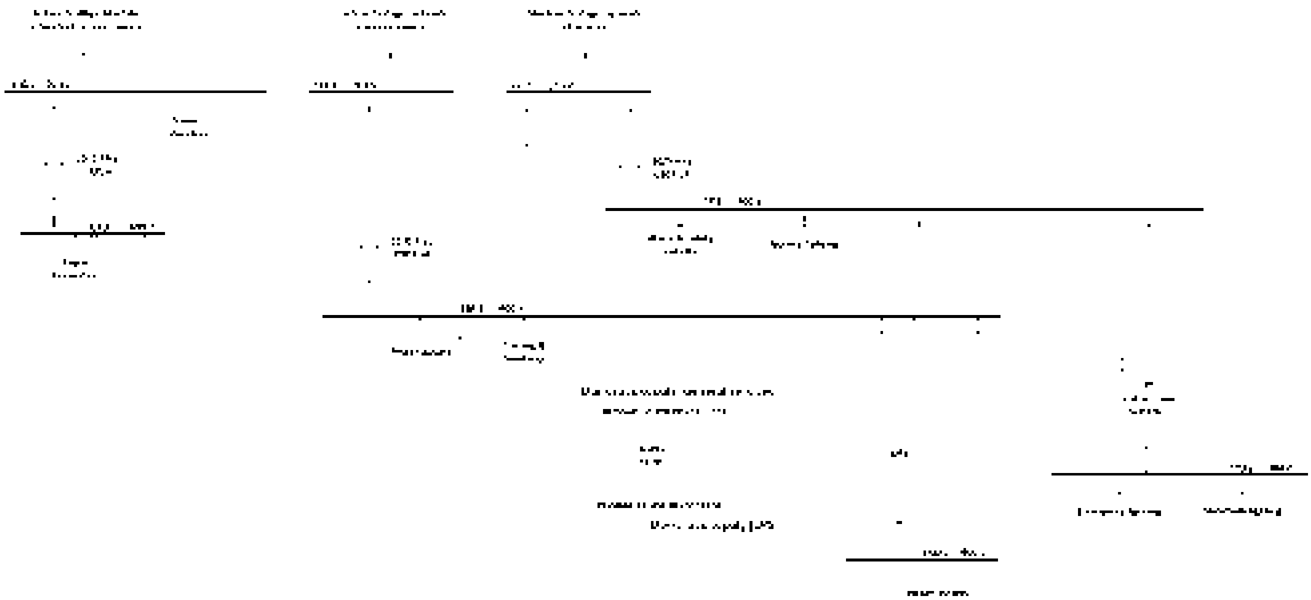

Fig. 8.68 Typical single line diagram of the power distribution of a big alcove at the end of LSS

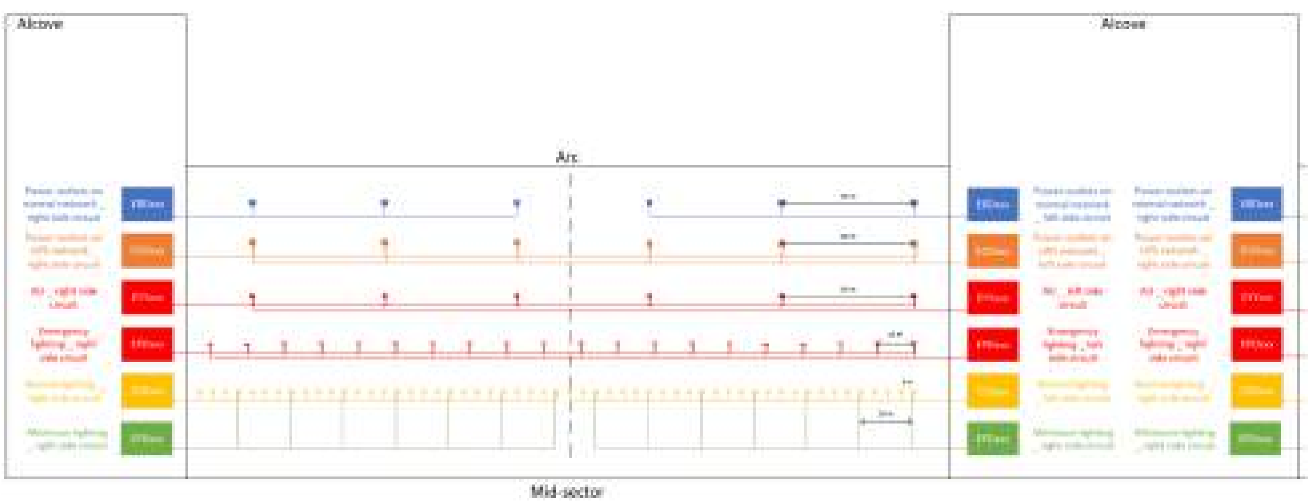

Fig. 8.69 Electrical distribution in the arc

For the same reason, the signal and control cables and the optical fibres used by other systems and installed in the arc have also been estimated. This process started from the various system's owners when available, or from extrapolation from previous accelerator projects at CERN when the information was not available. The list of these cables is given in Table 8.25.

The collection of the powering and cables' requirements in the tunnel will be constantly updated in the next stages of the study to consider every possible modified or new request and to adapt the technical solution accordingly. Furthermore, the use of optical fibres should be prioritised over copper cables to minimise space occupancy when developing users' cable requirements.

The information summarised in Table 8.24 and Table 8.25 allows the selection and dimensioning of the cable containment systems to be installed (mainly cable trays). This is one of the most important factors for the determination of the layout and cross section of the arc tunnel. The number and dimensions of cable trays are:

- Twelve 500 mm wide and 60 mm high cable trays for: DC cables (five cable trays considered), MV power cables, LV power cables, signal cables and optical fibres.
- Two 200 mm wide, 60 mm high and fire-resistant cable trays for safety systems.
- One 520×500 mm concrete duct for the HV cables.

Table 8.24 Estimation of the power cables in the arc

User	Load	Cable tray	Cable type	Size (mm)	Number of lines in the tunnel
Powering	MV power of alcoves	MV	$3\times(1\times400\ mm^2) + (1\times120\ mm^2)$ Cu	3×d = 50 + d = 21	1
	Power outlets on GS network	LV	$3\times(1\times150\ mm^2) + (1\times95\ mm^2)$ Cu	3×d = 21 + d = 18	1
	Power outlets on UPS	LV	$3\times(1\times150\ mm^2) + (1\times95\ mm^2)$ Cu	3×d = 21 + d = 18	2
	Classic lighting	LV	$(5\times10\ mm^2)$ Cu	d = 22	1
	Emergency lighting	Safety	$(5\times2.5\ mm^2)$ Cu, flat	24x6	2
	Emergency stops link (AU)	Safety	$14\times(2\times1\ mm^2)$ Cu	d = 21	2

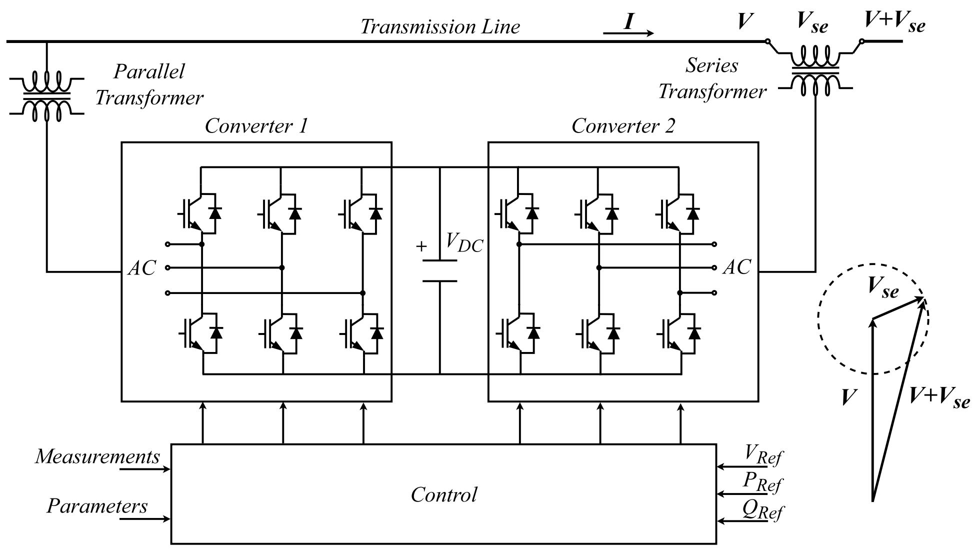

Fig. 8.70 Diagram of a unified power flow controller (UPFC) used to enhance controllability of the FCC network

8.4.5 Control of FCC grid

AC network control using unified power flow controllers Unified power flow controllers (UPFCs) are power-electronic-based network controllers capable of performing voltage control, power flow control, reactive power compensation, and protection against network perturbations. The versatility of these systems makes them highly suitable for controlling and stabilising the FCC AC transmission network, offering an alternative to systems such as static var compensators (SVCs) or DC networks.

A UPFC consists of two back-to-back converters, each connected to the network via a transformer. One converter is connected in parallel, enabling reactive power or voltage control at the associated network node. The other converter is connected in series, allowing active and reactive power flow control, voltage control, and voltage dip mitigation by injecting a specific voltage between the network and the loads. Figure 8.70 illustrates the basic structure of the UPFC.

The application of UPFCs in the FCC network can be tailored to specific protection and reactive power compensation requirements. In the high-voltage transmission ring, UPFCs can be installed at each network connection point to manage the accelerator's reactive power using the parallel converter. At the same time, the series converter provides protection against voltage dips and prevents undesired power flows, particularly under closed-loop operation.

At the medium-voltage level, UPFCs enable voltage control and protect access points from voltage dips. To optimise equipment efficiency, protection can be focused on critical sections of the network by connecting the series transformer to selected feeders. This approach creates a dedicated machine network, effectively decoupling it from general services, following the model already employed in CERN's existing infrastructure.

Compared with existing compensating equipment such as SVCs, UPFCs offer enhanced functionality. While they perform the same tasks of reactive power compensation and voltage control, UPFCs are more robust to network perturbations, exhibit faster response times, and, through the series converter, provide load protection against transients - an advanced feature not currently available in SVCs.

Table 8.25 Estimation of the control and signal cables, and optical fibres crossing the arc

User	Load	Cable tray	Cable type	Size (mm)	Number of lines in the tunnel
Fibre optics	Backbone	FO	3 cables (×24 fibres)	d = 25	1
	Underground	FO	9 cables (×24 fibres)	d = 25	2
	BI (only BPMs)	FO	13 cables (×12 fibres) +8 cables (×24 fibres)	d = 25	4
	Sensing	FO	2 cables (×6 fibres)	d = 25	1
Vacuum	ion pumps	Signals	1×0.63(HV) + 2×0.25 mm^2 Cu	d = 10.7	28
	NEG (power)	Signals	3×2.5 mm^2 Cu	d = 13	16
	Penning	Signals	3-axis 0.8/8.4 mm Cu	d = 10.3	12
	Pirani	Signals	1× (4×1 mm^2) Cu	d = 6.5	12
	BA power	Signals	6× (2×0.75 mm^2) Cu	d = 14.5	6
	BA collector	Signals	3-axis 0.5/5.7 mm Cu	d = 7	6
	Sector valve	Signals	6× (2×0.75 mm^2) Cu	d = 14.5	6
	Profibus	Signals	2× (1×0.35 mm^2) Cu	d = 8	1
Access & Alarms	Sector doors	Safety	13× 2×0.5	d = 17	1
	Fire doors - magnet	Safety	2×1.5	d = 10.5	3
	Fire doors - position contacts	Safety	2×1	d = 5	3
	Fire doors - flashing lights	Safety	4×1.5	d = 10.5	3
	Call points - break-the-glass	Safety	2×1	d = 5	2
	Call points - telephones	Safety	1× 4×0.6)	d = 7.4	2
	Evacuation - voice alarm	Safety	2×2.5	d = 13	2
Cooling & Ventilation	Fancoils	Signals	1×70 mm^2	d = 16.6	16
	Dampers	Signals	1×35 mm^2	d = 12.1	21
	Valves & other equipments	Signals	1×35 mm^2	d = 12.1	3
Radiation protection	Radiation detectors ($t\bar{t}$ phase only)	Safety	2×CEH50 + 2× (2×0.22 mm^2)	d = 9.5	2
Magnet	WIC fieldbus	Signals	1×50 mm^2	d = 14	4
Protection	BIS fibres	FO	1 duct	d = 25	1
Power Converters	DC cables				
Others	Unknown				

At this stage of the project, the exact compensating requirements are not fully defined. However, it is anticipated that the reactive compensation needs for each access point will be approximately 10 MVAr. Regarding voltage dip compensation, most of the recorded voltage dips at CERN exhibit a depth of less than 30% of the nominal voltage. With this figure in mind, and assuming a power rating of 10 MVA for the loads to be protected at each access point, the UPFC must be designed to inject up to 3 MVA during such events. Based on these considerations, the total installed UPFC power per access point can be estimated at approximately 15 MVA.

DC distribution alternative Recent developments in power electronics have enabled the use of DC for power transmission and distribution. Compared with conventional AC distribution, DC networks offer lower transmission losses, as only active power flows through the cables and the skin effect is absent. Additionally, DC networks provide precise power flow control and mitigate perturbations originating from the AC network.

The use of DC to transmit power from network connection points to accelerator loads is under consideration. In this transmission scheme, loads are supplied by high-voltage converters with energy buffers that decouple them